

LIB.

P199324 N°002

AGARD-AG-175

AGARD-AG-175

AGARD

ADVISORY GROUP FOR AEROSPACE RESEARCH & DEVELOPMENT

7 RUE ANCELLE 92200 NEUILLY SUR SEINE FRANCE

AGARDograph No. 175

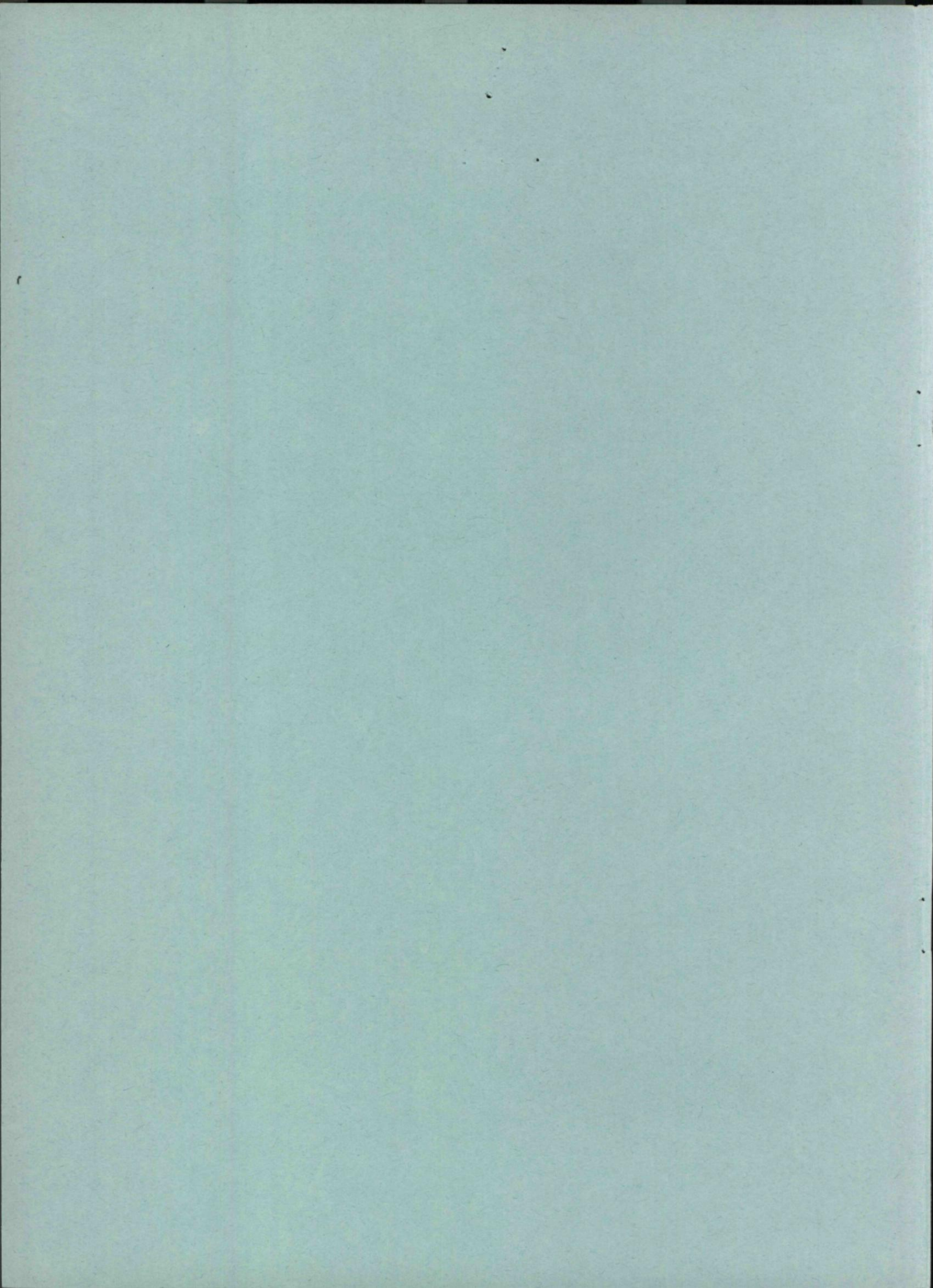
on

Active Control Systems for Load Alleviation, Flutter Suppression and Ride Control

NORTH ATLANTIC TREATY ORGANIZATION



DISTRIBUTION AND AVAILABILITY
ON BACK COVER



NORTH ATLANTIC TREATY ORGANIZATION
ADVISORY GROUP FOR AEROSPACE RESEARCH AND DEVELOPMENT
(ORGANISATION DU TRAITE DE L'ATLANTIQUE NORD)

AGARDograph No.175
ACTIVE CONTROL SYSTEMS FOR LOAD ALLEVIATION,
FLUTTER SUPPRESSION AND RIDE CONTROL

THE MISSION OF AGARD

The mission of AGARD is to bring together the leading personalities of the NATO nations in the fields of science and technology relating to aerospace for the following purposes:

- Exchanging of scientific and technical information;
- Continuously stimulating advances in the aerospace sciences relevant to strengthening the common defence posture;
- Improving the co-operation among member nations in aerospace research and development;
- Providing scientific and technical advice and assistance to the North Atlantic Military Committee in the field of aerospace research and development;
- Rendering scientific and technical assistance, as requested, to other NATO bodies and to member nations in connection with research and development problems in the aerospace field;
- Providing assistance to member nations for the purpose of increasing their scientific and technical potential;
- Recommending effective ways for the member nations to use their research and development capabilities for the common benefit of the NATO community.

The highest authority within AGARD is the National Delegates Board consisting of officially appointed senior representatives from each member nation. The mission of AGARD is carried out through the Panels which are composed of experts appointed by the National Delegates, the Consultant and Exchange Program and the Aerospace Applications Studies Program. The results of AGARD work are reported to the member nations and the NATO Authorities through the AGARD series of publications of which this is one.

Participation in AGARD activities is by invitation only and is normally limited to citizens of the NATO nations.

Part of the content of this publication has been reproduced directly from material supplied by AGARD or the authors; the remainder has been set by Technical Editing and Reproduction Ltd.

Published March 1974

629.73.062 - 52 : 533.6.013.422 : 533.6.048.1



*Printed by Technical Editing and Reproduction Ltd
Harford House, 7-9 Charlotte St. London. W1P 1HD*

PREFACE

In view of the ever increasing performance of modern aircraft, wing safety must be improved, without any weight penalty, through devices permitting the suppression of critical flutter speeds, on the one hand, and, on the other, the alleviation of maneuver or gust induced loads. Such devices are always "active" systems based on the feed-back principle.

The present AGARDograph collects, in a single volume, several papers on this theme presented on the occasion of a Specialists' Meeting organized in The Hague in October 1973 under the joint sponsorship of two separate Working Groups of the AGARD Structures and Materials Panel: one of these groups deals with the interactions and maneuverability of aircraft in flight, the other with aeroelasticity and unsteady aerodynamics.

Major current problems such as flutter suppression and the reduction of loads induced by lateral gusts are reviewed by the authors who describe the solutions either developed or in the course of development in their respective countries: United States, Great Britain, Germany and France. When reading these texts, one is struck by the ingeniousness and variety of the solutions presented, as well as by the fact that some devices which have been used for a long time to improve maneuverability prove efficient in a much broader field; this would justify, if such a justification was still needed, the necessity of an increasing collaboration between research workers specialized in closely related subjects.

We express the hope that, by presenting solutions which may still be unknown by many, this AGARDograph will promote useful thoughts and contribute to the development of the means used to increase the safety and comfort of aircraft simultaneously with their speed.

R.MAZET
Chairman of the Working Group on
Aeroelasticity and Unsteady Aerodynamics

CONTENTS

	Page
PREFACE	iii
INTRODUCTION	v
EFFECT OF YAW DAMPER ON LATERAL GUST LOADS IN DESIGN OF THE L-1011 TRANSPORT by F.M.Hoblit	1
THE EFFECT OF ACTIVE CONTROL SYSTEMS ON STRUCTURAL DESIGN CRITERIA by N.F.Harpur	11
STATUS OF TWO STUDIES ON ACTIVE CONTROL OF AEROELASTIC RESPONSE AT NASA LANGLEY RESEARCH CENTER by I.Abel and M.C.Sandford	23
CONTROLE DU FLOTTEMENT PAR DEPLACEMENT D'UNE VALEUR PROPRE par J.Angélini	49
ACTIVE FLUTTER SUPPRESSION ON WINGS WITH EXTERNAL STORES by G.Haidl, A.Lotze and O.Sensburg	57

INTRODUCTION

ACTIVE CONTROL SYSTEMS FOR LOAD ALLEVIATION, FLUTTER SUPPRESSION AND RIDE CONTROL

Modern active or feedback control technology has been applied for perhaps a quarter of a century now to augment handling qualities and stability and control characteristics of aircraft. Moreover, many important contributions have extended applications of active control technology in a broader manner and to other areas. Maneuver and gust load reductions, fatigue damage reductions, load distribution control, ride comfort improvement, and relaxation or reduction of unaugmented static stability requirements are some present or near-future applications. For many of the above phenomena, not only the more or less rigid body responses have been controlled, but also the significant responses of the lowest vibration modes of the flexible aircraft have been reduced. Novel and very important contributions are now being made to the theory and hardware pertinent to higher frequency ranges of flexible aircraft. "Active flutter suppression" is a distinct possibility in some applications.

In view of the above progress, the Working Group on Interaction of Handling Qualities, Stability and Control on Structural Loads together with the Working Group on Aeroelasticity and Unsteady Aerodynamics recommended a joint conference which was approved by the AGARD Structures and Materials Panel at the April 1973, 36th meeting in Milan, Italy. Consequently, and in consonance with the mission requirements of AGARD as stated on page ii, five pilot papers were presented during the Opening Ceremony (afternoon) Session of the 37th meeting of the Structures and Materials Panel, 8th October 1973, Den Haag, Netherlands. The purposes of the papers were to describe the status and impact of the rapidly expanding domain of aircraft active control relative to our Panel activities. In particular, these limited pilot papers were primarily selected to define (a) the present status of industrial applications of active control technology in reducing loads on modern aircraft, and (b) the future potential of active control for aircraft flutter suppression.

Both Working Groups and the Panel are grateful to Dr Mazet for competently acting as Chairman of this joint meeting, to the authors for their high quality papers, and to the audience for the lively and interesting discussions. In view of the success of this meeting and accelerating progress in this most important technological domain, further such joint meetings are envisioned.

WALTER J. MYKYTOW
Vice Chairman
Working Group on Aeroelasticity
and Unsteady Aerodynamics

Dr JOHN C. HOUBOLT
Chairman
Working Group on Interaction of
Handling Qualities, Stability and Control



EFFECT OF YAW DAMPER ON LATERAL GUST LOADS IN
DESIGN OF THE L-1011 TRANSPORT

by

Frederick M.Hoblit

Commercial Project Loads
Lockheed-California Company, P.O. Box 551
Burbank, California 91520, USA

EFFECT OF YAW DAMPER ON LATERAL GUST LOADS IN DESIGN OF THE L-1011 TRANSPORT

by

Frederic M. Hoblit

SUMMARY

In the design of the L-1011 transport, the reduction of lateral gust loads, in continuous turbulence, due to the presence of a yaw damper was reflected in the limit design loads. The resulting load reduction was about 27 percent. In establishing the limit design loads, both the mission analysis and design envelope forms of continuous turbulence gust loads criteria were used. Account was taken, under both forms of criteria, of the fraction of time the damper might be inoperative. The effect of saturation of the damper at the limit-load level was also taken into account. This effect was determined by means of time-history analyses in which the input was a random gust velocity and the rudder angle limits (governed by available hinge moment) were included in the simulation.

INTRODUCTION

In the design of the L-1011, it was known from the start that this airplane, like virtually all other modern transports, would have a yaw damper. It was also known that in actual flight the gust loads — on the vertical tail — would be lower because of the damper. And it was decided, therefore, at an early stage of design to reflect this reduction in the limit design loads.

The purpose of this paper is to provide further background relative to this decision, to indicate how the presence of the damper influenced the procedures by which the design loads were obtained, and to comment briefly on what was learned from loads measurements in flight through turbulence.

For the purpose of gust loads determination, two mathematical idealizations of the atmospheric gust structure have been in wide use. The first is the discrete gust idealization, in which the gust structure is considered to consist of individual gusts of standard (usually one-minus-cosine) shape, variable gust length or gradient distance, and a maximum gust velocity independent of gust length. The other is the continuous turbulence idealization, in which a stationary Gaussian gust structure is assumed. Neither idealization even approaches describing accurately all atmospheric turbulence. But there seems to be a growing acceptance of the continuous turbulence idealization as being by far the more realistic for the purpose of predicting airplane loads at the limit or ultimate load level, as well as at lower load levels pertinent to structural fatigue. In the design of the L-1011, limit design gust loads were determined by application of continuous turbulence criteria. Static discrete gust loads were also obtained, but were at no point critical.

Under a continuous turbulence input, any lightly damped mode will tend to resonate, reaching an amplitude, relative to the input, perhaps many times that possible in response to a single pulse input of the same magnitude. For most transport airplanes, and especially swept-wing configurations at cruise altitude, the Dutch roll mode is such a mode. In the absence of effective damping action by means of either a yaw damper or the pilot, yaw oscillations of sufficient amplitude are developed so that the sideslip angle reached can be several times that associated with the lateral gust velocity directly. Great potential exists, therefore, for utilization of a yaw damper to reduce the lateral gust loads.

From the initial stages of design of the Lockheed L-1011 transport, provision was made for a yaw damper in order to assure good handling qualities. Use of a yaw damper for this purpose is, of course, characteristic of large swept-wing aircraft generally. But for the reason discussed above, a damper also results in a substantial reduction in the structural loads due to lateral gust encounter. Early in the design of the L-1011, it was decided to reflect this loads reduction in the limit design loads.

Care was taken in the development of the damper to assure its effectiveness from a loads reduction as well as a handling qualities standpoint. Initially a Dutch roll damping ratio of at least 0.30 was set as a design objective. It was found, however, that substantially higher values, up to 0.50 or more, could be achieved over most of the climb, cruise, and descent flight regimes. It was also found, contrary to earlier expectations, that these higher damping ratios provided a further reduction in loads. In addition, in establishing the damper authority, consideration was given to the need for the damper to remain effective at fairly high turbulence intensities.

AIRPLANE AND YAW DAMPER DESCRIPTION

The Lockheed L-1011 TriStar, in service since April 1972, is a wide-body three-engine turbo-fan commercial transport, designed for short to medium range operation. It is of high-subsonic swept-wing design with two of the three engines pylon-mounted beneath the wing and the third located internally in the extreme aft end of the fuselage. Normal passenger capacity is 256, with mixed six and eight abreast seating. Wing span is 155 ft and design takeoff gross weight is 430,000 lb.

The nominal area of the vertical tail is 550 square ft including the rudder. The rudder is hinged at 71 percent chord, and is capable of 30 degrees travel in either direction; its area is 129 square ft.

The rudder is fully powered, driven by a pair of dual tandem hydraulic actuators, supplied by three hydraulic systems. Of the four actuator units, two are supplied by one hydraulic system each, and two are supplied jointly by a third hydraulic system. At speeds less than 164 knots EAS, all three systems are active. At speeds in the range 164 — 260 knots, only system "C" is active,

resulting in a reduction of available hinge moment to 41 percent of that available at low speeds. At speeds above 260 knots, the available hinge moment is further reduced to 28 percent of the three-system low-speed value by means of pressure reduction through a pressure regulator. Separately, a rudder deflection limit of 8 degrees is imposed when the flaps are retracted and the speed exceeds 164 knots.

A servo valve control module is located close to the actuators. It accepts mechanical inputs from the pilot and electrical inputs from the SAS (stability augmentation system) and autopilot, from which it commands hydraulic flow to the actuators. The SAS input is the source of the yaw damper action. (The terms SAS and yaw damper will be used interchangeably throughout this paper). Pilot and SAS inputs act in series — that is, the rudder angle is the sum of the angles commanded by the pilot and the SAS. The autopilot which affects rudder motion in the automatic landing mode, includes SAS inputs as well as the landing maneuver inputs.

The yaw damper action provides a rudder angle, δ_r , that is essentially proportional to and in phase with the yaw velocity, $\dot{\psi}$. The exact characteristic is shown in Figure 1. This characteristic applies to flight with flaps retracted; with flaps extended, higher gains are used. The washout below the Dutch roll frequency is provided to improve the airplane handling under pilot control in turns. The dropoff above the Dutch roll frequency is provided in order to minimize the effect of the SAS on elastic mode response. It was found, incidentally, that the lateral gust loads were about 8 percent higher for the damper as defined by Figure 1 than for a damper defined simply by $\delta_r = 1.30 \dot{\psi}$.

GUST LOADS CRITERIA

The continuous-turbulence gust loads criteria to which the L-1011 was designed were basically as developed in Reference 1 and summarized in Reference 2. These criteria involve the combined use of mission analysis and design envelope approaches. For the L-1011, the mission analysis loads were generally the more severe, and the primary effort, therefore, involved use of that criterion.

Under the mission analysis criterion, a set of typical flight profiles is first established. The gust structure is assumed to be characterized by the Von Karman shape of power spectral density, with $L = 2500$ ft. The probability density of the rms gust velocity is defined in a form such that frequency of exceedance of each load quantity is given by the expression,

$$N(y) = N_0 \left[P_1 \exp \left(-\frac{y/\bar{A}}{b_1} \right) + P_2 \exp \left(-\frac{y/\bar{A}}{b_2} \right) \right] \tag{1}$$

In this expression, y can be any load quantity — for example, bending moment at a particular wing station. $N(y)$ is the number of exceedances of y per unit time. \bar{A} is the ratio of the rms value of y to the rms gust velocity, and N_0 is a characteristic frequency of y , obtained as the radius of gyration of the power spectral density of y about zero frequency. Both \bar{A} and N_0 are obtained by appropriate dynamic analysis. The constants P_1 , P_2 , b_1 , and b_2 are parameters defining the gust environment and are specified in Reference 1 as functions of altitude. Exceedances are calculated by means of the above equation for each mission segment and added to give a total for over-all operation of the airplane. For the vertical gust analysis, the above equation for $N(y)$ is modified to include the contribution of the one-g steady flight loads, so that the exceedances obtained are of net loads. Curves of $N(y)$ vs y are obtained in this way for shears, bending moments, and torsions at as many locations on the wing, fuselage, horizontal tail, and vertical tail as considered necessary. Each curve is then entered at a limit design frequency of exceedance of 2×10^{-5} cycles per hour to give the limit design value of the load.

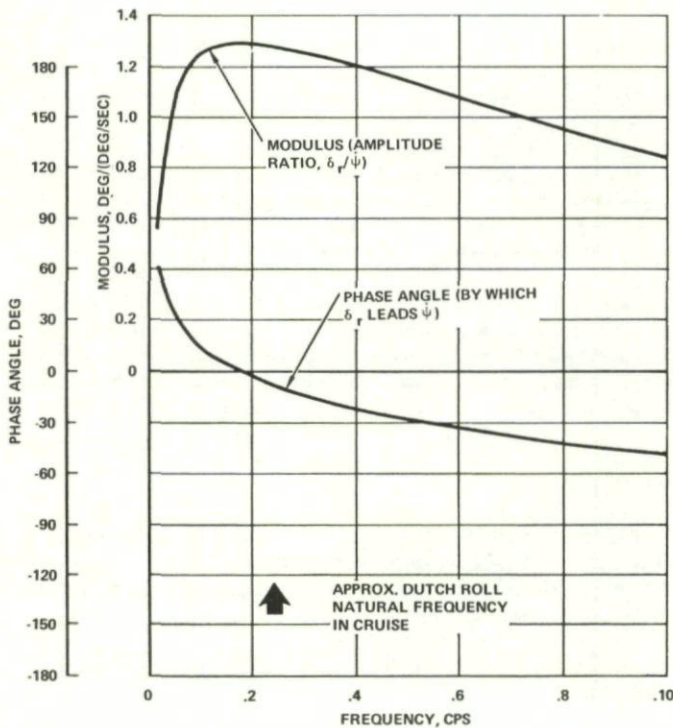


FIGURE 1. FREQUENCY-RESPONSE CHARACTERISTICS OF L-1011 YAW DAMPER

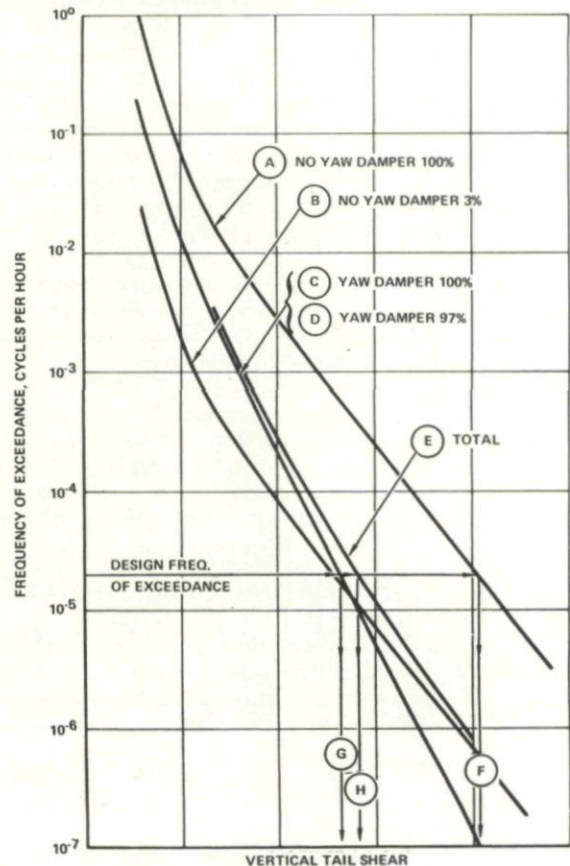


FIGURE 2. FREQUENCY OF EXCEEDANCE OF VERTICAL TAIL SHEAR WITH AND WITHOUT YAW DAMPER

Under the design envelope criterion, design is to the most critical points on the specified design envelope of speed, altitude, gross weight, fuel weight, zero-fuel weight, and CG position. In this respect, the criterion is similar to the past discrete gust criteria, as well as to limit design maneuver loads criteria. A quantity $\sigma_w \eta_d$, analogous to a design gust velocity, is specified as a function of altitude. In the expression $\sigma_w \eta_d$, σ_w is a design rms gust intensity and η_d is a factor representing the ratio of design load to rms load. The design load at any point is then given by multiplying $\sigma_w \eta_d$ by \bar{A} :

$$y_d = \sigma_w \eta_d = (\bar{A} \sigma_w) \eta_d = \bar{A} (\sigma_w \eta_d) \quad (2)$$

In applying these criteria to obtain design loads for the L-1011, \bar{A} and N_0 values were obtained by means of digital computer programs as described in Reference 2.

EFFECT OF YAW DAMPER — MISSION ANALYSIS CRITERION

Basic Approach; SAS Reliability

A key concern in any attempt to reduce limit design loads by accounting for the beneficial effects of a stability augmentation system is that the system will not be 100 percent reliable — i.e., it will not be in operation 100 percent of the time.

Under the mission analysis concept, the fraction of time that the system is inoperative can be accounted for easily and quantitatively.

Typical frequency-of-exceedance curves for a representative load quantity — fin shear at a location near the root — are shown in Figure 2. These curves were obtained by means of Eq (1) and represent the total exceedances contributed by all segments of all profiles. Curve A is obtained on the assumption of no yaw damper. The design load, under this assumption, would be as indicated by F on the figure. Curve C reflects the load reduction due to the presence of the yaw damper, under the assumption that the yaw damper is always operating. The design load with a fully reliable yaw damper would be as indicated by G on the figure.

In the development of the L-1011, early estimates indicated that the yaw damper might be inoperative as much as 3 percent of the time. The exceedances accumulated during that portion of the total flight time during which the SAS is not in operation are then given by 0.03 of Curve A; the result is Curve B, obtained by shifting Curve A down by a factor of 0.03. The exceedances accumulated during the 97 percent of flight time during which the SAS is operating are then given by shifting Curve C down in the ratio 0.97 to give Curve D. (Curves D and C differ imperceptibly and are shown by a single line.) The total exceedances are then given by the sum of Curves B and D, or Curve E. This is the curve from which the actual design load is obtained, indicated by H on the figure.

As the design of the airplane progressed, it became evident that the estimate of 3 percent for time inoperative was extremely conservative. The yaw damper system as finally defined is a two-channel system; there is no degradation of performance and no loss of authority upon single-channel failure. Further, to preclude the possibility that an airplane might be flown for a protracted period with a totally inactive yaw damper, certification provisions require that at least one channel be operative for dispatch. Utilizing guaranteed values of mean-time-until-removal of the various SAS elements, it was calculated that the average failure rate of the second channel, conservatively assuming the first channel never to be operative, would be 0.00086 per flight hour. Actual service experience to April 1973 showed reliabilities of the individual components that differed considerably from the specification values, but an over-all value that agreed very closely. With time, the reliability of the system should increase. On the basis of an average flight duration of 2 hours, with the loss of the SAS occurring — when it does — midway during the flight, it follows that the fraction of time SAS inoperative would be

$$.00086 \times 1/2 \times 2 = .086 \text{ percent}$$

As noted, even this estimate is conservative in that it ignores the likelihood that on most flights both SAS channels will be operative on takeoff. Normal maintenance practices of the airlines are such that, once a SAS channel becomes inoperative, the equipment will be replaced within a reasonable time, ordinarily two days at the most. Thus the value of 3 percent for time inoperative, used in defining the design loads, was found to be much higher than necessary. The effect on loads, however, of using a more realistic value — 0.1 percent or less — would not be great. Even with the fraction of time inoperative reduced to zero, the reduction in load would be only in the ratio G/H in Figure 2, or 7 percent. An increase in percent of time inoperative above 3 percent, however, would have a much more potent effect.

Saturation

A second concern is the saturation of the yaw damper at high load levels. The power-spectral analysis as ordinarily performed requires an assumption that the dynamic system is completely linear. In contrast, the angle to which the rudder can be moved by the SAS is subject to a well-defined limit governed by the hinge moment that is available from the hydraulic actuators. As a result, in turbulence of limit-load severity, the yaw damper may be less effective than indicated by the linear analysis.

In order to evaluate the effect on lateral gust loads of a rudder angle limit, time-history analyses were performed using an electric analog computer. The airplane simulation utilized the three rigid-airplane degrees of freedom of sideslip, yaw, and roll, and included the yaw damper. Provision was made for a rudder angle limit, which could be set at any desired value. The lateral gust input was provided by a white noise generator in conjunction with a filter to give approximately the desired shape of power spectral density.

Runs of 600 seconds duration were made, first with no rudder angle limit and then with various rudder angle limits. The important time history records were of rudder angle, δ_r , and side load on the vertical tail, P_y .

The flight condition represented was one for which the computer was already set up for handling-qualities studies. It was similar, but not identical, to the condition that predominated in defining the design frequency of exceedance curves.

The intensity of the lateral gust input could be rather arbitrary, inasmuch as the only significant nonlinearity was the limiting rudder angle, and the results would be interpreted on a non-dimensional basis. Nevertheless, it was desired to use a realistic gust intensity

in order to facilitate a complete understanding of the results. To determine an appropriate gust intensity, it was noted, first, that the design loads read from the exceedance curves, if expressed in the form of Eq (2),

$$Y_D = (\sigma_w \eta_d) \bar{A},$$

required a $\sigma_w \eta_d$ value of about 107. Here \bar{A} is the value calculated for the predominant mission segment. Actually the $\sigma_w \eta_d$ value thus obtained differs slightly from one load quantity to another, so that 107 is an average value. Assuming a peak-to-rms ratio, η_d , of 3.0, $\sigma_w = 107/3 = 36$ fps. Values of approximately this value, therefore, were used.

It may be remarked that for a given value of $\sigma_w \eta_d$, the "most likely" combination of σ_w and η_d can be determined by appropriate integrations of the joint probability density of the two statistically independent quantities, σ_w and η_d . The probability density of σ_w is available through its use in the derivation of Eq (1). Inasmuch as the second term in Eq (1) predominates, at the limit load level, this probability density is defined simply by means of the parameter b_2 . The probability density of η_d , or y/σ_y , is Gaussian. It is found that the "most likely" value of η_d is a function only of $\sigma_w \eta_d / b_2$. For the 28,000 ft altitude of the L-1011 predominant mission segment, b_2 is given by Reference 1 or Reference 2 as 11.8. For $\sigma_w \eta_d = 107$ and $b_2 = 11.8$, $\sigma_w \eta_d / b_2 = 107/11.8 = 9.1$. The resulting value of η_d is 2.95. This is approximately the same as the value 3.0 assumed above. For other values of $\sigma_w \eta_d / b_2$, values of η_d are: $\sigma_w \eta_d / b_2 = 5$, $\eta_d = 2.20$; $\sigma_w \eta_d / b_2 = 10$, $\eta_d = 3.10$; $\sigma_w \eta_d / b_2 = 15$, $\eta_d = 3.75$. These values are consistent with values that are readily obtained from data given in Reference 3, Figures 75 - 78 and Table 12. The existence of a "most likely" combination of σ_w and η_d is plausible. At high σ_w 's, the given $\sigma_w \eta_d$ is unlikely to be reached because the airplane is seldom in turbulence of that intensity. At low σ_w 's, requiring high η_d 's, the high η_d would seldom be reached even if the airplane were in turbulence of the given σ_w all the time.

A frequency-of-exceedance curve for rudder angle, obtained with no rudder-angle limit, is shown in Figure 3. This was obtained from the 600-second time-history record. The horizontal coordinate was taken as δ_r^2 instead of δ_r in order that Rice's equation for positive slope crossings at a given level (Reference 4, page 39) would plot as a straight line. It is seen that the value of δ_r expected to be reached once in the 600-second run is $\sqrt{14.3} = 3.78$ degrees.

Runs were then made with rudder angle limits of 2.40, 1.95, 1.50 and 1.05 degrees. Exceedance curves of vertical tail load were obtained for all five runs. Three of these are shown in Figure 4. It is seen that the value of tail load expected to be reached once in the 600-second run gradually increases as the available rudder angle is decreased.

The once-in-600-seconds value of P_y is then plotted vs. limiting rudder angle in Figure 5. In the non-dimensional form in which the data are plotted, it is expected that the curve would not change significantly with flight condition or even with modest changes to the yaw damper characteristic.

It might be remarked that entering Figures 3 and 4 at the once-in-600-seconds frequency of exceedance in obtaining the curve of Figure 5 is arbitrary. A more rational approach for establishing this frequency of exceedance would involve use of the most

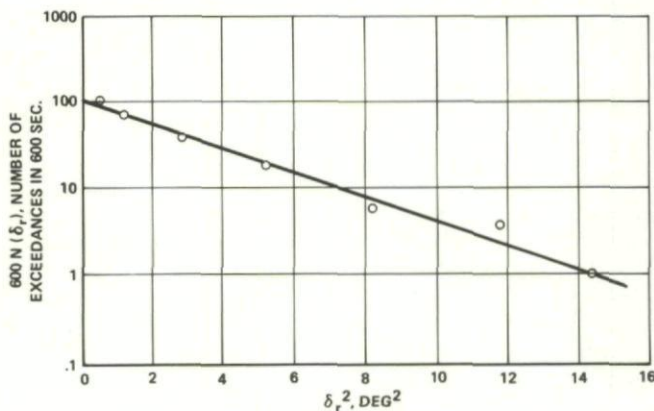


FIGURE 3. FREQUENCY OF EXCEEDANCE OF δ_r WITH NO AUTHORITY LIMIT, CONSTANT σ_w

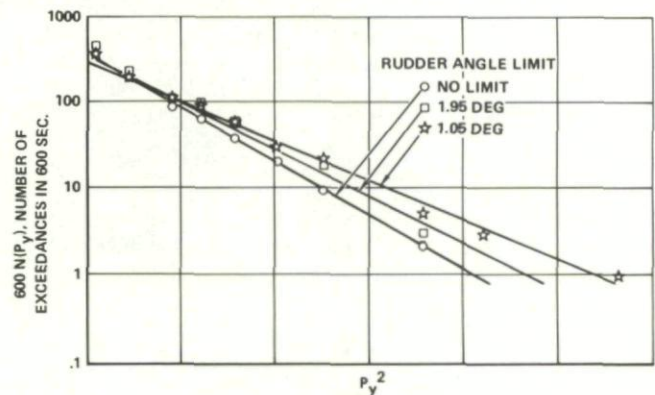


FIGURE 4. FREQUENCY OF EXCEEDANCE OF VERTICAL TAIL LOAD WITH VARIOUS AUTHORITY LIMITS, CONSTANT σ_w

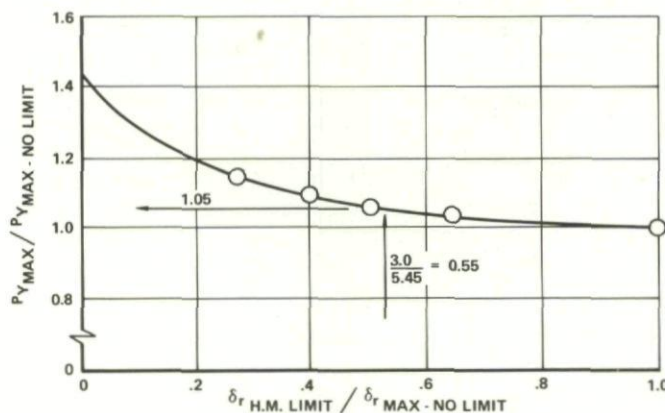


FIGURE 5. EFFECT OF RUDDER AUTHORITY LIMIT ON VERTICAL TAIL LOAD

probable value of η_d obtained as discussed earlier in this section. Substitution of this value of η_d , or γ/σ , into Rice's equation,

$$N(\gamma) = N_0 \exp \left[-1/2 \left(\frac{\gamma}{\sigma} \right)^2 \right],$$

then gives the frequency of exceedance. It is found that a better value is about 3 exceedances in 600 seconds, instead of one. The effect on the curve of Figure 5, however, has been found to be negligible.

The frequency of exceedance curves for δ_r obtained in the design loads analysis indicated a value at the limit-load frequency of exceedance of 5.45 degrees. For the predominant mission segment, the rudder angle that can be reached with the available hinge moment is 3.0 degrees. (For other segments, the value generally is close to this.) Entering the curve of Figure 5 at a value on the horizontal scale of $3.0/5.45 = 0.55$, one finds the increase in tail loads due to saturation to be 5 percent.

All lateral gust loads were increased by this percentage. The percentage increase in loads elsewhere than on the vertical tail should generally be less than this. For the vertical tail, the response is almost purely static. For other parts of the airplane, however — in particular for the fuselage in side bending — elastic mode dynamic response is substantial. But the yaw damper is designed to have negligible effect on the dynamic response at elastic-mode frequencies. With saturation increasing the static contribution 5 percent but not affecting the dynamic response, the total load will increase by some amount between 0 and 5 percent. Thus the treatment of saturation for loads other than on the vertical tail was slightly conservative.

In view of the care that was taken to input a realistic limit-design lateral gust intensity, one might have expected closer agreement between the maximum rudder angle recorded in the analog runs (3.78 degrees) and obtained from the exceedance curves (5.45 degrees). Part of the difference may be due to the use of a slightly different flight condition in the analog work. The primary source of the difference, however, appears to be an increase in the yaw damper gain reflected in the design frequency of exceedance curves but not in the analog runs, which were made much earlier.

Load Reduction Achieved

From Figure 2, it is seen that a fully reliable linear yaw damper would have reduced the design loads in the ratio $G/F = 0.65$. As a result of assuming the yaw damper to be inoperative 3 percent of the time, the reduction is seen to be less — $H/F = 0.70$. Increasing the loads 5 percent to account for saturation of the yaw damper results in an actual reduction in the ratio $(1.05)(0.70) = 0.73$.

FLIGHT LOADS MEASUREMENTS

As part of the L-1011 flight test program, an extensive set of flight and ground loads measurements was made. This program is summarized in Reference 5. Included in the tests was flight through continuous turbulence, with the gust velocities measured by means of a probe mounted on a boom 23 ft ahead of the nose. Sixteen samples of turbulence were obtained, varying from 1 to 5 minutes in duration. These samples totaled 5 minutes at an altitude of 30,000 ft, representative of normal cruise, and 30 minutes at about 5,000 ft. Flight was included both with and without SAS, and over a range of speeds and fuel weights.

It is of interest to note the load reduction obtained by use of the SAS and to compare this with the theoretical indications.

First, as a matter of background, flight-measured and theoretical power-spectral densities of fin shear are shown in Figure 6. Only the frequency range from 0 to 0.6 cps is included, inasmuch as the fin response at the higher frequencies, including elastic mode resonances, is virtually nonexistent. The theoretical psd's were obtained in the usual way, multiplying the Van Karman gust spectrum by the square of the modulus of the theoretical frequency-response function. The test psd's were obtained similarly, except that the frequency-response function was determined from the test data by means of the cross-spectrum method (Reference 6).

The Dutch roll peak is seen to occur at about 0.2 cps. The vast difference in sharpness of peak, for the SAS-off cases, between the test and theoretical curves is due largely to the smearing effect of the numerical procedures used in determining the test psd's. (The smearing effect is roughly equivalent to that given by a weighting function having the shape of an isosceles triangle with base equal to 0.20 cps.)

\bar{A} values for fin shear are compared in Figure 7. These were obtained by integrating the respective psd's.

The results shown in Figure 7 are seen to be similar for the two flight conditions. With SAS on, the test and theoretical values agree very well. (From the standpoint of structural adequacy of the L-1011, the small amount by which the test values exceed the theoretical was more than offset by conservatism in other aspects of the analysis.) With SAS off, both test and theory show a load increase relative to the SAS-on value; but the test data show this increase to be substantially less than indicated by theory.

The substantial difference between test and theory SAS-off is believed to be due, in large part, to the tendency of the pilot to act as a yaw damper. Thus the test \bar{A} SAS-off (pilot as yaw damper) is intermediate between the SAS-on \bar{A} (test or theory) and the no-SAS-at-all \bar{A} (as indicated by theory). This view is supported by the measured coherencies (defined as in Reference 6) between rudder angle and lateral gust velocity. These are shown in Figure 8. With SAS on, the coherency is generally fairly close to unity, especially in the key frequency range from 0.1 to 0.4 cps. This is expected, inasmuch as the rudder angle is linearly related in a simple way to ψ , which in turn is produced primarily (although not exclusively) by the lateral gust velocity. But even with SAS off the coherency is seen to be substantial. Thus it is seen that the rudder motion is, to a substantial degree, linearly related to the lateral gust input. The pilot clearly is doing something directly in response to the gusts; and it is likely that when the frequencies are as low as 0.20 cps he can be a fairly effective yaw damper. Further, rudder angle rms values SAS-off are found to be about 40 percent of the SAS-on values in the high altitude cases and 60 percent in the low altitude cases. Thus a potential for substantial damping action is indicated.

In view of the apparent effectiveness of the pilot as a yaw damper, the question arises whether it might not be appropriate to reflect this damping in the limit design loads, in the event a yaw damper either is not provided or, if provided, is inadequate in either reliability or saturation characteristics. Indeed, it would appear that the adequacy of some existing aircraft is due in part to the additional damping provided by the pilot. Reference 1, for example, notes that two of the existing successful airplanes analyzed would not meet the gust loads criteria recommended, with respect to lateral gust loads, unless such additional damping were considered. On the other hand, it would appear difficult to establish quantitatively the damping increment that could safely be attributed to the pilot. The pilot's

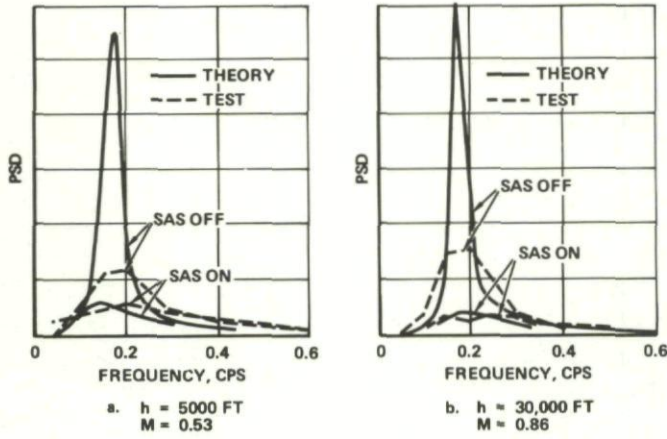


FIGURE 6. COMPARISON OF THEORETICAL WITH MEASURED POWER-SPECTRAL DENSITIES OF VERTICAL TAIL SHEAR

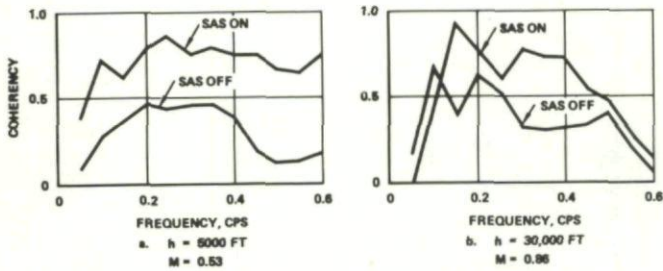


FIGURE 8. COHERENCIES BETWEEN RUDDER ANGLE AND LATERAL GUST VELOCITY, SAS-ON AND SAS-OFF

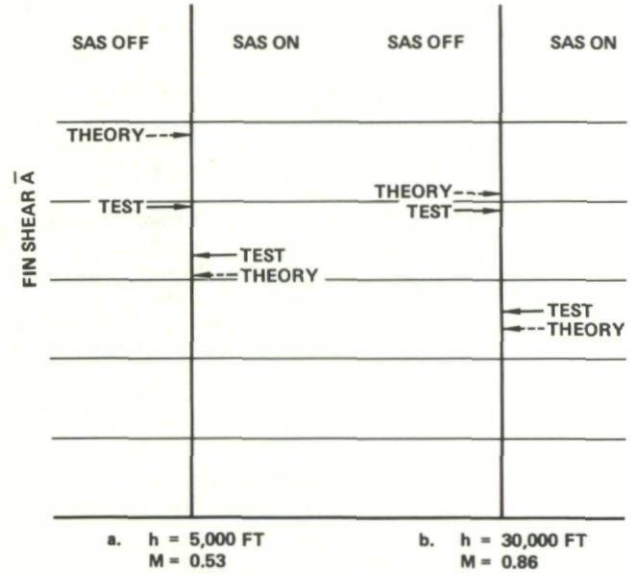


FIGURE 7. EFFECT OF SAS ON \bar{A} FOR VERTICAL TAIL SHEAR - COMPARISON OF THEORY AND TEST

effectiveness can be expected to vary from day to day and from pilot to pilot. His reliability and especially his saturation characteristics would be difficult to establish. It would appear preferable by far, in view of the widespread use of yaw dampers in modern airplanes, to assure that the damper is designed to be adequate from a loads standpoint. The design loads can then reflect not estimates but quantitative, substantiable data.

EFFECT OF YAW DAMPER - DESIGN ENVELOPE CRITERION

Under the design envelope criterion, as under the mission analysis criterion, it is necessary to account quantitatively for the fraction of time that the yaw damper may be inoperative.

Figure 9 shows the variation with altitude of the design gust velocity, $\sigma_w \eta_d$, at various levels of severity. Each curve of the family represents a constant frequency of exceedance as measured by $N(y)/N_0$. When using the design envelope criterion in combination with the mission analysis criterion, the recommended level of severity corresponds to $N(y)/N_0 = 1.2 \times 10^{-6}$. The corresponding curve in Figure 9 is one of the two indicated by heavy short-dash lines. At $h = 7000$ ft, the design $\sigma_w \eta_d$ is seen to be 62 fps.

To account for the presence of the yaw damper, separate $\sigma_w \eta_d$ values for the SAS-on and SAS-off cases are needed. These are obtained by arbitrarily allocating the allowable exceedances between SAS-on and SAS-off operation. This involves selecting any combination of $N(y)/N_0$ values SAS-on and SAS-off such as to satisfy the equation,

$$P \left(\frac{N(y)}{N_0} \right)_{\text{SAS-off}} + (1 - P) \left(\frac{N(y)}{N_0} \right)_{\text{SAS-on}} = \left(\frac{N(y)}{N_0} \right)_{\text{basic value}} \quad (3)$$

↑ Fraction of time SAS-off
 ↑ Fraction of time SAS-on

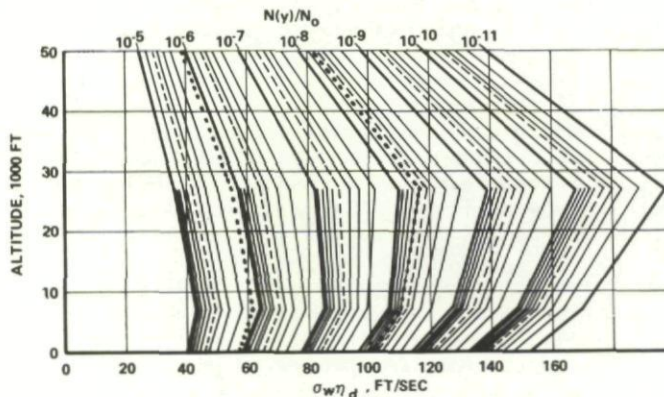


FIGURE 9. DESIGN VALUES OF $\sigma_w \eta_d$ AT SPEED V_c

The corresponding $\sigma_w \eta_d$ values SAS-on and SAS-off are then read from the curves of Figure 9 for the two $N(y)/N_0$ values selected. Any combination of values satisfying Eq (3) will assure adequate loads; the particular combination of values selected, however, should be such as to give the lowest loads. To find this combination will call for a trial-and-error, iterative, or similar approach.

For the L-1011, a potentially critical flight condition occurred at design cruise speed at $h = 7000$ ft. \bar{A} values for vertical tail shear at a particular fin station for this condition were

SAS-on	414 lb/fps
SAS-off	640 lb/fps

As noted earlier, the SAS was conservatively considered to be inoperative 3 percent of the time.

If the design $N(y)/N_0$ of 1.2×10^{-6} were allocated equally to SAS-on and SAS-off operation, the two $\sigma_w \eta_d$ values would be obtained by use of Eq (3) as follows:

$$\begin{array}{rcl}
 .60 \times 10^{-6} & + & .60 \times 10^{-6} & = & 1.20 \times 10^{-6} \\
 (.03) (20 \times 10^{-6}) & + & (.97) (.618 \times 10^{-6}) & = & 1.20 \times 10^{-6} \\
 \sigma_w \eta_d \downarrow = 36 & & \sigma_w \eta_d \downarrow = 68 & & \sigma_w \eta_d \downarrow = 62 \\
 \bar{A} (\sigma_w \eta_d) = 640 \times 36 & & \bar{A} (\sigma_w \eta_d) = 414 \times 68 & & \\
 = 23,000 \text{ lb} & & = 28,100 \text{ lb} & & \\
 \text{(With fully reliable SAS, } \bar{A} (\sigma_w \eta_d) = 414 \times 62 = 25,600 \text{ lb)} & & & &
 \end{array}$$

On the second line, the factors .03 and .97 are the p and $(1 - p)$ values. The quantities that these factors multiply are $N(y)/N_0$ values such as to give the products appearing on the first line. The $\sigma_w \eta_d$ values on the third line were read from Figure 9 for these $N(y)/N_0$ values.

The design load would be the higher of the two $\bar{A} (\sigma_w \eta_d)$ values, 23,000 lb and 28,100 lb. It is seen that, for SAS-off operation, the $\sigma_w \eta_d$ value of 36 fps is much lower than the basic design value of 62 fps. But the $\sigma_w \eta_d$ value for SAS-on operation must be somewhat higher than 62 fps, in order to "make room" for the exceedances contributed by SAS-off operation.

The equal allocation of exceedances between SAS-on and SAS-off operation is seen to result in different design loads for the two cases. To equalize these two loads and thus minimize the higher of the two, the allocation will be changed. Noting that the design load will be less than 28,000 lb, but greater than 25,600 lb, say 27,000 lb, $\sigma_w \eta_d$ for SAS-off can be increased to about $(27,000/23,000) 36 = 42$. The corresponding $N(y)/N_0$, from Figure 9, is about 12×10^{-6} . The allocation then becomes,

$$\begin{array}{rcl}
 .36 \times 10^{-6} & + & .84 \times 10^{-6} & = & 1.20 \times 10^{-6} \\
 (.03) (12 \times 10^{-6}) & + & (.97) (.87 \times 10^{-6}) & = & 1.20 \times 10^{-6} \\
 \sigma_w \eta_d \downarrow = 41.5 & & \sigma_w \eta_d \downarrow = 64.5 & & \sigma_w \eta_d \downarrow = 62 \\
 \bar{A} (\sigma_w \eta_d) = 640 \times 41.5 & & \bar{A} (\sigma_w \eta_d) = 414 \times 64.5 & & \\
 = 26,600 \text{ lb} & & = 26,700 \text{ lb} & &
 \end{array}$$

The design load is thus found to be 26,700 lb, about 4 percent higher than the 25,600 lb value that would be obtained with a 100 percent reliable SAS.

The reduction in load achieved by use of the yaw damper is in the ratio $(1.05)(41.5)/(62) = .70$, where the 1.05 factor accounts for the load increase due to SAS saturation. This .70 factor is comparable to the .73 factor attained under the mission analysis criterion.

CONCLUDING REMARKS

From the experience gained in the design and flight testing of the L-1011, it is evident that:

1. For an airplane of this type, the presence of a yaw damper can substantially reduce the lateral-gust-induced loads that the airplane experiences in flight.
2. This reduction can be reflected, rationally and safely, in the limit loads to which the structure is designed.

REFERENCES

1. Hoblit, F.M., Paul, N., Shelton, J.D., and Ashford, F.E., "Development of a Power-Spectral Gust Design Procedure for Civil Aircraft," FAA-ADS-53, Washington, D.C., Federal Aviation Agency, Jan. 1966.
2. Stauffer, W.A., and Hoblit, F.M., "Dynamic Gust, Landing, and Taxi Loads Determination in Design of the L-1011," Journal of Aircraft, Vol. 10, No. 8, Aug. 1973.
3. Fuller, J.R., Richmond, L.D., Larkins, C.D., and Russell, S.W., "Contributions to the Development of a Power-Spectral Gust Design Procedure for Civil Aircraft," FAA-ADS-54, Washington, D.C., Federal Aviation Agency, Jan. 1966.
4. Houbolt, J.C., Steiner, R., and Pratt, K.G., "Dynamic Response of Airplanes to Atmospheric Turbulence Including Flight Data on Input and Response," TR R-199, Washington, D.C., NASA, June 1964.
5. Stauffer, W.A., Lewolt, J.G., and Hoblit, F.M., "Application of Advanced Methods to Design Loads Determination for the L-1011 Transport," Journal of Aircraft, Vol. 10, No. 8, Aug. 1973.
6. Coleman, T.L., Press, H., and Meadows, M.T., "An Evaluation of Effects of Flexibility on Wing Strains in Rough Air for a large Swept-Wing Airplane by Means of Experimentally Determined Frequency-Response Functions with an Assessment of Random-Process Techniques Employed," TR R-70, Washington, D.C., NASA, 1960.

THE EFFECT OF ACTIVE CONTROL SYSTEMS ON
STRUCTURAL DESIGN CRITERIA

by

N.F.Harpur

British Aircraft Corporation Ltd
Commercial Aircraft Division, P.O. Box 77
Filton, Bristol BS99 7AR, UK

THE EFFECT OF ACTIVE CONTROL SYSTEMS ON STRUCTURAL DESIGN CRITERIA

N.F.Harpur

1. INTRODUCTION

Interest in the use of active control systems is increasing and they are being considered not only to improve stability but also structural efficiency. This greater interest is in a large measure due to the improved reliability of the necessary electronic systems and also to their considerably reduced weight and bulk. This makes it possible nowadays to envisage quite complex control system requirements and to ensure very high integrity (by duplication, triplication, etc.) without using unduly large equipment.

Active control systems, for the purpose at least of this paper, may be defined as systems which operate any or all of the controls on the aircraft (including flying controls, flaps, spoilers, throttles, etc.) to some degree independently of the action of the pilot.

They can be used for

- (a) improving aircraft stability thus enabling the size of the fixed and moveable control surfaces to be reduced,
- (b) reducing the static design loads (manoeuvres, gusts, etc.),
- (c) reducing the fatigue design loads,
- (d) increasing flutter speeds thus reducing the additional stiffness or mass which might otherwise be required,
- (e) reducing the margin required between normal operating speed and design diving speed due to upsets, entry into wind shears, temperature gradients, etc.,
- (f) improving the ride comfort and reducing vibration effects on stores, for example.

It is not intended to discuss here the structural weight savings which will obviously accrue from (a) above, nor the criteria which will determine whether (f) is worthwhile since these must be closely associated with the role of the aircraft.

However (b) to (e) can all significantly affect the structural design criteria. The extent to which weight can be saved depends on the particular aircraft but it is probable that the weight savings will be limited unless a number of the objectives (b) to (e) can be achieved simultaneously. There is little point in reducing structural scantlings in static design cases unless the fatigue loads can also be reduced and the resulting more flexible structure made flutter free.

The active control system is therefore likely to be quite complex and consideration must be given to the consequences of failures in the system when deciding by just how much the structure weight may be safely reduced.

Each of the objectives (b) to (e) will be considered separately. The discussion is confined to fixed wing aircraft since it appears that active control systems in helicopters will be largely limited to objective (a) and (f) above. The paper refers mainly to civil aircraft and their airworthiness requirements, chiefly because of the author's greater familiarity with this field, but the principles are equally applicable to military aircraft.

2. REDUCTION OF STATIC DESIGN LOADS

2.1 Manoeuvre Loads

Autostabilisers have been in use for many years but their prime objective has been to improve the stability or control of the aircraft and normally the lifting surfaces of the aircraft have been sized on the basis that a minimum degree of controlability is retained in the event of autostabiliser failure. As far as the structure was concerned the main concern was to ensure safety in the event of system malfunction (e.g. a runaway) and the structural design criteria were based on the most severe cases arising from either operative, inoperative or malfunctioning autostabilisers. Such devices are now being envisaged as means of directly reducing structural loads.

Autostabilisers operate by sensing a rate of rotation signal (yaw, roll, pitch) and moving the appropriate control surface. A typical example is the yaw autostabiliser or damper. Figure 1 shows the variation of fin load with altitude, with yaw autostabiliser both operative and also inoperative, on the BAC/AS Concorde. The fin load plotted is that arising from the specified pilot induced manoeuvre at design cruising speed V_C i.e. application of maximum rudder except as limited by pedal force, servo-control power etc.^{1,2}.

The variation with altitude is complex due to the considerable variation of V_C with altitude (and hence Mach number) on this aircraft. Figure 2 shows the side-slip, rudder angle and consequent load variation with time.

It will be seen that the effect of the autostabiliser is to reduce the peak loads by about 20%. This was achieved even though the autostabiliser had limited authority ($\pm 3^\circ$), since it was designed primarily to meet stability and control requirements.

No reduction is seen at altitudes above 30,000 ft because, at this altitude and above, the rudder servo-control jacks become saturated during the manoeuvre and the autostabiliser is obviously ineffective.

An additional requirement which has to be considered is one where the pilot induces yaw by a sinusoidal operation of the rudder control at a frequency such that the maximum lateral response of the aircraft is induced. Usually only one or two complete cycles are required to be considered and the peak fin loads do not, of course, occur in phase with the achievement of peak rudder angle. In these cases the autostabiliser may well prove effective in reducing loads even if the demanded rudder angle is so large that the servo-control jacks will stall at periods during the cycle. Figure 3 shows significant reduction in fin load on the Concorde with autostabiliser operative even when the peak demand rudder angle is in excess of the sum of the stall angle plus autostabiliser authority (about 20°).

To realise such load reductions requires that the airworthiness authorities accept that a reduced severity loading case may be assumed when the autostabiliser is inoperative; otherwise the inoperative case would always produce the critical design loads. The concept of reducing safety factors or the severity of the loading cases for combinations of flight conditions which can be shown to be rare, has been accepted in principle for some time. A typical example is the reduction of gust and manoeuvre load levels prescribed for flight with landing flaps extended where (except in cases where these flaps are used en-route as well as on take-off or landing) the design gust intensity for example is reduced from 50 ft/sec to 25 ft/sec as a crude basis of assessing the combined probability of gust encounter and flap position³. It is obviously a relatively small step to include, under aircraft condition, the probability of autostabiliser failure.

Perhaps the closest analogy lies in the requirements for fail-safe evaluation of structures⁴. Here it is accepted that safety will be ensured if, after a failure or partial failure of a single principal structural element, the structure remains capable of carrying a reduced load, typically between 53% and 67% of the design ultimate load. Again this is a rough and ready way of assessing the combined probability of the structural failure and of the applied load condition.

It would seem reasonable therefore to associate the autostabiliser inoperative conditions with a reduced severity loading case. A simple approach would be to take autostabiliser failure as being equivalent to the structural failure in a fail-safe evaluation and require, say, an ultimate factor of 1.0 on limit loads i.e. reducing the strength requirement to 67%. However this would imply the assumption that the frequency of autostabiliser failures was roughly the same as that of structural failures.

Nowadays it is possible to assess system reliability with a fair degree of confidence and a more quantitative approach might be considered.

Assessment of the overall probability of the event occurring, i.e. the combination of the loading case and the system failure, requires a knowledge of the probability of the loading case. Acceptance of a figure for the overall probability of structural failure, taking all loading cases and parts of the structure into consideration, would be required before an acceptable probability could be established for each such event. It would involve replacing all the existing structural safety criteria with a single statement such as "the probability of structural failure from any cause shall be less than 10^{-12} per hour". Such a statement, while quite logical, is not very practical when it comes to demonstration of compliance, although it must be admitted that some requirements are already heading part way down this road e.g. the power spectral gust criteria, referred to later.

An alternative is simply to consider the probability of the system failure and permit a reduction in ultimate strength as a function of this probability (i.e. analogous to the fail-safe rules) taking no quantitative account of the probability of the design case occurring. A compromise is suggested here by the author, which is to take some note of the greater proportion of flight time spent within the normal speed envelope i.e. up to design cruising speed V_C/M_C and the very much smaller time spent outside this envelope i.e. up to design diving speed V_D/M_D . The suggestion is that the loads be calculated assuming the device has failed and then these loads be reduced according to the failure probability of the device and the design speed associated with the loading case as indicated in Figure 4. This implies that:

- if the device has a failure probability of 10^{-3} /hr or worse, the full strength must be achieved for the failed case at both V_C and V_D .
- if the device has a failure probability of 10^{-7} /hr, the full strength must still be achieved at V_C but this may be reduced to 67% of full strength at V_D .
- if the device has a failure probability of 10^{-11} /hr or better, the strength to be achieved is 67% of the loads derived from the device failed case at both V_C and V_D .

The adoption generally of such an approach would leave the way clear to utilising systems of proven reliability to reduce structural loads by up to $\frac{1}{3}$. For example in the case illustrated in Figure 1 the design loads (which occur at V_C) would be

autostabiliser operative	—	$62,000 \times 1.5 = 93,000$ lb
autostabiliser inoperative (failure rate 10^{-11} per hour)	—	$78,000 \times 1.0 = 78,000$ lb
autostabiliser inoperative (failure rate 10^{-7} per hour)	—	$78,000 \times 1.5 = 117,000$ lb

Thus to achieve the maximum load reduction of 21% (i.e. $\frac{93,000 \text{ lb}}{117,000 \text{ lb}}$)

The autostabiliser inoperative ultimate factor should be less than 1.19 and using Figure 4 this would require a total system failure probabilities factor less than about 3×10^{-10} per hour of flight. With duplicated systems this is quite practicable.

Of course the reliability computation must take into account any possible operational considerations such as the desire to despatch the aircraft with part of the system failed. If it were intended that a duplicated system be regarded as a "go" item even in the event of failure of one channel, then the remaining channel must itself show a reliability close to that derived by the above method.

Manoeuvre loads can also be reduced by restricting the control movements of the pilot to the maximum which he needs to meet the handling requirements of the aircraft. This can be most conveniently done by means of an artificial feel system but this cannot truly be described as an active control system. However it is often difficult to restrict manoeuvres this way, particularly when these involve simultaneous use of more than one control e.g. in a rolling pull-out. Strike aircraft require a high rate of roll combined with high "g" but the resulting rolling power at low "g" can be excessive. Figure 5 indicates, for a modern strike aircraft, the variation of rolling power with "g" at high equivalent air speeds. Without use of active control systems, the low "g" rate of roll is over 8 times that at high "g". An active control system is installed which boosts the high "g" rate of roll, i.e. where it is needed, while limiting the rate of roll at low "g", thus cutting down the design loads, in this case mainly wing tank pressures, wing distributions and wing store loads. The controls are active in that, when full lateral stick is used, the rate of roll is sensed and the feedback system tries to maintain a constant rate of roll regardless of "g" i.e. a roll rate command system.

The extent to which the load alleviation at low "g" can be exploited depends on the reliability of the system. If the previously described criterion is adopted (see Figure 4) the maximum alleviation possible achieved with failure probabilities better than 10^{-11} /hr of flight, would be a $\frac{1}{3}$ reduction of load in design cases related to V_C .

2.2 Engine Failure Loads

Fin and rudder loads arising from engine failure cases may also be dealt with in the same way. Figure 6 shows the fin loads arising from single engine failures on the Concorde. In this case, in addition to the autostabiliser, an alleviation is obtained at Mach numbers greater than 1.4 by the use of an autorudder which applies rudder angle in response to a signal from a transducer sensing lateral acceleration. This figure shows also the adverse effect of corrective rudder applied by the pilot at or about peak sideslip. In this example the failure rates of the autostabiliser and autorudder systems should be combined with the chance of adverse pilot action, and also with the chance of an engine failure itself, to arrive at the overall probability of the event. However a conservative approach might be to ignore any adverse pilot corrective action, off-setting it against the low probability of engine failure, and to use just the combined system failure rates to derive a reduced ultimate factor based, say, on Figure 4. A critical design condition is that of 50,000 ft, associated with the higher structural temperature at Mach 2, and therefore the autostabiliser operative case becomes the design case with an ultimate load at V_C of $37,500 \times 1.5 = 56,250$ lb. For the inoperative case to give no greater loads it must have an ultimate factor less than $56,250 \text{ lb}/41,500 \text{ lb}$ i.e. 1.35.

Based on Figure 4 this would mean that the combined system failure rate must be better than 6.5×10^{-9} per hour of flight.

The autorudder system was installed primarily to limit yaw angles within the range acceptable for engine intake flow considerations and the reduction in structural loads might therefore be greater if the system were optimised for this objective as well.

2.3 Engine Surge Loads

The loads arising due to engine surge, or hammershock, can give critical design conditions for supersonic intakes and, to a lesser extent, for subsonic intakes. The surges can arise due to malfunctions of the engine or air-intake control systems, both of which can be complex in supersonic aircraft. They may also arise due to external perturbations, such as gusts and manoeuvres, which may affect the flow conditions at the engine face such as to induce surge. While the design of the intake and engine control systems will be such as to minimise the frequency of such surges, it is nevertheless necessary to design the intake structure and systems to meet the surge loads.

The peak surge pressure is a function of both airspeed and engine conditions. An example is given in Figure 7, which shows the peak engine-face surge pressures for the Concorde at Mach 2 as a function of calibrated airspeed (CAS) and low pressure compressor speed (N_1). There is little variation of the surge pressures with Mach number which affects primarily the probability of surge occurring. The intake strength is sized on the loads occurring at V_C , 530 knots at cruise altitudes. In order both to reduce the chances of surges occurring and also to limit their peak pressures a device has been installed which reduces the engine compressor speed in the event of the airspeed increasing beyond V_C towards V_D . The speed increments above V_C , due to upset manoeuvres, sudden temperature changes or wind shears, are themselves reduced by the consequent reduction in engine thrust.

Failure of the device would result in loads at V_D (565 knots) some 14% higher than those at V_C and an ultimate factor of not more than 1.30 would be required to ensure that the failed case did not design. Again using the criterion of Section 2.1 (Fig.4) the maximum failure probability permissible is 2.5×10^{-5} /hr. A system reliability of this order is practical.

2.4 Gust Loads

2.4.1 Discrete Gusts

Possibly the first attempt to alleviate the loads arising in discrete gust encounters was made in the design of the Bristol Brabazon long-range transport which first flew in 1949. This aircraft, with a predicted all-up weight of 330,000 lb in the production version, was obviously structure weight sensitive. A gust alleviation system was therefore designed to reduce wing bending loads by operating the ailerons symmetrically in response to signals from a gust vane mounted on the nose of the aircraft. Such faith was placed in the practicability of this system, that the wing structure of the prototype was some 20% weaker than would have been required to meet the design gust cases without gust alleviation. The gust alleviation system was not proved in flight before the aircraft was scrapped in 1953, although the response of the vane to turbulence had been measured. A complete system had, however, been flown in an Avro Lancaster⁵ in 1952 and some problems had arisen. The main one was that the large pitching moment contributed by the ailerons resulted in a considerable loss of stability such that at large gust gradient distances the alleviator effectiveness decreased.

Furthermore it is obvious that, in the limited flying time available (57 hours), it was not possible to find really severe turbulence although sufficient had been found to indicate non-linearity in alleviation with gust magnitude.

This illustrates a major problem with the use of an active control system for alleviating the large static design gusts i.e. the difficulty of demonstrating that it works. Assuming that a device can be engineered to cope with the very high response rates required to cope with the large limit gust velocities (e.g. 50 ft/sec), the behaviour of the whole system, and in particular that of the power operated controls, should be checked under these limit gust conditions and these, by definition, will be almost impossible to find. Assumption of extrapolation from lower level gusts may be difficult to justify.

The failure cases may be dealt with as indicated in Section 2.1 and the criteria suggested in Figure 4 would be equally appropriate to the gust cases.

2.4.2 Continuous Turbulence

Power spectral gust criteria have been under discussion between the FAA, the European civil airworthiness authorities and the aircraft manufacturers for some time. A proposal for a standard was put forward by FAA for the SST and is, in fact, a special condition on Concorde⁶. In the "mission analysis" approach the overall frequency of exceedance of load levels is determined taking into account the combinations of flight conditions (e.g. speed, altitude, payload, etc.) with turbulence intensities. The strength level is set by that load which will have a frequency of exceedance of 2×10^{-5} per hour. Active control systems are specifically referred to, viz:—

"If a stability augmentation system is utilized to reduce the gust loads, consideration must be given to the fraction of flight time that the system may be inoperative."

With the order of system failure probabilities which can nowadays be assumed e.g. 1×10^{-7} per hour or better, it is clear that consideration of system failures will have virtually no effect on the strengths required to meet the power spectral gust criteria.

This is simply because the probability of system failure is being combined with the probability of requiring the system to operate (i.e. of encountering the maximum load level). This is a much less severe criteria than that considered in previous paragraphs where a certain minimum strength level has been envisaged as a function of system failure probability alone, regardless of how infrequent the critical design loading conditions may be (except for some consideration of the low probability of being at V_D , for example).

The whole idea of the "mission analysis" while certainly being logically based, is not consistent with the past practice of defining a series of static strength cases which must be satisfied regardless of the probability of their occurrence. For example previous rules required the large discrete gust of 50 ft/sec velocity to be withstood over the whole flight envelope bounded by the chosen design cruising speed V_C at all practical combinations of weight, altitude and centre of gravity. The critical combination may only occur for a very short period on each flight but nevertheless the required strength must be provided. It is for such reasons, and because of doubts about the validity of the linearising assumptions necessary, that the European Airworthiness authorities have so far declined to accept the power spectral approach, as a replacement of the discrete gust, for static strength cases. If and when this is done, it would be very easy to incorporate the effects of active controls and their failure probabilities.

3. REDUCTION OF FATIGUE DESIGN LOADS

In contrast to the remarks made in the previous section, it is certainly true that the power spectral approach may be used with confidence for assessing the affect of active control systems on the lower levels of gust and manoeuvre loads i.e. those of greatest significance in causing fatigue defects. Furthermore it is quite simple to carry out the necessary flight demonstrations. The effects of system failures may be taken into account on the same basis as indicated in Section 2.4.2, and are likely to be insignificant with the level of system reliabilities now possible.

4. IMPROVEMENT OF FLUTTER CHARACTERISTICS

In the form of autostabilisers, active control systems have been involved in flutter evaluations for some time. It is rare that they have ever been modified, let alone designed, with the object of improving the flutter behaviour. The main reason is that the operating frequency range of the autostabiliser is usually well below the critical flutter frequencies so that there was very little coupling.

However if active control systems are used to improve flutter behaviour the effect of a system failure must be considered.

This is already covered in the FAR standards⁷ which say

"It must be shown by analysis or tests, that the airplane is free from such flutter or divergence that would preclude safe flight, at any speed up to V_D , after any other reasonably probable single failure, malfunction, or adverse condition affecting flutter or divergence."

This is a reduction in standard from the non-failed case where flutter freedom must be shown in principle up to $1.20 V_D$.

This rule can be used for active control system failures. It is suggested that a system failure probability not worse than $10^{-5}/\text{hr}$ is required so that the chance of a failure may be deemed no more than "reasonably probable".

5. REDUCTION OF SPEED MARGINS

A device can be envisaged which will sense increases above cruising speed, V_C , and operate the flying or engine controls in such a way as to return the aircraft to V_C . The autopilot normally does this via the flying controls. Autothrottles are often used to aid control on the approach and landing phase, where the aircraft is operating below the minimum drag speed, and it is not very difficult to contemplate using them on other flight regimes to control airspeed. A more sophisticated device has already been described under engine surge loads in Section 2.3. Since the critical static strength cases are often associated with design diving speed, V_D , and this is also critical for flutter, anything which can be done to reduce V_D in relation to a given cruise speed requirement will have all-round benefits.

In the case of flutter described in Section 4, a system failure probabilities factor of better than $10^{-5}/\text{hr}$ of flight was suggested as adequate. The same order of reliability should be adequate for the speed control device provided it is only called upon to operate on rare occasions. However, the more closely the device is called upon to control speed, the more often it will operate and then lower system failure rates will be required.

6. CONCLUDING REMARKS

This paper has suggested a number of ways in which the structural design criteria may be related to the design of active control systems. It seems desirable to look at all the varieties of active control systems in a consistent way and one such way has been suggested in this paper; it is not the only way and not necessarily the best. Airworthiness regulations, both civil and military, should be based on agreed policy, if the full benefits of active control systems are to be realised.

ACKNOWLEDGEMENT

The author is grateful for the assistance received from his colleagues in the UK but would emphasise that the views expressed in this paper are his own.

REFERENCES

1. — *TSS Standards for Concorde, Certification Authorities of Great Britain and France.* (TSS 4-3 Section 3.5.)
2. — *Federal Aviation Regulations, Part 25, Airworthiness Standards, Transport Category Airplanes, Federal Aviation Administration.* (Section 25.351(a).)
3. — *FAR Part 25.* (Section 25.345.)
4. — *FAR Part 25.* (Section 25.571(c).)
5. Zbrozek, J.
et al. *Preliminary Report on a Gust Alleviator Investigation on a Lancaster Aircraft.* Reports and Memoranda No.2972, August 1953.
6. — *Tentative Airworthiness Standards for Supersonic Transports.* Revision 7 (January 1971), Federal Aviation Administration (Section 25.305(e) and Appendix G).
7. — *FAR Part 25.* (Section 25.629(d).)

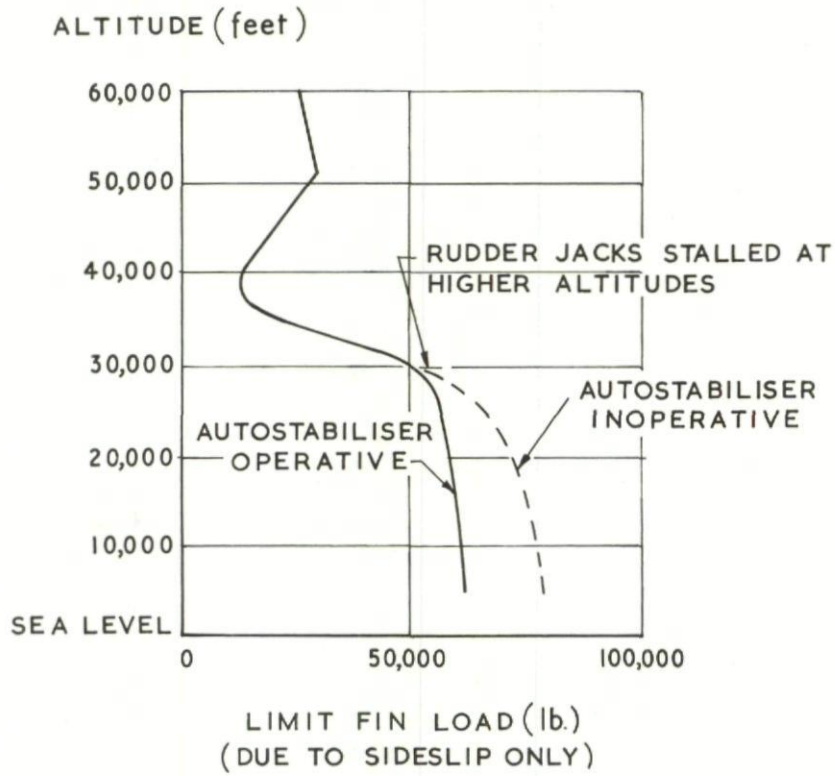


Fig.1 Fin loads from pilot induced yawing manoeuvres

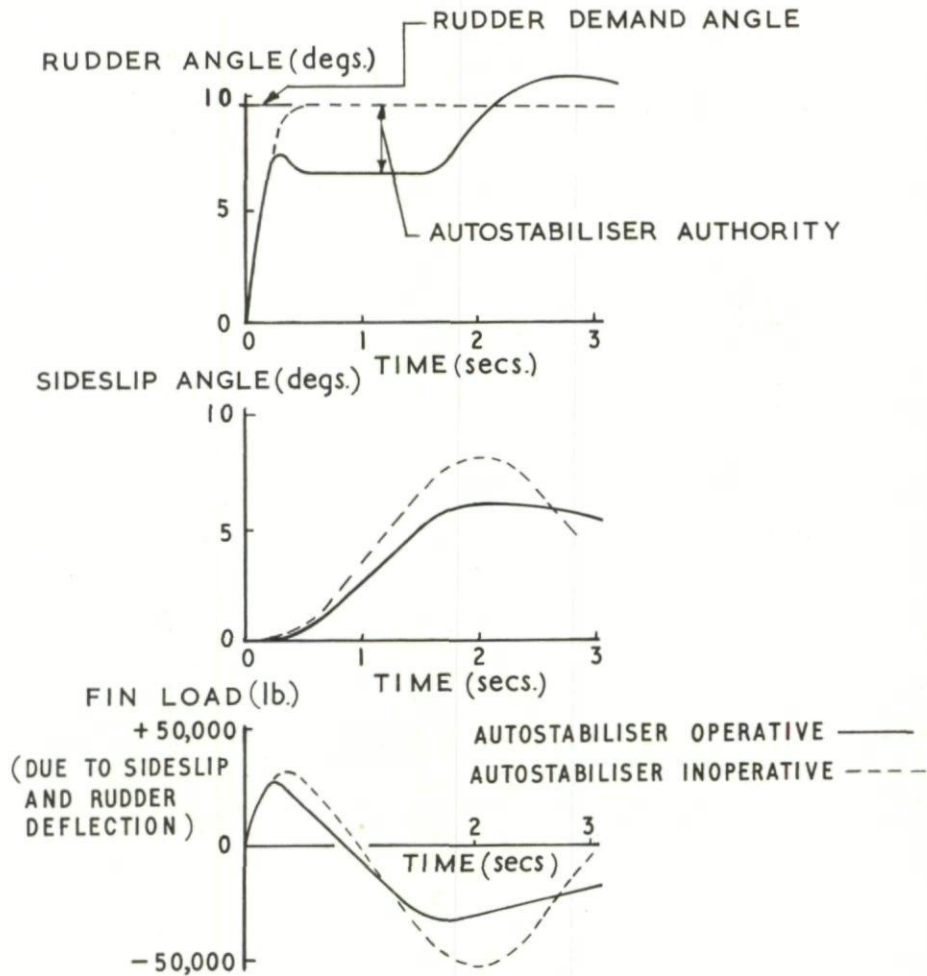


Fig.2 Responses during pilot induced yawing manoeuvres

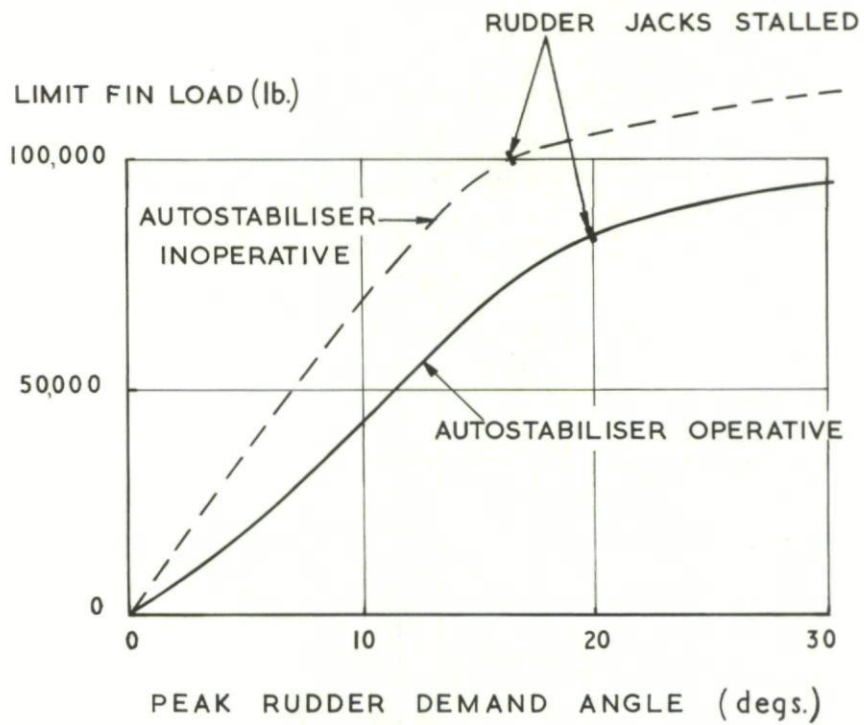


Fig.3 Fin loads from sinusoidal rudder application

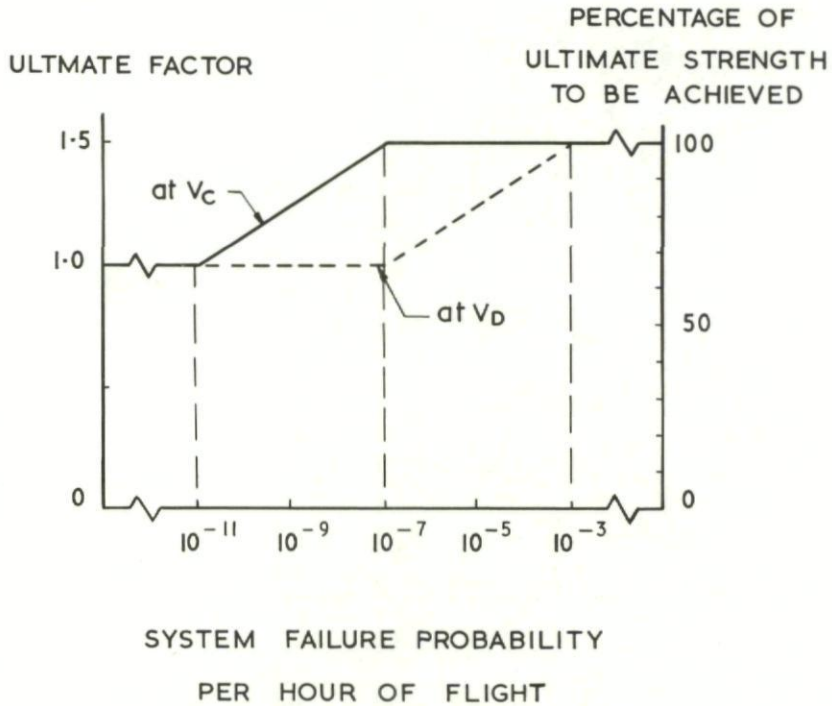


Fig.4 Relationship between system failure probability and choice of ultimate factor

RATE OF ROLL / CONTROL SURFACE ROTATION

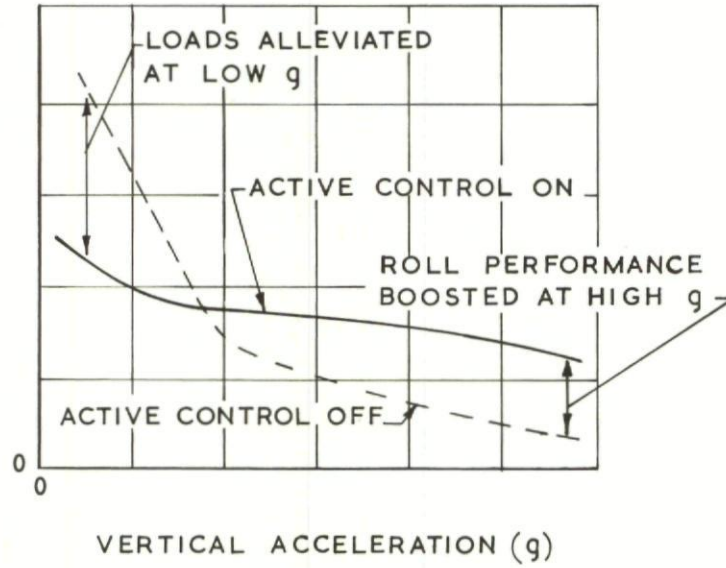


Fig.5 Strike aircraft rolling power with and without active control

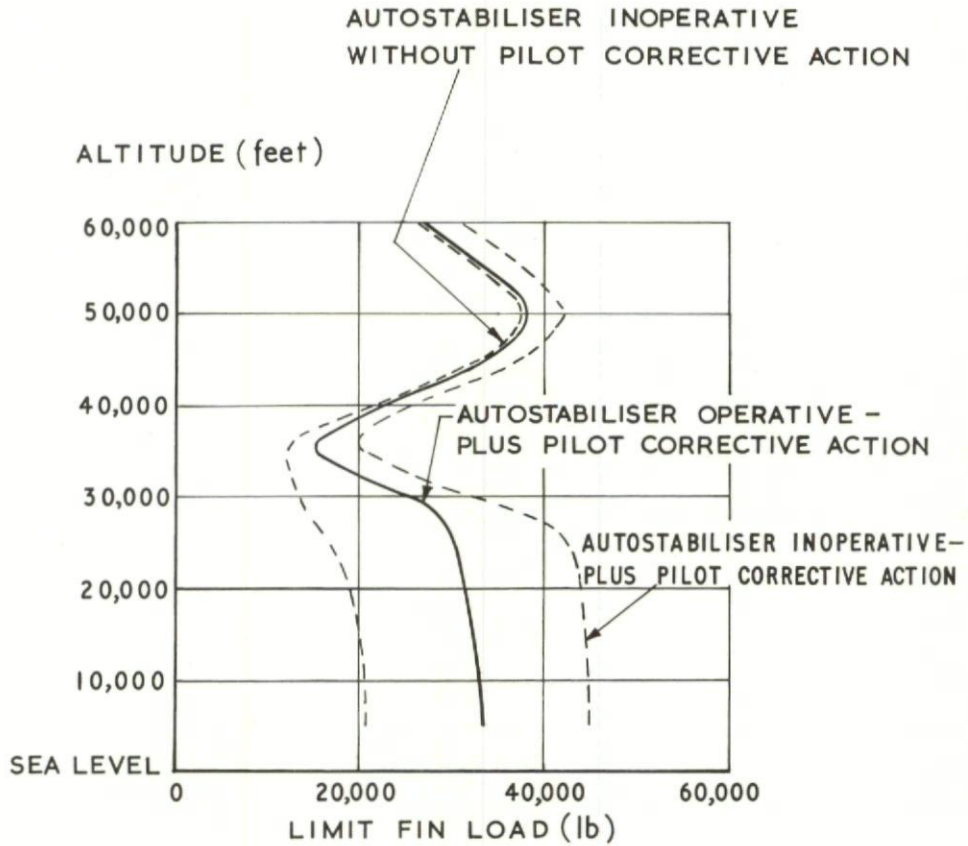
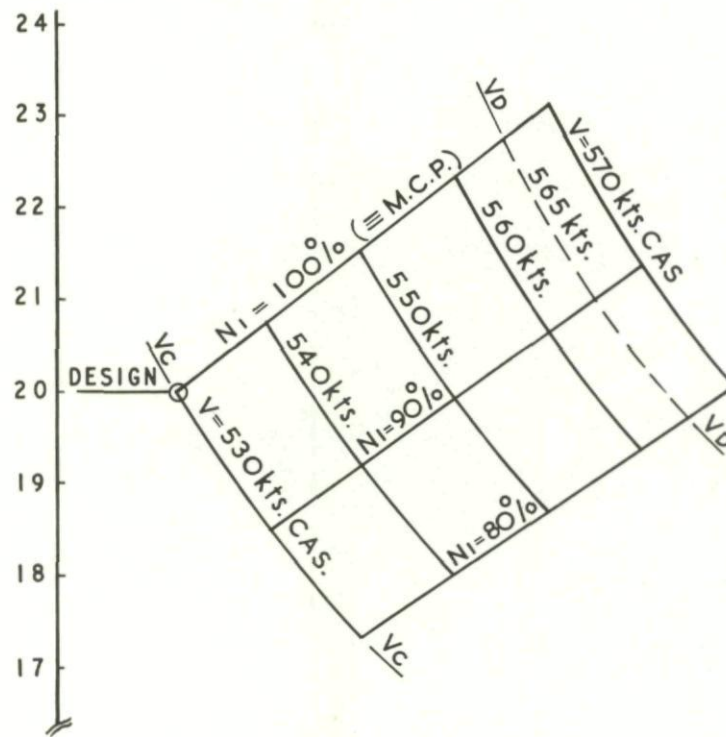


Fig.6 Fin loads due to single engine failures

ENGINE FACE PRESSURE (p.s.i.a.)

Fig.7 Variation of engine face surge pressure at $M = 2.0$

STATUS OF TWO STUDIES ON ACTIVE CONTROL OF
AEROELASTIC RESPONSE AT NASA LANGLEY
RESEARCH CENTER

by

Irving Abel and M.C.Sandford

NASA Langley Research Center
Hampton, Virginia, USA

STATUS OF TWO STUDIES ON ACTIVE CONTROL
OF AEROELASTIC RESPONSE AT NASA LANGLEY RESEARCH CENTER

Irving Abel and Maynard C. Sandford

SUMMARY

The application of active control technology to the suppression of flutter has been successfully demonstrated during two recent studies in the Langley transonic dynamics tunnel. The first study involved the implementation of an aerodynamic-energy criterion, using both leading- and trailing-edge controls, to suppress flutter of a simplified delta-wing model. Use of this technique has resulted in an increase in the flutter dynamic pressure of approximately 12 percent for this model at a Mach number of 0.9. Analytical methods used to predict the open- and closed-loop behavior of the model are also discussed. The second study, which is a joint effort with the Air Force Flight Dynamics Laboratory, was conducted to establish the effect of active flutter suppression on a model of the Boeing B-52 Control Configured Vehicle (CCV). Some preliminary results of this study indicate significant improvements in the damping associated with the critical flutter mode.

INTRODUCTION

Considerable interest has emerged over the last few years toward applying active control technology to suppress aeroelastic response of present and future aircraft configurations. Potential gains in aerodynamic efficiency and weight savings can be realized through ride-quality control, reduction of gust and maneuver loads with a consequent reduction in fatigue damage, reduction of static-stability requirements, and suppression of flutter. The use of active controls to suppress aeroelastic response is not new. It has already been used, to a limited degree, on such airplanes as the XB-70 and B-52 to improve ride quality by reducing structural response to turbulence (refs. 1 and 2).

The use of active controls to suppress flutter seems further from realization than other active control concepts, partly because of the lack of a thorough experimental evaluation. A review of the recent literature (e.g., refs. 3, 4, and 5) indicates that most of the work in this area is analytical. In an effort to fill the need for experimental results, wind-tunnel model programs are underway in the Langley transonic dynamics tunnel to demonstrate the effectiveness of using active controls for flutter suppression.

The purpose of this paper is to describe some recent activities at Langley Research Center toward evaluating the use of active controls for flutter suppression. (Some early progress on these programs was reported in ref. 6.) The application of active controls to the suppression of flutter at transonic speeds on a simplified delta-wing model is described. Included is a brief summary of the analytical aspects of the problem, a description of the model, measured and calculated flutter points with and without active controls, and some experimental techniques used to establish the behavior of the model at subcritical test conditions.

In addition to the delta-wing program, a program is being conducted to evaluate the use of active controls for flutter suppression, maneuver-load control, ride-quality control, and reduction of static-stability requirements on a model of the Boeing B-52 CCV airplane. This program is a cooperative effort by Langley Research Center; the Air Force Flight Dynamics Laboratory; and The Boeing Company, Wichita Division, under NASA and Air Force contracts. These studies are being conducted in conjunction with a flight research program (ref. 7) in an effort to correlate model and flight data. This paper includes a brief summary of preliminary wind-tunnel flutter-suppression studies accomplished to date.

SYMBOLS

b	reference semichord
c	reference chord, $2b$
f_A, f_B	frequencies at half-power points of forced response
g	structural damping coefficient
$h(x,y,t)$	vertical displacement
h_1, h_2	vertical displacement of delta-wing model at 30 and 70 percent of the reference chord, respectively (fig. 5)
M_i	generalized mass of i th vibration mode
$m(x,y)$	mass distribution
$\Delta p(x,y,t)$	pressure distribution
q_i	generalized displacement of i th vibration mode
S	reference area
s	Laplace operator
t	time
U	aerodynamic-energy matrix defined in equation (2)
\bar{U}	complex conjugate of the matrix U
V	free-stream velocity
x,y	streamwise and spanwise coordinates, respectively
$Z_i(x,y)$	normalized deflection in i th vibration mode
α	angle of attack at section A-A (fig. 5)
β	leading-edge-control deflection

δ	trailing-edge-control deflection
δ_a	B-52 outboard-aileron deflection
$\delta_{a,c}$	deflection command signal to B-52 outboard aileron
δ_f	B-52 flaperon deflection
$\delta_{t,c}$	deflection command signal to delta-wing trailing-edge control
ω	circular frequency

Matrix notation:

$\{ \}$	column matrix
$[\]$	row matrix
$[\]$	square matrix
$[\]^T$	transpose of matrix

Dots above symbols indicate derivatives with respect to time.

FLUTTER SUPPRESSION BASED ON AERODYNAMIC ENERGY CONSIDERATIONS

Flutter is a self-excited oscillation in which energy is absorbed by the lifting surface from the airstream. The state of stability of the system is defined by the sign of the work per cycle when the lifting surface undergoes an arbitrary oscillatory motion. The use of energy techniques to investigate the stability of an aeroelastic system is not new (ref. 8); however, a recent contribution to the area of flutter suppression is the development of an aerodynamic energy criterion by Nissim (ref. 3). This criterion states that a necessary and sufficient condition for the prevention of flutter is that for all allowable oscillatory motions of an elastic system in an airstream, positive work must be done by the system on the surrounding airstream. A brief summary of the salient points brought out in reference 3 is given in the following section.

Energy Concept

Consider the equations of motion for a system with n degrees of freedom:

$$\langle \mathbf{F} \rangle = -\omega^2 \left[\mathbf{M} + \pi \rho b^4 \mathbf{S} \left[\mathbf{A}_R + i \mathbf{A}_I \right] \right] \langle \mathbf{q} \rangle + \mathbf{K} \langle \mathbf{q} \rangle \quad (1)$$

where, at flutter, the generalized force $\langle \mathbf{F} \rangle = 0$ and ω is the circular frequency of oscillation; \mathbf{M} is the mass matrix (called \mathbf{B} in ref. 3); \mathbf{A}_R and \mathbf{A}_I are the real and imaginary unsteady aerodynamic-force matrices, respectively; \mathbf{K} is the structural stiffness matrix (called \mathbf{E} in ref. 3); ρ is the fluid density; \mathbf{S} and b are a reference area and length, respectively; and $\langle \mathbf{q} \rangle$ is the generalized displacement vector.

Nissim shows that the work per cycle W (called P in ref. 3) done by the system on the airstream can be written as

$$W = \frac{1}{2} \pi^2 \rho b^4 S \omega^2 [q_R - iq_I][U] \{q_R + iq_I\} \quad (2)$$

where

$$\{q\} = \{q_R + iq_I\} e^{i\omega t}$$

and

$$[U] = \left[-\left[[A_I] + [A_I]^T \right] + i \left[[A_R] - [A_R]^T \right] \right]$$

A positive value for W indicates a transfer of energy from the system to the airstream, and hence stability. The matrix U is Hermitian (i.e., $\bar{U}^T = U$) and therefore possesses real eigenvalues. By use of these eigenvalues it is shown in reference 3 that the energy input per cycle into the airstream can be reduced to a principal quadratic form as

$$W = \frac{1}{2} \pi^2 \rho b^4 \omega^2 S \left[\lambda_1 (\xi_{R1}^2 + \xi_{I1}^2) + \lambda_2 (\xi_{R2}^2 + \xi_{I2}^2) + \dots + \lambda_n (\xi_{Rn}^2 + \xi_{In}^2) \right] \quad (3)$$

where $\lambda_1, \lambda_2, \dots, \lambda_n$ are the eigenvalues of the matrix U and ξ denotes generalized coordinates associated with the aerodynamic energy. It can be seen from equation (3) that the work W will always be positive if all the eigenvalues λ are positive. Therefore, a sufficient condition for flutter stability is that all the λ terms are positive. A notable characteristic of the energy method is that the criterion for flutter stability is determined by the characteristics of the aerodynamic-force matrices alone. Therefore, if a particular system has undesirable flutter characteristics (i.e., too low a flutter speed), the flutter characteristics can be improved if a mechanism can be found which changes the U matrix in an appropriate manner. One such mechanism is the addition of control surfaces to the basic system. The motions of these surfaces generate aerodynamic forces which modify the aerodynamic terms in the U matrix for the basic system. For flutter suppression the control-surface deflections are related by a "control law" to the plunging and pitching motion of the main surface. Nissim points out in reference 3 that a suitable configuration is one employing both leading- and trailing-edge controls since the two working together provide independent control of lift and pitching moment.

Delta-Wing Flutter Suppression Model

To evaluate the practical aspects of the aerodynamic-energy concept, The Boeing Company, Wichita Division, under contract to NASA, performed an analytical study of the application of this concept to an early supersonic transport (SST) configuration. Some results of this study, as described in reference 9, indicate increases in the flutter speed from 11 to 29 percent for several spanwise locations of leading- and trailing-edge controls.

Because of these positive results, an experimental program aimed at providing evaluation and validation of the energy concept was initiated by using a wall-mounted 1/17-size simplified semispan model of a recent SST configuration. The Boeing Company, under contract to the Langley Research Center, is providing general support for this program in the area of controls implementation and analysis. A photograph of the model installed in the Langley transonic dynamics tunnel is shown in figure 1, and a sketch of the model is presented in figure 2.

The wing has a clipped-delta planform without twist or camber, a symmetric circular-arc airfoil section with a maximum thickness-to-chord ratio of 0.03, and hydraulically actuated leading- and trailing-edge controls. The trailing-edge control was approximately 20 percent of the local chord, while the leading-edge control varied from about 15 percent of the chord inboard to 20 percent of the local chord outboard. Both controls were located between 73 and 84 percent of the wing span. These locations are approximately those referred to in reference 9 that resulted in the largest increase in flutter speed. Simulated engine nacelles are mounted on the underside of the wing. The model construction consists of an internal aluminum alloy plate that was tapered in thickness in the spanwise direction and had cutouts to simulate spars and ribs. The plate was covered with balsa wood to provide the proper aerodynamic contour.

Because of the large hinge moments required and the necessity of keeping the control-surface actuation system within the physical constraints imposed by the model, that is, small and light, it was necessary to design and fabricate an electrohydraulic actuation system. Within these constraints an actuator was designed that weighs only 56.7 grams yet can produce approximately 4.52 N-m of torque throughout the operating range of interest (approximately from 0 to 25 Hz). Because of the limited thickness of the wing, it was also necessary to design and fabricate special control-surface position indicators. This was accomplished by mounting silicon solar cells to the actuator control shaft and illuminating them with a stationary light source. As the control shaft rotates, a voltage proportional to the angular position of the surface is produced. A photograph of the model showing the actuator and position indicator is presented in figure 3. A complete description of the design and fabrication of the control actuation system for the model is given in reference 10.

In order to perform analytical calculations for the model, it was necessary to specify a set of generalized masses, mode shapes, and natural frequencies. These properties were determined experimentally for the first nine structural modes of the model by using methods similar to those described in reference 11. The measured modal contours, natural frequencies, and generalized masses are given in figure 4.

Control Law

A simplified block diagram of the delta-wing flutter-suppression system is presented in figure 5. The control law used is of the form

$$\begin{Bmatrix} \beta \\ \delta \end{Bmatrix} = \begin{bmatrix} C_{11} & C_{12} \\ C_{21} & C_{22} \end{bmatrix} \begin{Bmatrix} h_1/b \\ \alpha \end{Bmatrix} + i \begin{bmatrix} G_{11} & G_{12} \\ G_{21} & G_{22} \end{bmatrix} \begin{Bmatrix} h_1/b \\ \alpha \end{Bmatrix} \quad (4)$$

where β is the leading-edge control deflection; δ is the trailing-edge control deflection; h_1 and α are the plunging and pitching motions, respectively, of a representative streamwise section of the wing (section A-A in fig. 5); b is a reference length; and C and G are constant coefficients which were evaluated from an aerodynamic-energy analysis.

The motions of h_1 and h_2 are measured by accelerometers located at 30 and 70 percent of the local chord c . The control law is mechanized on an analog computer which has been programmed to perform the operations indicated in figure 5 to determine h_1 , \dot{h}_1 , α , and $\dot{\alpha}$, and pass the proper command signal as expressed in equation (4) to the control surfaces. Figure 5 indicates that the period of oscillation $1/\omega$ must be determined. However, reference 3 showed that essentially the same results can be obtained if the value of $1/\omega$ is taken to be constant and equal to the open-loop flutter

period. This result was confirmed by preliminary wind-tunnel investigations.

Flutter Analysis

In order to illustrate the mechanism of flutter suppression, a flutter analysis, both with and without active controls, is presented. The flutter equations for a three-dimensional lifting surface are obtained from Lagrange's equation of motion by assuming that the unknown mode of motion is described by a linear combination of orthogonal modes, that is, the undamped natural modes of the system, in the following manner:

$$h(x,y,t) = \sum_{i=1}^n q_i(t) Z_i(x,y) \quad (5)$$

If structural damping is neglected, then the equations of motion become

$$M_i \ddot{q}_i(t) + \omega_i^2 M_i q_i(t) = Q_i(t) \quad (6)$$

where

$$M_i = \iint_S m(x,y) Z_i^2(x,y) dx dy$$

is the generalized mass and

$$Q_i(t) = \iint_S \Delta p(x,y,t) Z_i(x,y) dx dy$$

is the generalized aerodynamic force. The total pressure distribution $\Delta p(x,y,t)$ is composed of contributions due to each flexible mode plus those due to the leading- and trailing-edge controls. Therefore,

$$\Delta p(x,y,t) = \sum_{j=1}^n \Delta p_j(x,y) q_j(t) + \Delta p_\delta + \Delta p_\beta$$

where Δp_j is the pressure distribution due to each flexible mode, and Δp_β and Δp_δ are the pressure distributions due to leading- and trailing-edge controls, respectively. Substituting this expression for the pressures into equation (6) and expanding results in the following form of the equations of motion:

$$\begin{aligned} (-\omega^2 M_i + \omega_i^2 M_i) q_i(t) = & \sum_{j=1}^n \left(q_j(t) \iint_S \Delta p_j Z_i dx dy \right) \\ & + \beta \iint_S \Delta p_\beta Z_i dx dy + \delta \iint_S \Delta p_\delta Z_i dx dy \end{aligned} \quad (7)$$

From equation (5), the nondimensionalized deflection of the wing for the responses h_1 and h_2 can be written as

$$\frac{h_1}{b} = \frac{1}{b} \sum_{i=1}^n q_i(t) Z_i(x_1, y_1) \quad \frac{h_2}{b} = \frac{1}{b} \sum_{i=1}^n q_i(t) Z_i(x_2, y_2)$$

Assuming that a straight line between the locations of the two sensors gives a reasonable approximation to the angle of attack at the reference station and noting that the sensors are $0.8b$ apart lead to the following equation for angle of attack:

$$\alpha = \frac{1}{0.8} \left(\frac{h_2}{b} - \frac{h_1}{b} \right) = \frac{1}{0.8b} \sum_{i=1}^n (Z_i(x_2, y_2) - Z_i(x_1, y_1)) q_i(t)$$

Substituting the above results into the control law (eq. (4)) results in a matrix equation relating the control-surface motions to the generalized coordinates in the following form:

$$\begin{Bmatrix} \beta \\ \delta \end{Bmatrix} = \begin{bmatrix} A_1 + iB_1 & A_2 + iB_2 & \dots & A_n + iB_n \\ C_1 + iD_1 & C_2 + iD_2 & \dots & C_n + iD_n \end{bmatrix} \begin{Bmatrix} q_1 \\ q_2 \\ \vdots \\ q_n \end{Bmatrix} \quad (8)$$

where the parameters A_i , B_i , C_i , and D_i are constant coefficients defined as follows:

$$A_i = Z_i(x_1, y_1) \left(\frac{C_{11}}{b} - \frac{C_{12}}{0.8b} \right) + Z_i(x_2, y_2) \frac{C_{12}}{0.8b}$$

$$B_i = Z_i(x_1, y_1) \left(\frac{G_{11}}{b} - \frac{G_{12}}{0.8b} \right) + Z_i(x_2, y_2) \frac{G_{12}}{0.8b}$$

$$C_i = Z_i(x_1, y_1) \left(\frac{C_{21}}{b} - \frac{C_{22}}{0.8b} \right) + Z_i(x_2, y_2) \frac{C_{22}}{0.8b}$$

$$D_i = Z_i(x_1, y_1) \left(\frac{G_{21}}{b} - \frac{G_{22}}{0.8b} \right) + Z_i(x_2, y_2) \frac{G_{22}}{0.8b}$$

Substituting equation (8) into equation (7) results in the final form of the equations of motion:

$$\begin{aligned} (-\omega^2 M_i + \omega_i^2 M_i) q_i(t) = & \sum_{j=1}^n q_j \left(\iint_S \Delta p_j Z_i \, dx \, dy + (A_j + iB_j) \iint_S \Delta p_\beta Z_i \, dx \, dy \right. \\ & \left. + (C_j + iD_j) \iint_S \Delta p_\delta Z_i \, dx \, dy \right) \end{aligned} \quad (9)$$

It should be noted from the form of the equations presented here that the active controls serve only to modify the aerodynamic forces of the wing alone. The Hermitian matrix U described earlier can be derived directly from the aerodynamic terms appearing in this equation and the effect of active controls on this matrix determined. Flutter calculations without active controls are performed by setting the coefficients A , B , C , and D equal to zero.

Flutter calculations were performed for the delta-wing model at Mach numbers of 0.6, 0.7, 0.8, and 0.9. The generalized aerodynamic forces appearing in equation (9) were formulated through the use of doublet-lattice aerodynamics as described in reference 12. This method requires the subdivision of the lifting surface into an array of trapezoidal boxes arranged in streamwise columns with a line of pulsating doublets located at the quarter chord of each box. The geometric boundary condition of tangential flow is satisfied at the 3/4-chord location for each box. The delta-wing model was divided into 160 boxes arranged in 16 streamwise strips with 10 boxes per strip. This arrangement provided six boxes on each control surface. All flutter calculations were made using the first nine measured structural modes, generalized masses, and natural frequencies. It should be noted that the equations of motion did not include control-surface dynamics since the natural frequency of rotation for each surface was considerably above the frequency of interest.

Results

Flutter.- Flutter characteristics of the model without active controls were experimentally determined in the Langley transonic dynamics tunnel at Mach numbers of 0.6, 0.7, 0.8, and 0.9. For these tests the control surfaces were kept at 0° deflection by applying hydraulic pressure to the actuators. The pressurized system acted as a very stiff spring and kept the rotational frequencies of the controls many times higher than the flutter frequency. Once the flutter boundary of the wing was established, an evaluation of the effect of active controls on raising the boundary was begun. However, these studies were conducted only at a Mach number of 0.9 because of an unexplained high-frequency, large-amplitude oscillation of the leading-edge control above a certain range of dynamic pressure at the lower Mach numbers. This phenomenon occurred around 65 Hz, whereas the flutter frequency was 11 to 12.5 Hz. This problem is not believed to be a result of the control law, since this motion is also observed with the control loop open, but has been introduced in some manner by the mechanization of the controls on the model.

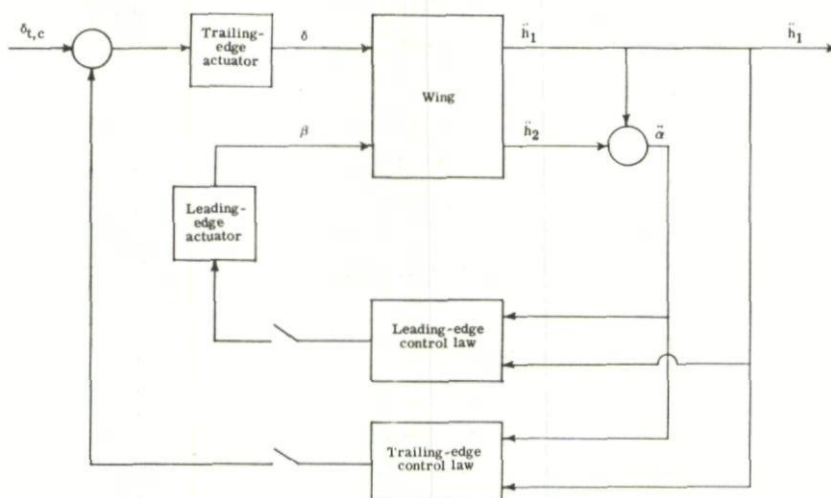
The experimental flutter results are presented in figure 6. At a Mach number of 0.9 the basic wing model fluttered at a dynamic pressure of 5.879 kN/m^2 . With active controls the flutter point was raised to 6.607 kN/m^2 , reflecting an increase of approximately 12 percent in dynamic pressure. The degree of confidence in the control system was such that when open-loop flutter was encountered, the active control loop was closed to suppress the motion. The observed flutter motions for both open- and closed-loop operation were similar in nature and closely resembled the second natural vibration mode with some slight primary bending.

A comparison of calculated and experimental data is also presented in figure 6. The calculations for the basic wing show excellent agreement at all Mach numbers; however, the calculations with active controls predict a higher flutter point than was measured. At a Mach number of 0.9 the calculated increase in flutter dynamic pressure was approximately 21 percent compared with the measured increase of 12 percent. This difference is believed to be due to the inability of the aerodynamic theory to predict adequately the pressure distributions resulting from actuating the control surfaces, the lack of control-surface dynamics in the equations of motion, and the amplitude and phase lags incurred between the desired and actual control-surface deflections introduced by implementing the control loop on the model.

On the basis of these calculated results, it was decided to investigate analytically the sensitivity of the system to phase lag between the desired and actual control-surface deflections. A separate set of calculations were made which included a phase lag for both

leading- and trailing-edge controls. The phase angle was experimentally determined for the model by measuring the frequency response of the actuator systems. At the flutter frequency of about 12 Hz, both surfaces had a phase lag of approximately 18° , and this value was used in the calculations. The results of these calculations are presented in figure 6. At a Mach number of 0.9 the phase angle reduced the increase in flutter dynamic pressure from 21 percent to 16 percent and resulted in a more favorable comparison with experiment.

Subcritical response.- In order to explore fully the behavior of the model below the flutter boundaries, two techniques for estimating the damping associated with the flutter mode were used. The first of these techniques (described in ref. 13) involves measuring the forced response of the model to an input generated by the trailing-edge controls as indicated in sketch 1. A measure of the damping in each mode can be obtained for both open- and closed-loop operation if the transfer function relating the forced response to the command signal ($\ddot{h}_1/\delta_{t,c}$) is determined as a function of frequency. During the wind-tunnel test an electronic signal analyzer was used to determine the in-phase and out-of-phase components of the response \ddot{h}_1 with respect to the trailing-edge command signal. Figure 7 presents a typical plot of this response at a Mach number of 0.9 and a dynamic pressure of 5.429 kN/m^2 . The curves in the upper portion of this figure represent the response of the basic wing; the lower curves, the response with the control loop closed. The damping in the modes can be estimated from the out-of-phase component by the frequencies labeled f_A and f_B . For an equivalent system with a single degree of freedom, these



Sketch 1

are the frequencies at the half-power points, and the damping can be expressed in terms of these frequencies:

$$g = \frac{(f_A/f_B)^2 - 1}{(f_A/f_B)^2 + 1}$$

The data shown in figure 7 are for a 3-minute logarithmic sweep from 5 to 25 Hz.

A qualitative measure of the effect of active controls in reducing the forced response of the system is evident from figure 7. The closed-loop system significantly alters the response by adding appreciable damping to the model. However, a quantitative measure of the damping is quite difficult to estimate because of the noise in the signal resulting from the model responding to tunnel turbulence. As the dynamic pressure is further increased, the signal-to-noise ratio becomes extremely high and results in very poor

response plots. For this model the forced-response technique did not provide very useful information, but it will be shown later that this procedure can be an extremely useful tool in estimating the subcritical response.

The second technique that was used is referred to as "randomdec" and is described in reference 14. Basically, the technique extracts the damped sinusoidal response of the model vibration modes from the response of the model to tunnel turbulence. This is accomplished by assuming that the measured response is composed of the response to a step, an impulse, and a random force. By averaging the measured response over a number of time sweeps, the response of the system to a step is determined, since the response to an impulse and to a random force average to zero. Damping is then obtained in the same manner as from a free-vibration decay which would be obtained if the model were given an initial displacement in the critical mode and then released. For a system with multiple degrees of freedom a filter is required to isolate the modes of interest. It should be pointed out that when the frequencies of the structural modes are closely spaced, both the randomdec and forced-response techniques suffer from the problem of accurately determining the damping value.

The randomdec technique was used to obtain the plot in figure 8, which is the measured system damping in the critical flutter-mode frequency range as a function of dynamic pressure at a Mach number of 0.9. The hatched area represents the experimental scatter of the data. Typical randomdec signatures are presented at a dynamic pressure of 5.841 kN/m^2 , which is within 1 percent of the flutter dynamic pressure. The open-loop damping is about 0.008; the closed loop, about 0.075. Also shown are the measured open- and closed-loop flutter points. Because of the frequency spectrum of the structural modes of interest, this technique proved to be quite valuable in establishing the subcritical behavior of the model. For test conditions at which the forced-response technique described earlier gave meaningful results, these results also fell within the scatter indicated in figure 8.

B-52 FLUTTER-SUPPRESSION PROGRAM

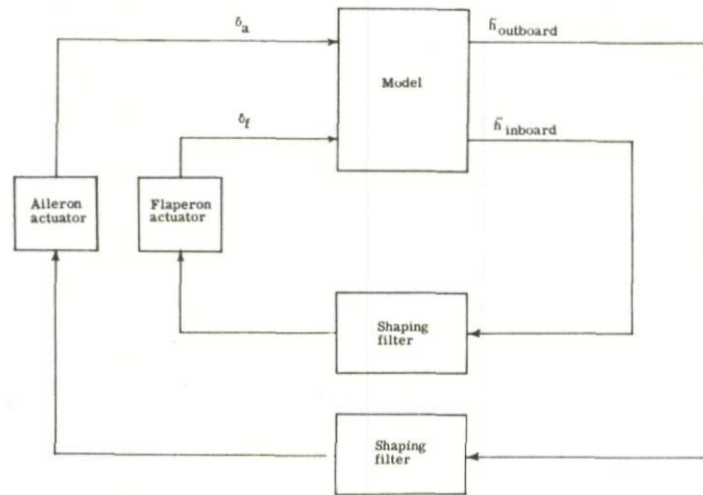
In addition to the delta-wing program, the Langley Research Center is engaged in a cooperative program with the Air Force Flight Dynamics Laboratory to study symmetric flutter suppression on a model of the B-52 CCV airplane. As mentioned in the Introduction, the B-52 program will include studies of the application of other active control systems including maneuver-load control, ride-quality control, and relaxed static stability.

Model Program

The model program uses a 1/30-size dynamically and aeroelastically scaled model of the B-52. A photograph of the model installed in the Langley transonic dynamics tunnel is shown in figure 9. In order to provide a simulation of the free-flight dynamics, the model is mounted on a modified version of the two-cable mount system described in reference 15. This mount provides the model with a soft support in that the natural frequencies associated with the mount are well below those of the free-flight and elastic modes.

The active flutter-suppression system designed for the model is indicated in the simplified block diagram shown in sketch 2. This control system was not designed with the use of the energy approach discussed earlier. It is a result of previous experience and analysis of the B-52 which have indicated that aerodynamic forces on the wing are stabilizing for 360° of the flutter oscillation cycle when the incremental lift generated by the control surfaces lags the wing motion by 90° . The control law is essentially a shaping

filter which provides the required phase lag between wing lift and displacement at the flutter frequency. A summary of the analysis, synthesis, and hardware implementation being used for the flight program is presented in reference 16.



Sketch 2

As indicated in sketch 2, the control system incorporates an active flaperon and outboard aileron. The placement of these controls is indicated in figure 10. An outboard accelerometer is used to drive the ailerons. A second inboard accelerometer is used to drive the flaperons. Because of the smaller hinge moments required for this model and the substantially larger volume available than in the delta-wing model, an electromechanical system was designed to actuate the controls. This system consisted of separate dc torque motors mounted within the fuselage to drive the ailerons and flaperons. The linkages used to drive the controls were designed to isolate them from the structure so that they would not change the stiffness characteristics of the wing. A description of this system is presented in reference 10.

Results

Experimental studies of the B-52 model were performed in the Langley transonic dynamics tunnel. The prime objectives of these tests were to establish the behavior of the flutter-suppression system below the flutter boundary. A plot of estimated damping in the critical flutter mode (approximately 12.8 Hz), using the forced-response technique, against tunnel dynamic pressure is presented in figure 11. Experimental results for the open-loop system, the closed-loop system with nominal gains, and the closed-loop system with double the nominal gains are indicated in this figure. It is readily apparent from these results that the effect of active controls is appreciable. Even with nominal gains, the damping at a dynamic pressure 2.42 kN/m^2 is more than double that of the open-loop system. With twice the nominal gains, not only has the level of damping increased but even the trend with increasing dynamic pressure has reversed direction.

A typical plot of the measured in-phase and out-of-phase response of the model is presented in figure 12. For this model the ailerons were used to generate the forcing function. As indicated in figure 12 the damping was estimated by determining the ratio of the outboard-accelerometer response to the aileron command for a frequency range of 4 to 24 Hz. The randomdec technique did not provide useful results until the model was tested near the flutter boundary, at which time most of the wing response was predominantly in the lowly damped flutter mode.

CONCLUDING REMARKS

A description of two wind-tunnel studies used to evaluate active control of flutter suppression has been presented. A flutter-suppression method based on an aerodynamic-energy criterion has been described, and some results of the application of this method to a simplified delta-wing model are presented. An increase of approximately 12 percent in the flutter dynamic pressure for this model has been achieved at a Mach number of 0.9 through the use of leading- and trailing-edge controls. Analytical calculations have been compared with experiment and indicate excellent agreement for the open-loop system; however, calculations for the closed-loop system predicted a larger increase in dynamic pressure than was measured.

Some preliminary experimental results of a flutter-suppression study of an aeroelastic model of the B-52 CCV airplane have been presented. A flutter-suppression method based on the phasing between wing motion and control-surface deflections has indicated that significant improvements in the subcritical damping of the flutter mode can be achieved through the use of active controls.

ACKNOWLEDGMENTS

The authors wish to express their appreciation to the Air Force Flight Dynamics Laboratory for their participation and support during the B-52 model program. In addition, the authors are particularly indebted to Mr. Frank D. Sevart of the Boeing/Wichita Company for his technical contributions during all of the studies described in this report.

REFERENCES

1. Wykes, John H.; and Kordes, Eldon E.: Analytical Design and Flight Tests of a Modal Suppression System on the XB-70 Airplane. Aeroelastic Effects From a Flight Mechanics Standpoint, AGARD CP-46, 1970, pp. 23-1 - 23-18.
2. Burris, P. M.; Dempster, J. B.; and Johannes, R. P.: Flight Testing Structural Performance of the LAMS Flight Control System. AIAA Paper No. 68-244, Mar. 1968.
3. Nissim, E.: Flutter Suppression Using Active Controls Based on the Concept of Aerodynamic Energy. NASA TN D-6199, 1971.
4. Triplett, William E.; Kappus, Hans-Peter F.; and Landy, Robert J.: Active Flutter Control: An Adaptable Application to Wing/Store Flutter. AIAA Paper No. 73-194, Jan. 1973.
5. Thompson, Glenn O.; and Kass, Gerald J.: Active Flutter Suppression - An Emerging Technology. *J. Aircraft*, vol. 9, no. 3, Mar. 1972, pp. 230-235.
6. Rainey, A. Gerald; Ruhlin, Charles L.; and Sandford, Maynard C.: Active Control of Aeroelastic Response. Stability and Control, AGARD CP-119, 1972, pp. 16-1 - 16-5.
7. Kass, Gerald J.; and Johannes, R. P.: B-52 Control Configured Vehicles Program. AIAA Paper No. 72-747, Aug. 1972.
8. Hunt, Gerald L.; and Walberg, Gerald D.: Calculated Mode Shapes and Pressure Distributions at Flutter for a Highly Tapered Horizontal Tail in Subsonic Flow. NASA TN D-1008, 1962.

9. Garrick, I. E.: Perspectives in Aeroelasticity. Israel J. Technol., vol. 10, no. 1-2, 1972, pp. 1-22.
10. Bergmann, Gerald E.; and Severt, Francis D.: Design and Evaluation of Miniature Control Surface Actuation Systems for Aeroelastic Models. AIAA Paper No. 73-323, Mar. 1973.
11. Abel, Irving: A Wind-Tunnel Evaluation of Analytical Techniques for Predicting Static Stability and Control Characteristics of Flexible Aircraft. NASA TN D-6656, 1972.
12. Albano, Edward; and Rodden, William P.: A Doublet-Lattice Method for Calculating Lift Distributions on Oscillating Surfaces in Subsonic Flows. AIAA J., vol. 7, no. 2, Feb. 1969, pp. 279-285.
13. Keller, Anton C.: Vector Component Techniques: A Modern Way To Measure Modes. Sound & Vib., vol. 3, no. 3, Mar. 1969, pp. 18-26.
14. Cole, Henry A., Jr.: On-Line Failure Detection and Damping Measurement of Aerospace Structures by Random Decrement Signatures. NASA CR-2205, 1973.
15. Reed, Wilmer H., III; and Abbott, Frank T., Jr.: A New "Free-Flight" Mount System for High-Speed Wind-Tunnel Flutter Models. Proceedings of Symposium on Aeroelastic & Dynamic Modeling Technology, RTD-TDR-63-4197, Pt. 1, U.S. Air Force, Mar. 1964, pp. 169-206.
16. Hodges, Garold E.: Active Flutter Suppression - B-52 Controls Configured Vehicle. AIAA Paper No. 73-322, Mar. 1973.

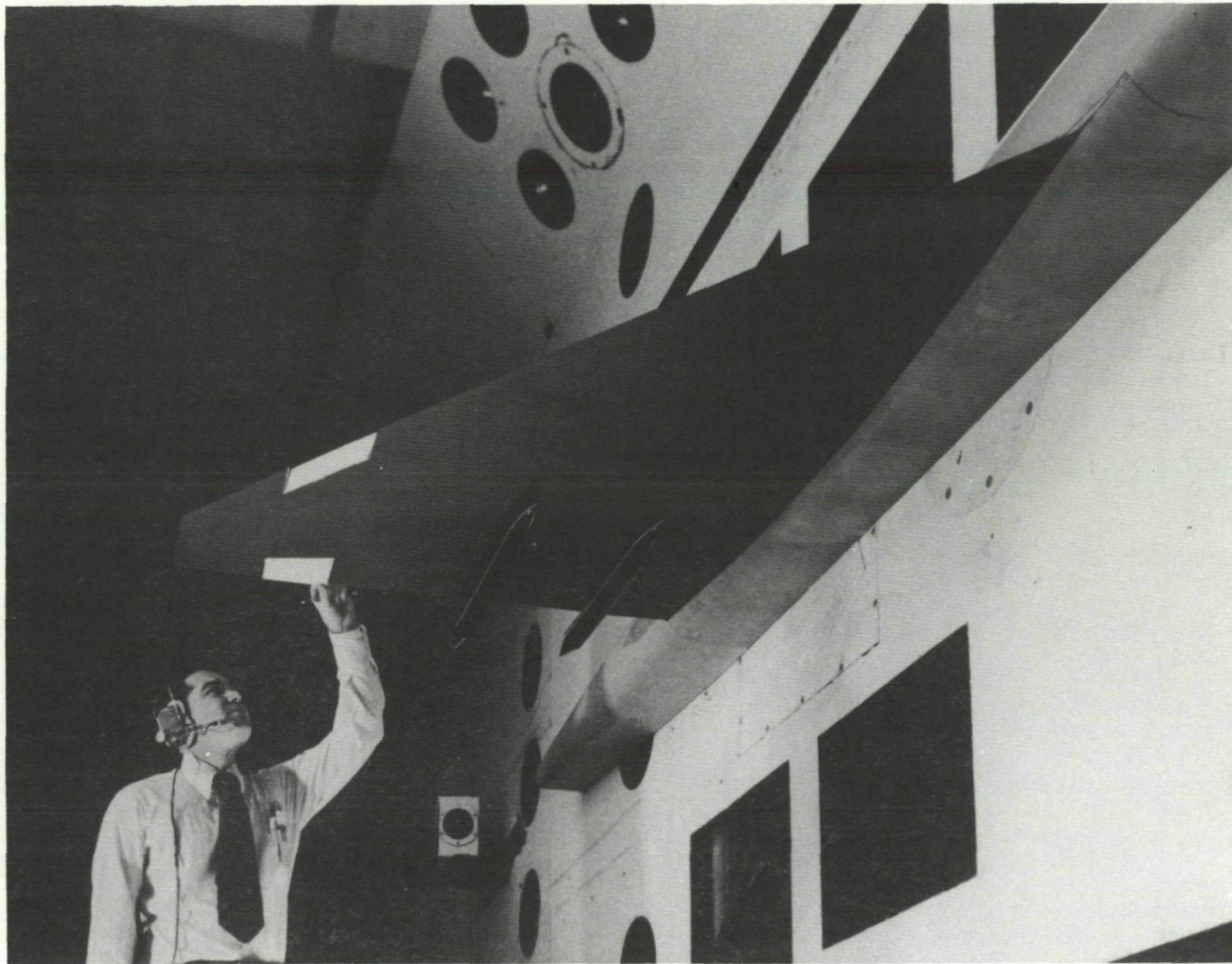


Fig.1 Delta-wing flutter-suppression model

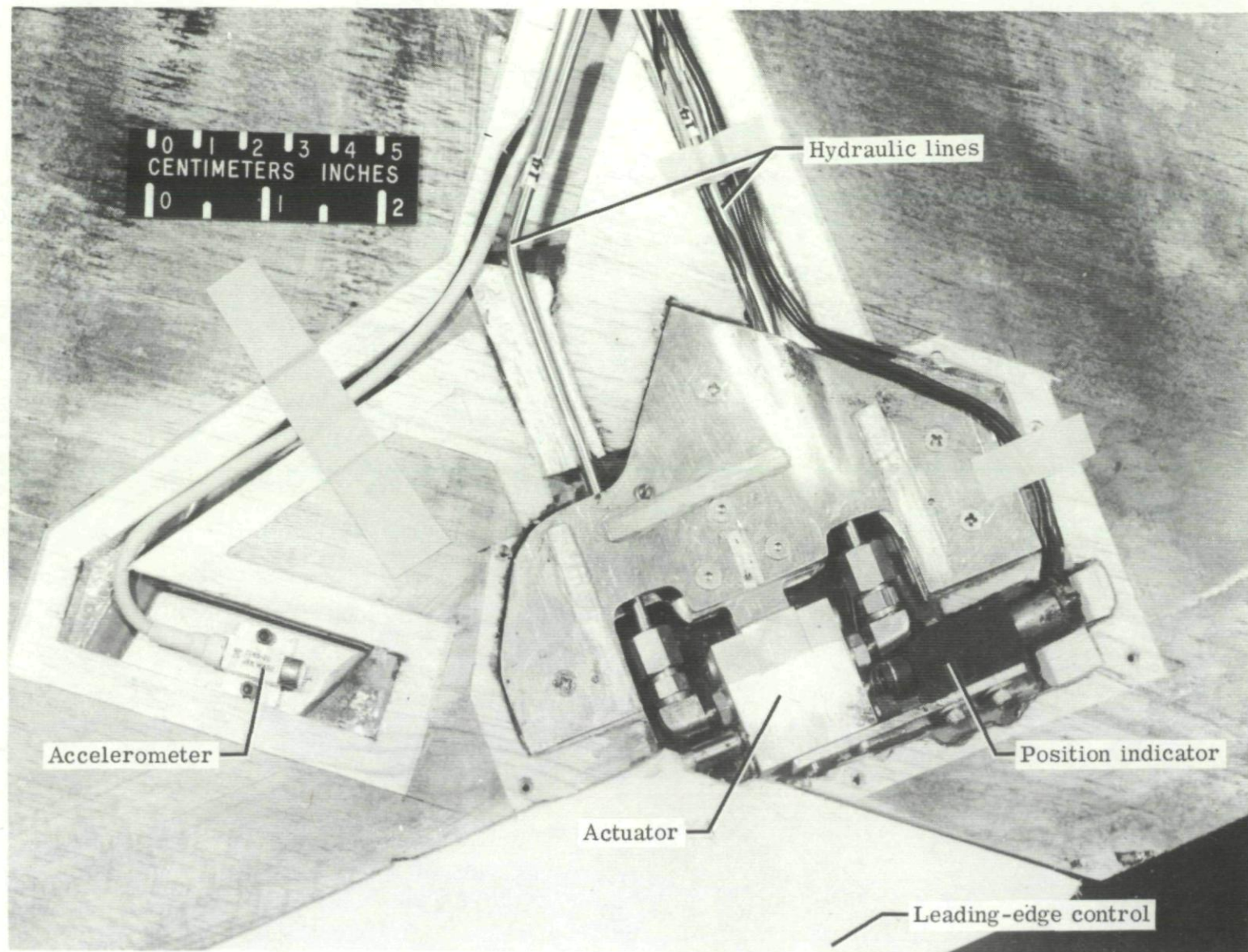


Fig.3 Delta-wing control system

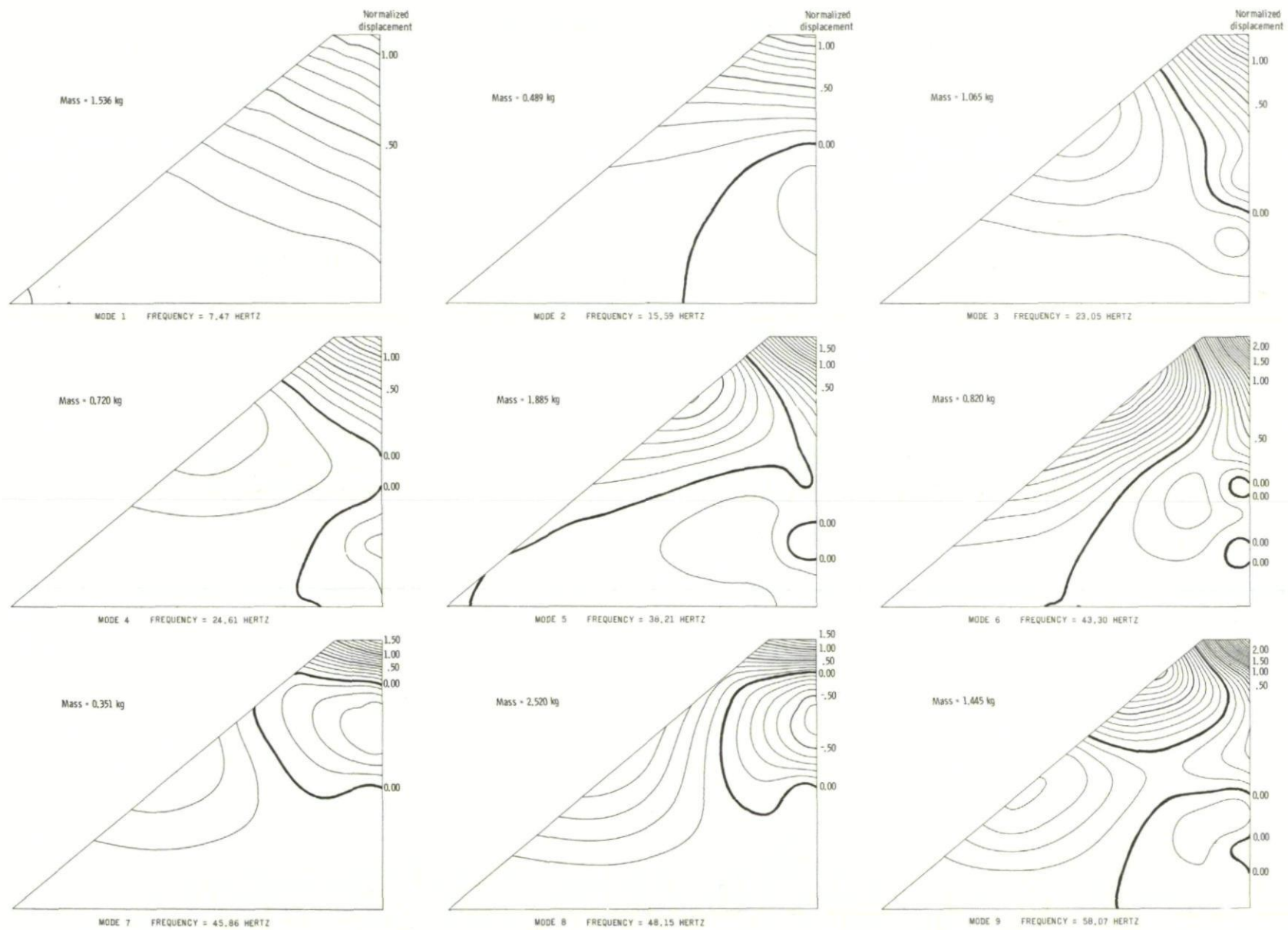


Fig.4 Measured modal contours, generalized masses, and frequencies of natural vibration modes. (Contour interval, 0.1 normalized displacement)

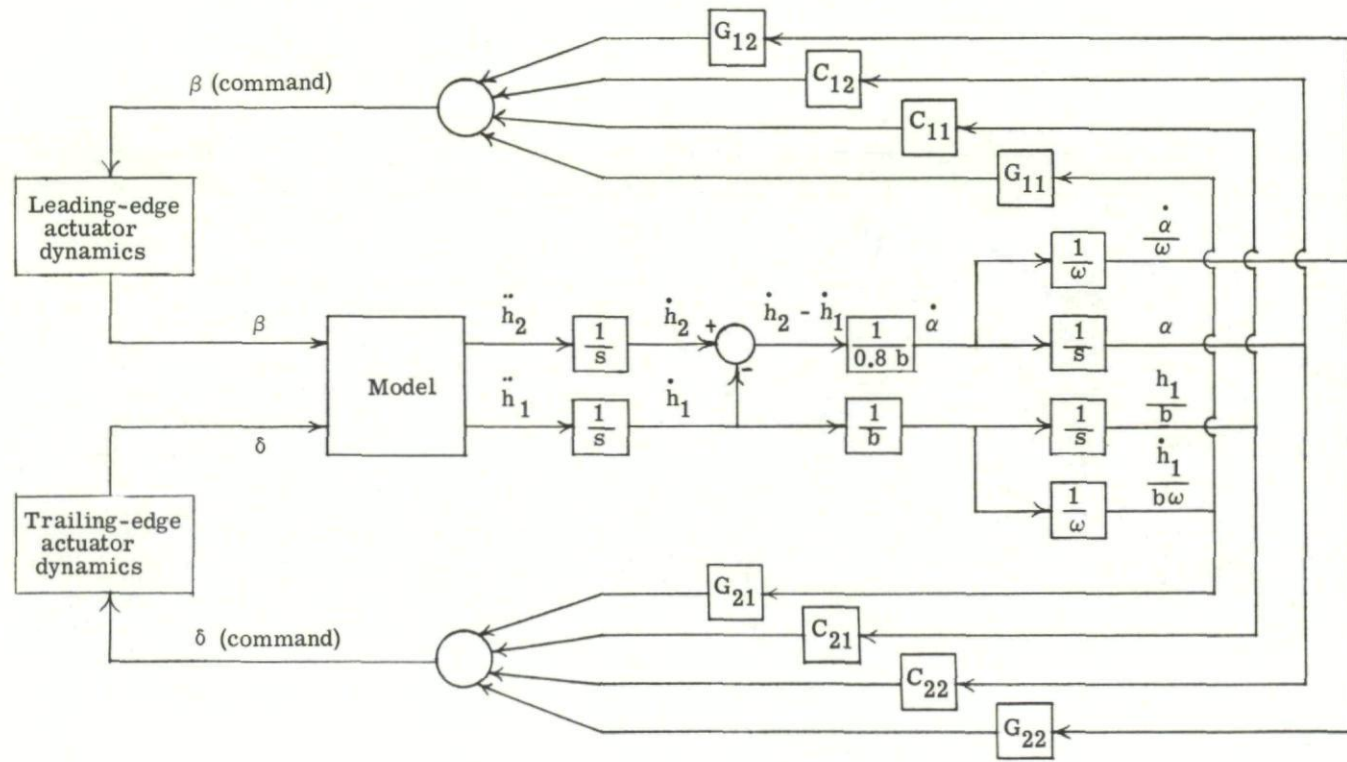
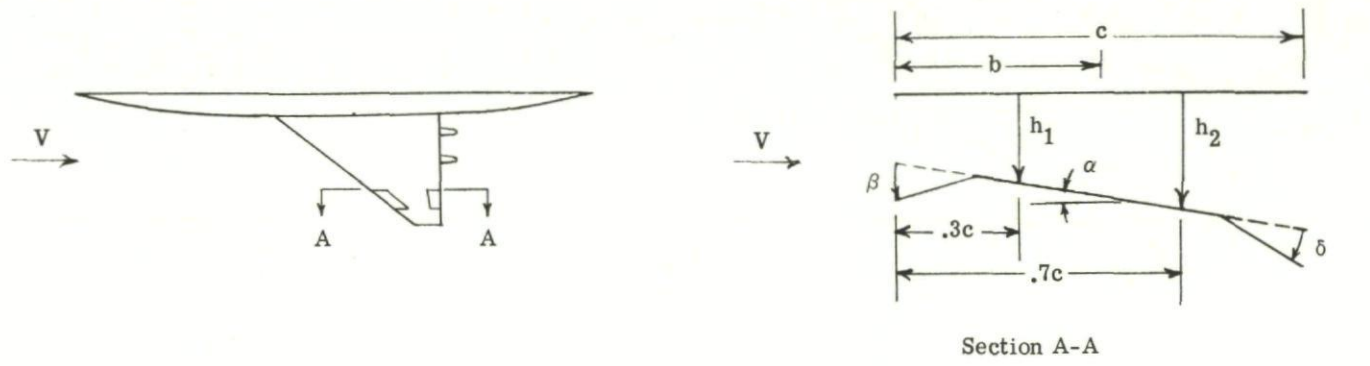


Fig.5 Block diagram of flutter-suppression system

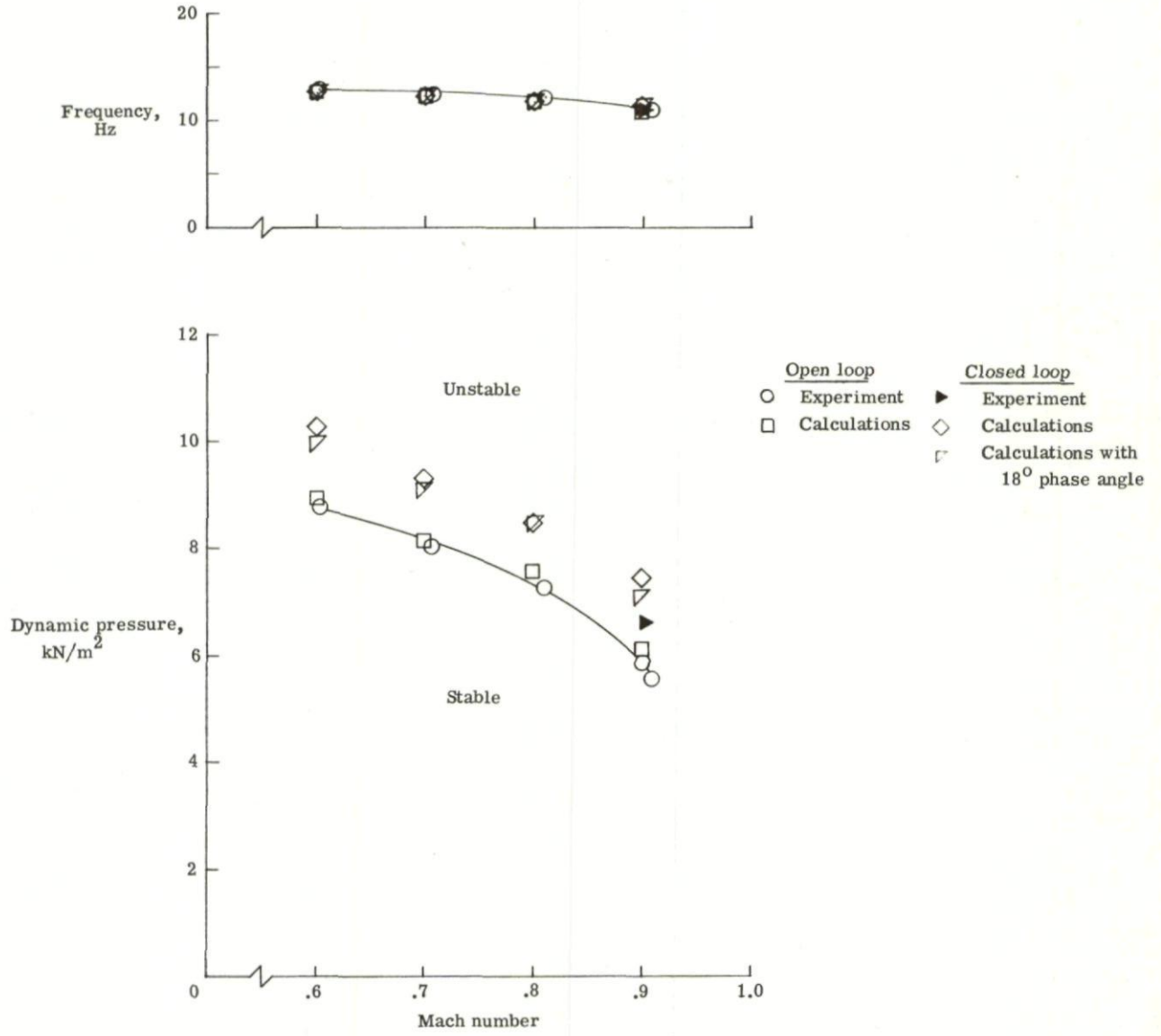


Fig.6 Measured and calculated model flutter boundaries

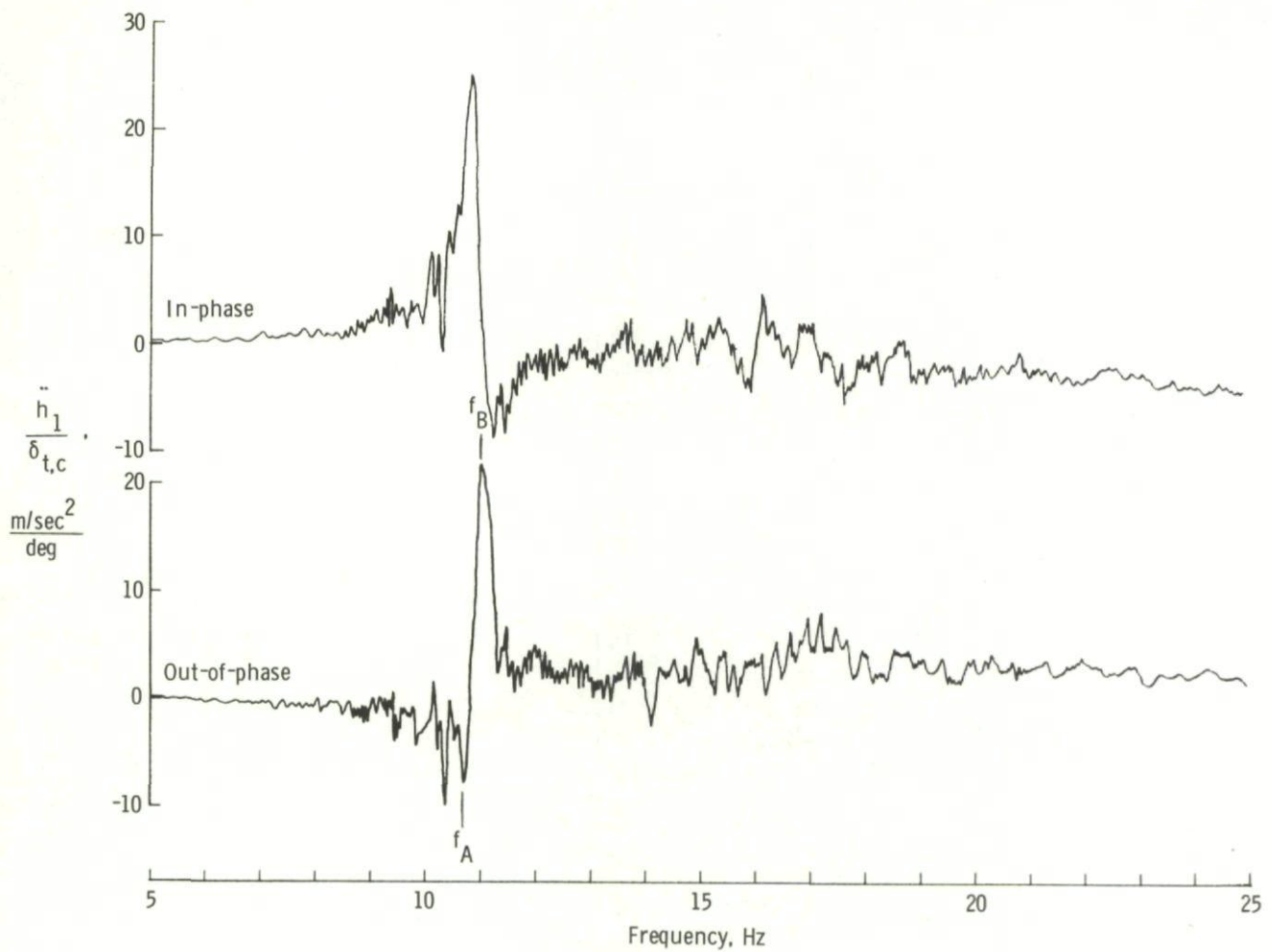
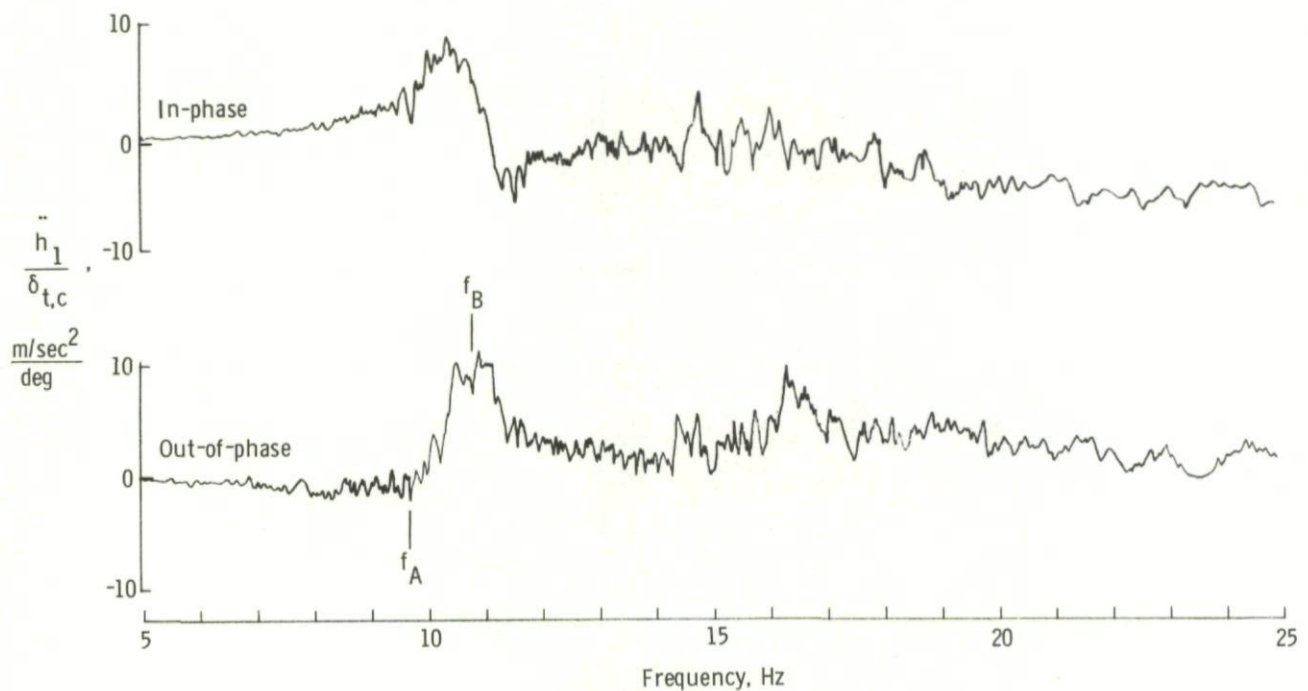
(a) Open-loop response. $g = 0.037$ (b) Closed-loop response. $g = 0.107$

Fig. 7 Measured forced response of model to trailing-edge-control excitation at Mach number of 0.9 and dynamic pressure of 5.429 kN/m^2

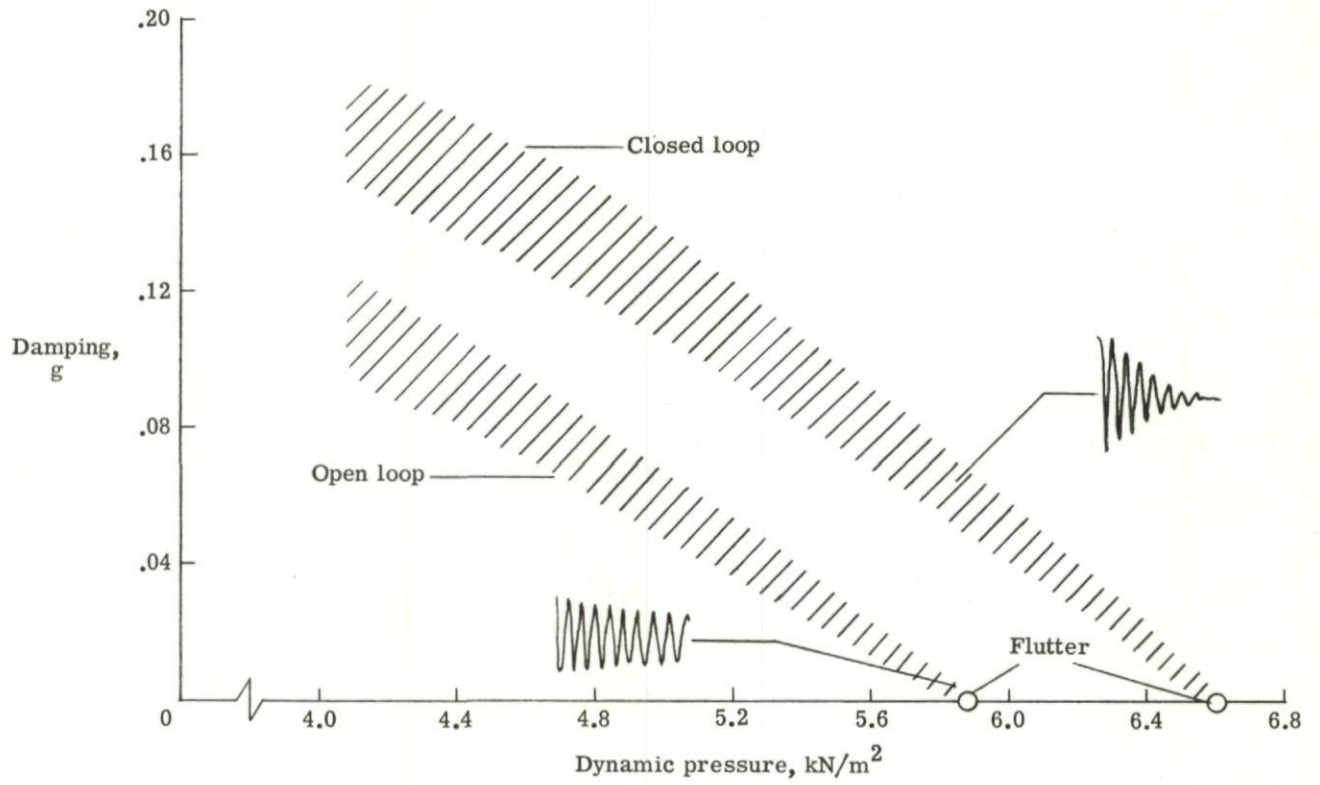


Fig.8 Measured subcritical damping at Mach number of 0.9

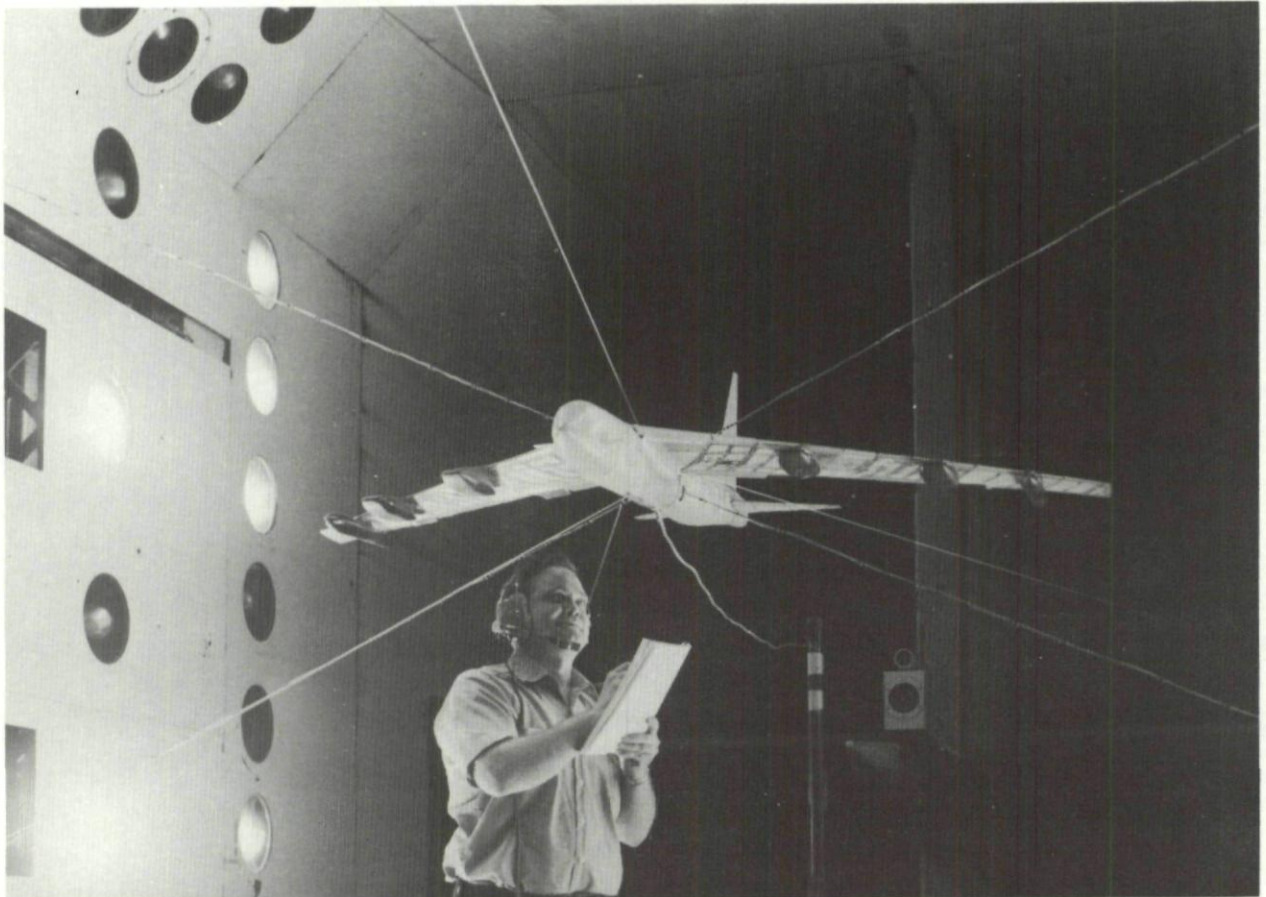


Fig.9 B-52 CCV model mounted in the Langley transonic dynamics tunnel

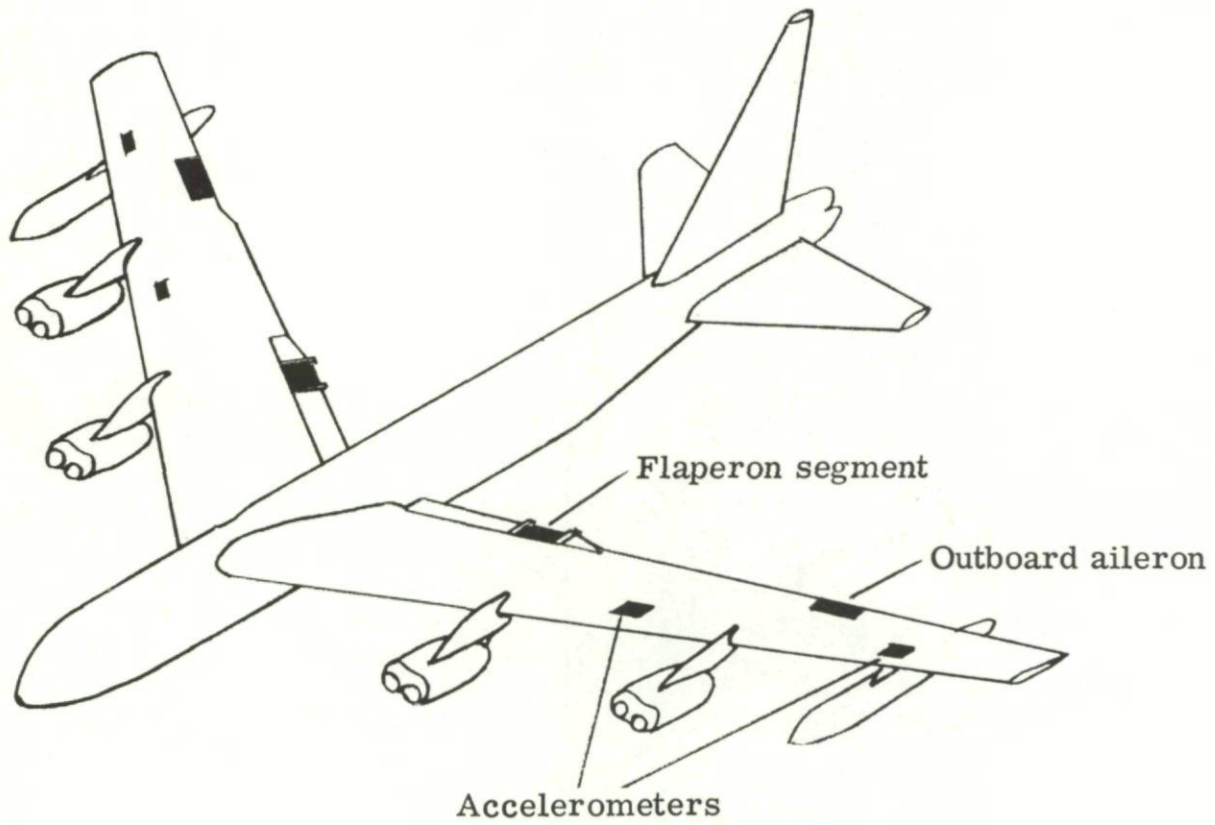


Fig.10 B-52 model control surfaces used for flutter suppression

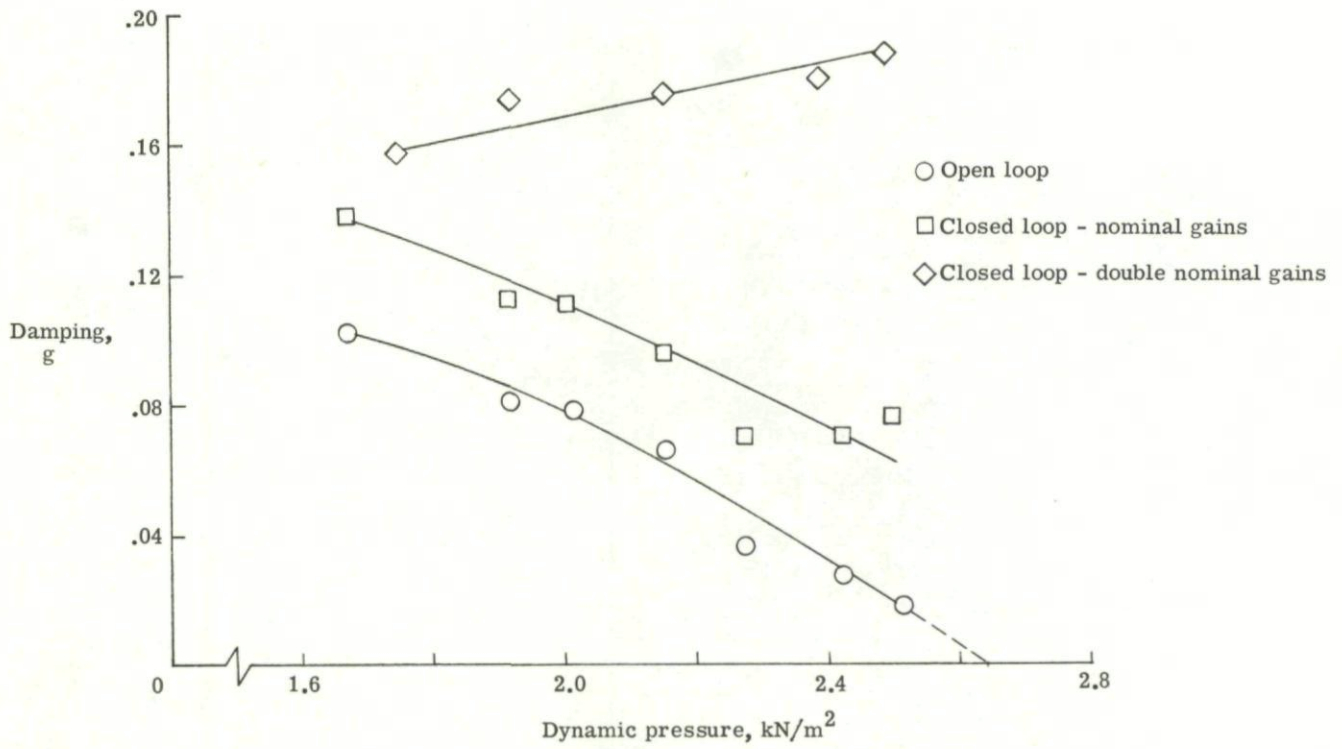
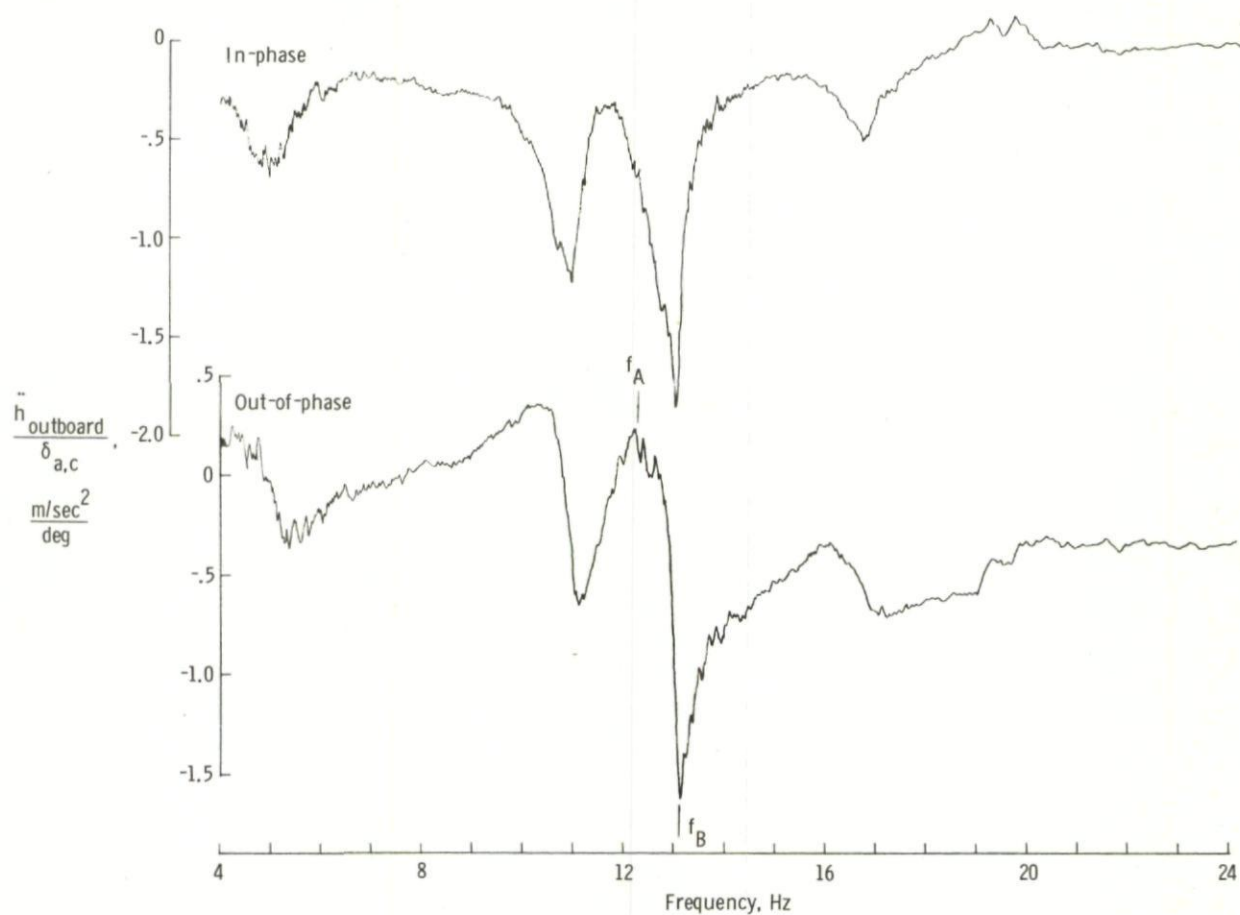
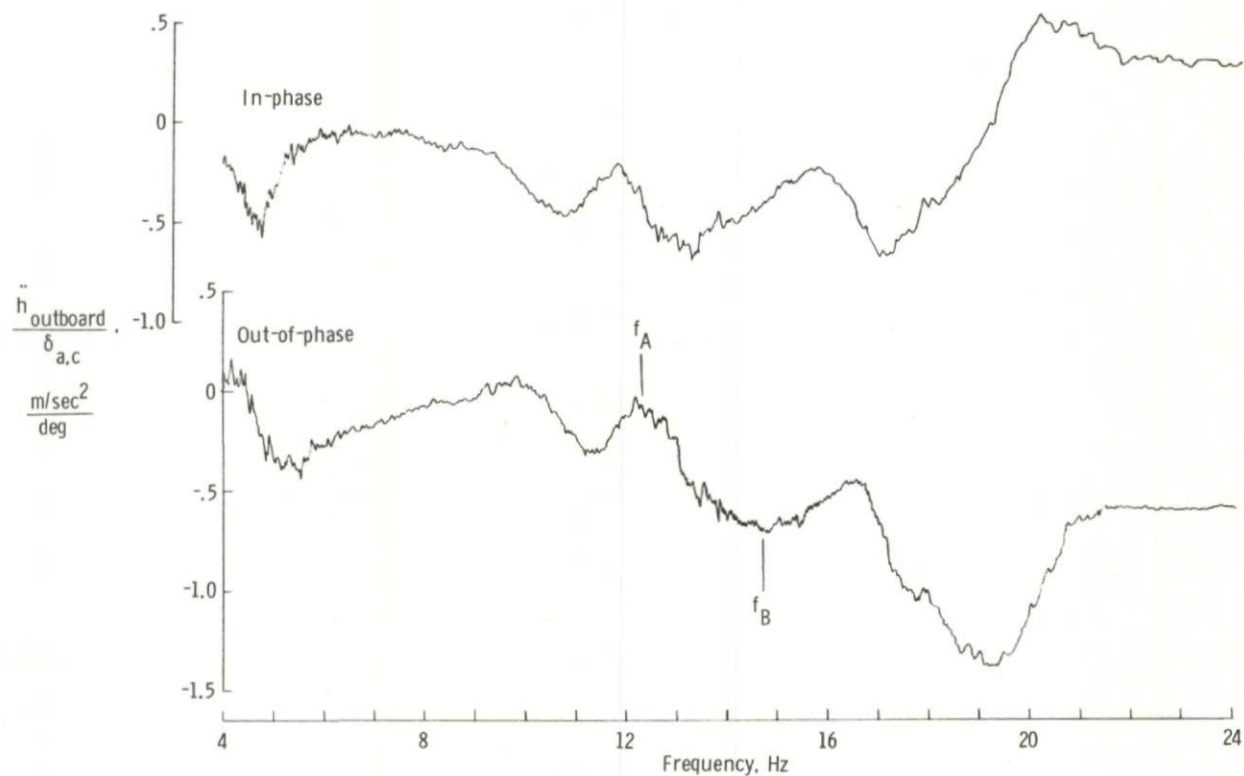


Fig.11 Measured damping for B-52 flutter-suppression model

(a) Open-loop response. $g = 0.062$ (b) Closed-loop response — double nominal gains. $g = 0.176$ Fig.12 Measured forced response of B-52 model to aileron command at a dynamic pressure of 2.154 kN/m²

**CONTROLE DU FLOTTEMENT PAR DEPLACEMENT
D'UNE VALEUR PROPRE**

par

J. Angélini

ONERA
29, ave de la Division Leclerc
92320 Châtillon-sous-Bagneux
France

Résumé

Le document propose une nouvelle méthode en vue du contrôle actif du flottement des avions. Cette méthode est caractérisée par le fait qu'elle permet de ne modifier que l'amortissement de la valeur propre instable, sans que les autres racines, ni les vecteurs propres soient modifiés.

Une telle approche permet d'espérer que le système actif concrétisé présentera le minimum d'interaction avec d'autres systèmes C.C.V. susceptibles d'être installés sur la structure.

FLUTTER CONTROL BY MODIFICATION OF AN EIGEN VALUE

Summary

The technique presented here aims at defining an active control system to stabilize a multiple degree of freedom coupling of modes on an aircraft.

This technique modifies only the value of the unstable root of the characteristic equation and keeps unchanged the corresponding eigen vector and the other generalized characteristics.

Considering this property, it is hoped that this method leads to the least possible interaction with the system.

I - INTRODUCTION

Le contrôle du flottement des avions est l'un des aspects de la doctrine C.C.V. dont la nécessité ne fait à présent aucun doute.

Cette nécessité ayant été dégagée il s'agit maintenant de rendre réalisables les principes qu'elle impose. Ainsi à l'ONERA, s'est posé naturellement le problème de définir, dans un cadre donné, le moyen de matérialiser les possibilités de contrôle du flottement.

Le cadre choisi, qui est loin d'être unique, est le suivant : on envisage un flottement fondamental sur une voilure munie d'une gouverne classique ; est-il possible de définir un moyen de contrôle qui, agissant par l'intermédiaire de la gouverne, supprime le flottement ?

L'idée de la construction de cette loi de contrôle est basée sur la remarque mathématique suivante :

soit une matrice A de valeurs propres λ , de vecteurs propres à droite $[V]$ de vecteurs propres à gauche U , on a alors la décomposition suivante :

$$A = [V]^{-1} \lambda [U]$$

soit λ_0, U_0, V_0^T une certaine valeur propre et ses vecteurs propres associés

alors la matrice $A + \nu U_0 V_0^T$

admet $\lambda_0 + \nu, V_0^T U_0^T$ comme nouvelle valeur propre et vecteurs propres associés. Cela permet d'envisager la possibilité de modifier une racine d'un système sans toucher aux vecteurs propres et aux autres racines, donc de peu perturber un système tout en le rendant stable.

II - DEFINITION DU MODELE REPRESENTANT LE FLOTTEMENT ET LA LOI DE CONTROLE

Le système suivant

$$(1) \quad \begin{bmatrix} \mu_{11} & \mu_{12} \\ \mu_{21} & \mu_{22} \end{bmatrix} \ddot{q} + \begin{bmatrix} \gamma & 0 \\ 0 & \delta \end{bmatrix} \dot{q} + PV^2 A q = \begin{bmatrix} \Gamma \theta_0 \\ 0 \\ \vdots \end{bmatrix}$$

donne les équations des petits mouvements de l'avion. q est la colonne des coordonnées généralisées où μ la matrice diagonale des masses généralisées.

La coordonnée θ représente le mouvement relatif de la gouverne et n'est pas en général orthogonale aux autres coordonnées, l'opérateur Γ est l'opérateur des forces aérodynamiques associées au mouvement et $\Gamma \theta_0$ représente la commande qui est un couple exercé sur la charnière de la gouverne.

Un certain nombre d'accéléromètres placés sur structure permettent d'identifier ses mouvements ou ses déformations. Nous supposons donc qu'à partir de ces mesures accélérométriques il est possible de remonter à la connaissance des coordonnées généralisées q_i .

Une mesure angulaire fournira par ailleurs la coordonnée θ

Effectuant la transformation de Laplace de (1),

on pose $D(s) = \mu s^2 + \delta q + PV^2 A(s)$

(s est le variable de Laplace).

La stabilité du système est définie par les racines de l'équation :

$$\text{Det}(D) = 0$$

Soit λ_i l'ensemble des racines stables, c'est-à-dire à partie réelle négative λ_i leur valeur conjuguée.

Soit λ_n une racine instable à la vitesse V on a par définition

$$\text{Det}(\lambda_n) = 0$$

Si l'on veut modifier la valeur de λ_n d'une quantité ν on aura donc :

$$\text{Det}(\lambda_n + \nu) \neq 0$$

Appelons V_n^T la première ligne de la matrice $D^{-1}(\lambda_n + \nu)$

Choisissons comme loi de pilotage la relation :

LOI DE CONTROLE

$$(2) \quad \Theta = \begin{bmatrix} K \frac{\prod_{i=1}^{n-1} (\frac{s}{V} - \frac{\lambda_i}{V}) \Delta^* V_n^T}{Q(\frac{s}{V})} + K^* \frac{\prod_{i=1}^{n-1} (\frac{s}{V} - \frac{\lambda_i}{V}) \Delta^* V_n^{T*}}{Q(\frac{s}{V})} \end{bmatrix} \begin{bmatrix} \theta \\ q_1 \\ q_2 \end{bmatrix}$$

$$\mu \dot{q} + V q + P V^T A q = \Gamma \Theta$$

$$\text{on } \prod_{i=1}^{n-1} \left(\frac{s}{V} - \frac{\lambda_i}{V} \right) = \left(\frac{s}{V} - \frac{\lambda_1}{V} \right) \dots \left(\frac{s}{V} - \frac{\lambda_{n-1}}{V} \right)$$

et $Q(\frac{s}{V})$ est un polynôme arbitraire de degré au moins égal à celui de \prod

On remarque que, pour le nouveau système d'équation :

- 1) les racines λ_i et les vecteurs propres associés sont inchangés
- 2) on peut choisir K pour que $\lambda_n + \nu$ soit la nouvelle valeur propre associée aux vecteurs propres de λ_n

Le dénominateur Q a été introduit uniquement pour avoir une loi représentable par une fraction rationnelle c'est-à-dire n'introduisant pas les dérivées des grandeurs mesurées.

Enfin il est logique de choisir ν de façon à n'agir que sur la partie réelle de λ_i , c'est-à-dire de façon à ne modifier que l'amortissement du système ce qui, en général, ne demandera que peu d'énergie.

III - APPLICATION

A partir des idées précédentes l'ONERA a décidé de réaliser un modèle en soufflerie pour étudier la faisabilité d'un système de contrôle et en vue d'étudier la sensibilité aux diverses perturbations et aux erreurs d'appréciation des paramètres.

Dans une première étape le modèle choisi est une aile rectangulaire montée à la paroi dans une soufflerie subsonique, voir figure n° 1.

Cette aile a été dimensionnée de façon à présenter un flottement flexion torsion vers soixante mètres seconde. Elle possède un gouverne dont la raideur est donnée par un moteur couple.

Ce moteur couple sert également à assurer le contrôle.

La réalisation matérielle de l'aile est actuellement en cours et le montage complet sera expérimenté en soufflerie au début de l'année 1974.

Des calculs de prévision de flottement pour cette aile sont réunis sur la figure n° 2 suivant la présentation classique à l'ONERA (fréquence et amortissement fonction de la vitesse).

Pour définir la loi de contrôle le dénominateur $Q\left(\frac{s}{V}\right)$ a été choisi de la forme

$$Q\left(\frac{s}{V}\right) = \left(\frac{s}{V} + \frac{1}{T}\right)^4$$

et on a décidé de rendre positive la partie réelle de la racine instable pour une vitesse de 75 m/s. On a donc refait le calcul de stabilité dans ces nouvelles conditions et les résultats sont résumés dans la figure n° 3.

Ces résultats amènent les commentaires suivants :

- 1) le flottement est bien contrôlé à 75 m/s
- 2) il l'est également entre 0 et 80 m/s, bien que la loi ait été établie seulement pour 75 m/s
- 3) le coefficient du terme en θ dans la loi calculée est extrêmement petit.

En conséquence on a simplifié la loi de commande en annulant le coefficient de θ ; les calculs ont donc été repris dans ces conditions et les résultats sont présentés sur la figure n° 4.

On peut constater le peu de sensibilité de ces résultats par rapport aux paramètres pris en compte.

n.b. Le fait que le contrôle établi à 75 m/s soit efficace sur plage (0 - 80 m/s) est une circonstance heureuse qui n'est pas une conséquence de la théorie. Dans d'autres problèmes il faudrait peut-être envisager une évolution des coefficients de la loi de contrôle en fonction de la pression dynamique et du nombre de Mach.

CONCLUSION

La méthode présentée ici est simplement une technique permettant de stabiliser un avion ayant un flottement à une certaine vitesse.

Cependant dans le cadre de la doctrine C.C.V. elle présente l'avantage important de ne pas interférer avec les autres systèmes de contrôle.

En effet si d'autres racines ont été modifiées, pour des raisons de pilotage par exemple, la méthode proposée ne les modifiera pas, à condition, bien sûr, qu'on les prenne en compte.

Signalons enfin que cette méthode peut être utilisée pour d'autres contrôles que celui de flottement, par exemple pour la stabilisation d'un avion à marge statique négative.

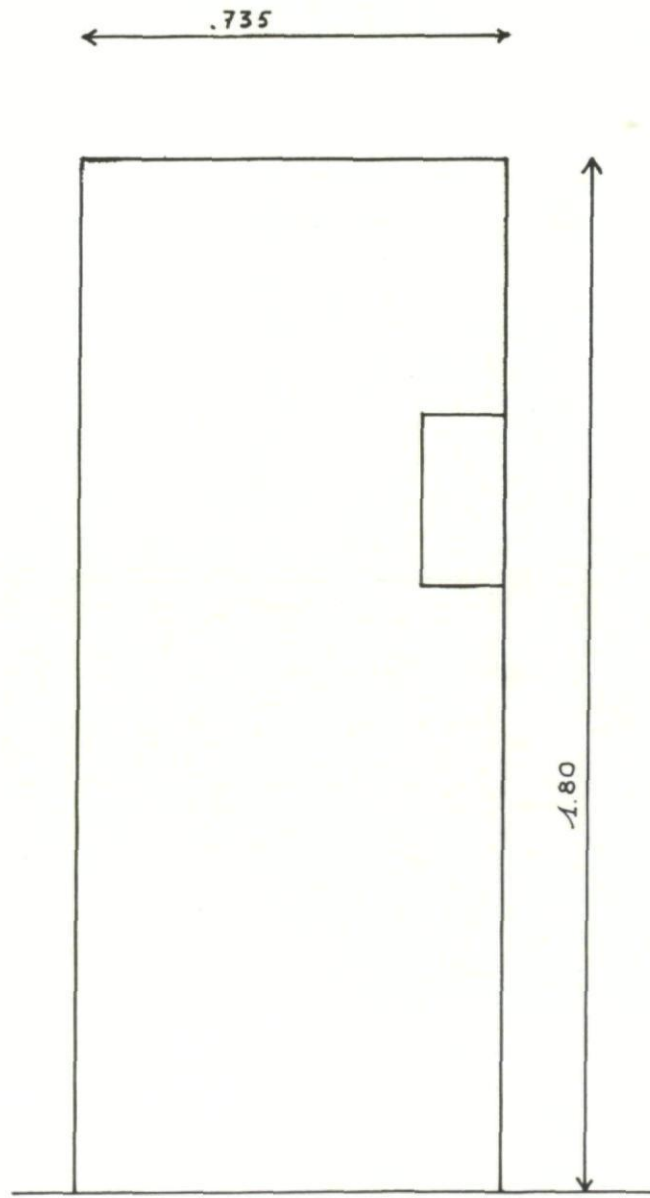


Fig.1 Dimension du modèle de soufflerie prévu pour 1974

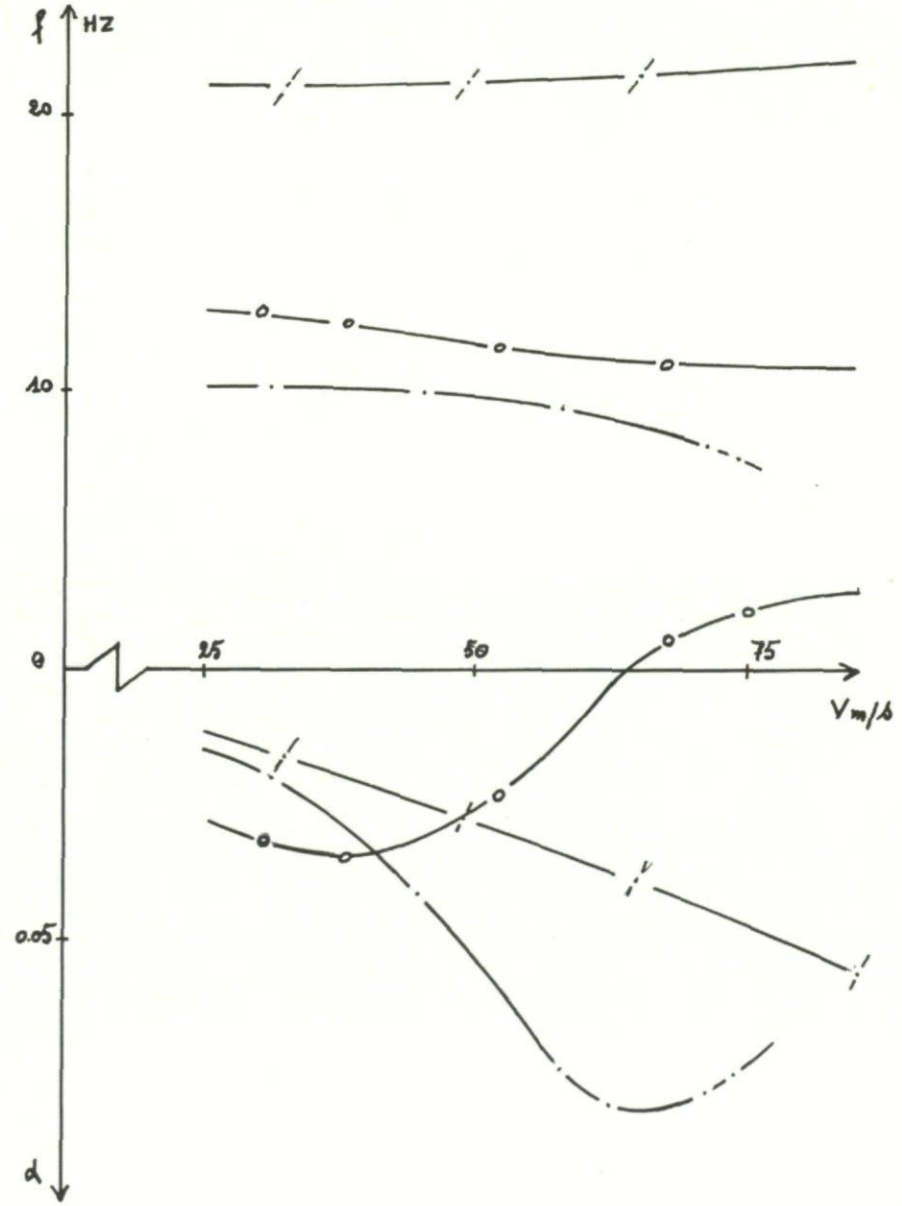


Fig.2 Calcul classique

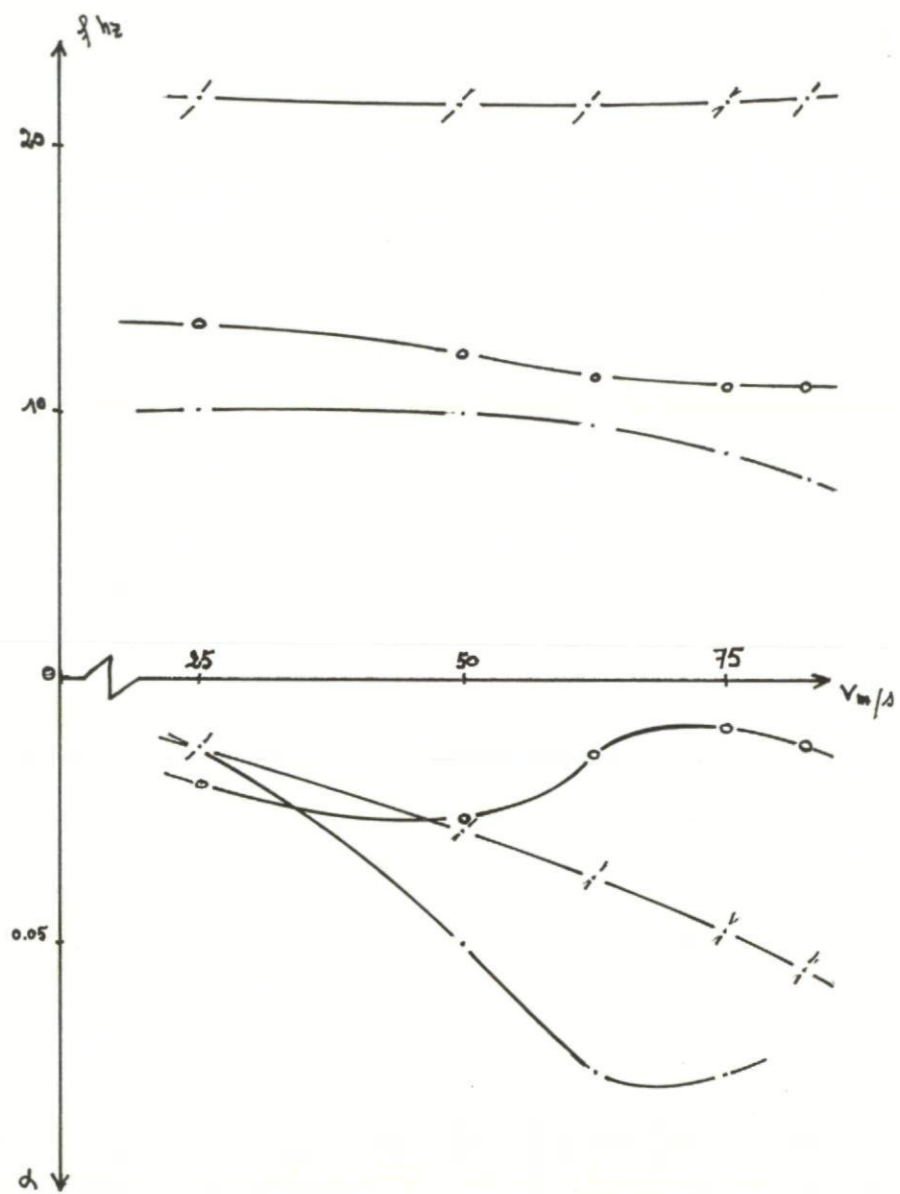


Fig.3 Avec controle

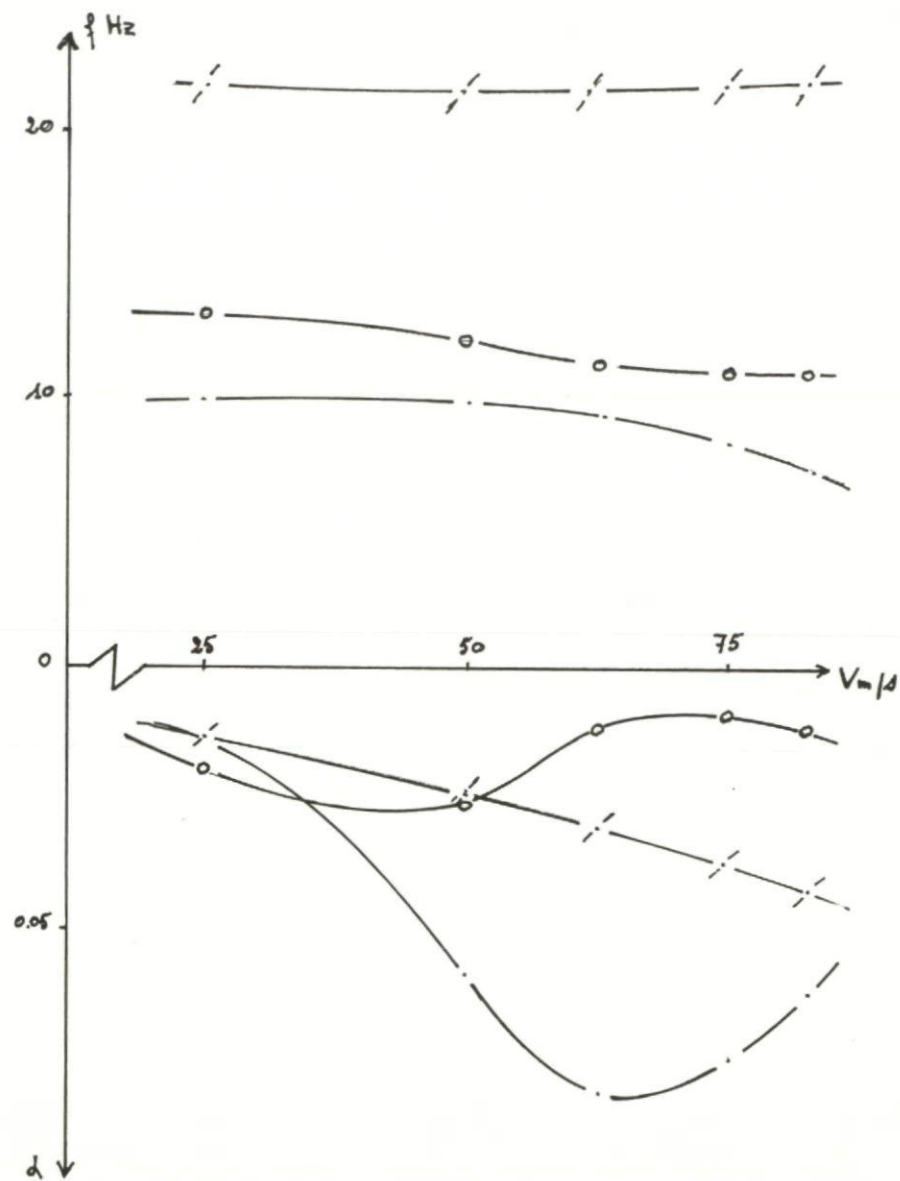


Fig.4 Avec controle simplifié

ACTIVE FLUTTER SUPPRESSION ON WINGS WITH
EXTERNAL STORES

by

G.Haidl, A.Lotze and O.Sensburg

Messerschmitt-Bölkow-Blohm GmbH
Unternehmensbereich Flugzeuge
Postfach 801160
8 München, 80, Germany

SUMMARY

A control system is described, which is able to suppress flutter of wing-external store combinations. The aerodynamic flutter suppression forces are generated by movable vanes, attached to the stores, which are moved by a feedback signal from the store motion in such a way, that these forces damp the store motion.

By adjusting the phase of the servoloop it is possible to have an active flutter-system below the flutter-speed of the passive system. This arrangement can be used to excite the flutter-mode at subcritical speeds. By switching off the servoloop, damping and frequency can be evaluated.

The active flutter suppression system can also be used for reducing the level of externally forced vibration on stores which could occur through excitation by buffet or gusts.

Tests results for an elastic wind-tunnel model are given and compared with analytical predictions. Correlation is very good, considering the complexity of the problem.

ACTIVE FLUTTER SUPPRESSION ON WINGS WITH EXTERNAL STORES

G.Haidl, A.Lotze and O.Sensburg

1. INTRODUCTION

External store carriage on wings of variable geometry fighters is posing a huge problem to the flutter analyst. Due to varying weight and inertia of stores together with changing wing sweeps and increased flight envelopes, no external store position on the wing nor a suitable store attachment stiffness can be selected that would make all possible stores flutter free. Stiffness increase or mass balance requirements penalize the aircrafts performance. Active flutter suppression (AFS) is a possible and promising solution to the problem.

A system which is capable of suppressing wing store flutter was developed and tested on a subsonic wing tunnel model in the flutter tunnel of the Eidgenössisches Flugzeugwerk in Emmen.

The control system drives a vane, attached to a store, controlled by a feed-back signal in a way so that it counteracts the store motion. The developed mechanism can also be utilized for conventional flight flutter testing excitation techniques, such as frequency sweep or harmonic signals, in addition to providing a method for quickly finding the frequency and damping of the flutter mode. Another application of the system is the reduction of external store amplitudes created by buffet or air turbulence, thus increasing the fatigue life of wing attachments, improving the target aiming of weapons and enhancing the clearness of pictures shot by reconnaissance cameras in wing mounted pods.

This paper concentrates on the development of a flutter suppression system, gives a mathematical description of it and shows the different applications on a dynamically scaled wind tunnel model. No attention is paid to the implementation of the system in an already existing flight control augmentation system such as is usually available on modern fighters. This aspect is covered to some extent in (1) and (2). There are indications from (2), that it might not be possible to use the already existing CSAS because of couplings introduced by the sensor mountings in the fuselage.

2. FLUTTER CONFIGURATION AND MECHANISM

Several configurations varying the number of stores and the sweep angle were tested. Analytical comparisons were only performed for a wing leading edge sweep angle of 45° .

Two flutter modes occur containing mainly the properties of the still air modes (Fig.1). One flutter mode can be described as the classical wing bending-torsion, store pitch flutter. The other flutter mode is a problem mainly introduced by the relatively low yaw attachment stiffness which is inherent on variable geometry airplanes.

The fore and aft motion of the wing (not producing any considerable unsteady aerodynamic forces), together with the large mass of the store hanging below the wing, induces a torsional angle on the wing which produces unsteady aerodynamic forces that can cause flutter together with the wing bending mode unsteady air force.

3. VANE EXCITATION AND CONTROL SYSTEM

Excitation created by oscillating aerodynamic vanes is considered to be the most effective way of exciting low frequency vibration modes. These vanes, together with a driving and control system, can be easily installed in empty fuel tanks. The different stages of fuel loading, simulated by masses installed in the tank whose distance from each other can be varied, can represent the mass and inertia properties of all stores that are considered to be flutter critical.

The vane system must fulfill the following tasks:

1. It must follow any specified input signal given to it, i.e., fixed frequency sine wave, variable frequency sine wave, stochastic signals, shocks (open loop operation).
2. It must either excite vibration modes or suppress flutter modes by a suitable control circuit (closed loop operation).

This vane system used on an aircraft would be driven by an electro-hydraulic energy source. For the model tests, an electro-dynamic system was used. Considering the frequencies involved there seems to be no major difference in those two systems.

Two electrical torque motors per tank were chosen for driving the vanes. The maximum total moment of the two motors working together was 480 cm p. The mass moment of inertia is $60 \cdot 10^{-4}$ cm p.sec², the motor weight being 109 gr per motor. A metal-balsa wood construction of vanes of different shapes and dimensions was used. The rotation axis was at 26% of the chord to minimize the aerodynamic moment. The angular position of the vane was controlled by a Hall generator which produces a voltage proportional to the angle. The maximum angle is $\pm 15^\circ$. The vane was located at the forward tank end in order to provide an undisturbed flow. It was also possible to turn the whole tank around, so that the vanes were at the rear tank end. Weight, radius of gyration and center of gravity of the tank could be varied independently. Figure 2 shows the tank with different vanes.

In Figure 3 a schematic picture of the AFS is given.

The ideal control law is described in Equation (5). The realized function is depicted in Figure 4.

From this figure it can be readily seen that the ideal control law is fulfilled in the frequency region of interest from 6 Hz to 8 Hz. It was possible to feed the integrated differential sensor signal ($\bar{z}_1/i\omega - \bar{z}_2/i\omega$) into the system, thus compensating for a translatory motion or to use only the signal of one sensor $\bar{z}_1/i\omega$. For the latter case the gain was halved. The angular position of the vane can only be controlled as long as the available moment of the servo motor is higher than the externally applied moment. This condition was always fulfilled in the tests. It should be considered that the vane angle must not be greater than the vane stall angle for the AFS to be effective.

4. ANALYTICAL MODEL

A vibration analysis was performed using component branch modes as generalized coordinates. Three-dimensional unsteady aerodynamic forces for the wing and the vanes were calculated. No aerodynamic forces on the tank and no interference air forces between wing, vane and tank were considered. Equation (1) describes in general the motion of the complete aeroelastic system including a control system. All generalized terms of Equation (1) are dimensionless

$$\left(\frac{p^2}{\omega_r^2} [M_{qq}] + \frac{p}{\omega_r} \cdot \frac{\rho/2A}{m_r \omega_r s} \cdot \frac{s}{k} \cdot v \cdot [C''_{qq}] + [K_{qq}] + \frac{\rho/2A}{m_r \omega_r s} \cdot v^2 \cdot [C'_{qq}] \right) \{q\} = [F_{q\alpha}] \{\alpha\} \quad (1)$$

where: $m_r \omega_r$ = reference mass and frequency

s = semispan of reference plane

A = area of reference plane

v = true air speed

$k = \frac{\omega s}{v}$ = reduced frequency

α = generalized coordinate of the control mode

q = generalized coordinates of the free airplane modes

p = $i\omega$ or d/dt respectively

C', C'' = real and imaginary part of the generalized air force coefficients

M = generalized mass

K = generalized stiffness

F = generalized forces

The right-hand side product of Equation (1) vanishes for the uncontrolled case.

If external forces generated by the control mode α are being introduced into the aeroelastic system, the right-hand side term $F_{q\alpha}$ is replaced by expression (2).

$$[F_{q\alpha}] = -\frac{p^2}{\omega_r^2} [M_{q\alpha}] - \frac{p}{\omega_r} \frac{\rho/2A}{m_r \omega_r s} \cdot \frac{s}{k} \cdot v \cdot [C''_{q\alpha}] - \frac{\rho/2A}{m_r \omega_r s} \cdot v^2 \cdot [C'_{q\alpha}] \quad (2)$$

For the controlled system the generalized coordinate of each control surface mode is a frequency dependent function of the structural displacements at the sensor location.

Considering only second order transfer functions

$$(T_4^* + pT_5^* + p^2T_6^*)\alpha = (|T_1^*| + p|T_2^*| + p^2|T_3^*|)\{q\} \quad (3)$$

for the analytical representation of each control loop, Equations (1), (2) and (3) can be combined to form the matrix system (4)

$$\left(\frac{p^2}{\omega_r} \begin{bmatrix} M_{qq} & M_{q\alpha} \\ T_3^* & T_6^* \end{bmatrix} + \frac{p}{\omega_r} \left(\frac{\rho/2A}{m_r \omega_r s} \cdot \frac{s}{k} \cdot v \cdot \begin{bmatrix} C''_{qq} & C''_{q\alpha} \\ 0 & 0 \end{bmatrix} + \begin{bmatrix} 0 & 0 \\ T_2^* & T_5^* \end{bmatrix} \right) + \begin{bmatrix} K_{qq} & 0 \\ 0 & 0 \end{bmatrix} + \frac{\rho/2A}{m_r \omega_r s} \cdot v^2 \cdot \begin{bmatrix} C'_{qq} & C'_{q\alpha} \\ 0 & 0 \end{bmatrix} + \begin{bmatrix} 0 & 0 \\ T_1^* & T_4^* \end{bmatrix} \right) \begin{bmatrix} q \\ \alpha \end{bmatrix} = 0 \quad (4)$$

Using the QR-Algorithm, a computer program was used to solve Equation (4) for the complex eigenmodes and the corresponding complex eigenvalues.

Only symmetrical modes were considered because the mode was fluttering symmetrically.

In order to provide sufficient damping in the structural modes picked up by the sensor, the control system was designed to produce amplitudes of the vane displacement proportional to the velocity of the store oscillations over the frequency region of interest.

Equation (5) describes this relationship

$$\frac{\phi_{\text{control}}^{(\alpha)} \cdot \alpha}{\phi_{\text{sensor}}^{(q)} \cdot \dot{q}} = K \cdot e^{i\Delta\varphi} \quad (5)$$

where $\phi_{\text{sensor}}^{(q)}$ = local displacement at the sensor location in a free airplane mode q_i
 $\phi_{\text{control}}^{(\alpha)}$ = angular displacement of the vane in the control mode α .

The nominal value of K gives a ratio of angular displacements of vane and store of 8.5 at 8 (Hz). The nominal value of $\Delta\varphi$ is zero at 8 (Hz).

The phase setting $\Delta\varphi$ was provided in the model for corrections of possible phase shifts between the vane displacements and the unsteady air forces generated by the control mode α .

Using the measured transfer function of the total control loop, the control equation can be approximated by (6).

$$\phi_{\text{control}}^{(\alpha)} \cdot \alpha - (T_1 + pT_2)|\phi_{\text{sensor}}^{(q)}|\{q\} = 0 \quad (6)$$

Using Equation (6) the constants of (4) can be defined:

$$\begin{aligned} |T_1^*| &= -T_1 |\phi_{\text{sensor}}^{(q)}| \\ |T_2^*| &= -T_2 |\phi_{\text{sensor}}^{(q)}| \\ T_4^* &= \phi_{\text{control}}^{(\alpha)} = 1 \\ |T_3^*| &= 0 \\ T_5^* &= T_6 = 0 \end{aligned}$$

All calculations were performed for a wing sweep position of $\lambda_{WG} = 45^\circ$. For the system with AFS, two vanes (defined as standard vane surface) on each store tank were introduced into the calculations. In general, the forward stations of the store tank are used for location of sensor and vanes.

Because test results were only available for $Ma = 0.2$, most of the calculation was performed for this Mach number. In order to show the efficacy of the AFS at higher Mach number, unsteady aerodynamic forces for $Ma = 0.9$ were also introduced.

In the analysis the effect of the gain and the phase shift of the control system was investigated and depicted in $v-g$ and root locus plots. The application of the AFS to the classical wing-store pitch bending flutter problem was demonstrated by eliminating the wing pivot yaw mode.

5. WIND-TUNNEL TESTS

Dynamically scaled subsonic wind-tunnel flutter models are used to a large extent at MBB for flutter investigations³.

These tests are made at the flutter wind tunnel of the Eidgenössisches Flugzeugwerk in Emmen. This tunnel has a quick stop facility which allows an increase in speed until flutter occurs without destroying the model. At the flutter point, the frequency is measured and the flutter mode visually inspected and filmed.

For the mild flutter cases, existing when external stores are attached to the wings, there was a strong desire to also measure the damping trends by exciting the model, thus being able to exactly define the flutter point. This exact definition is especially needed for comparison of analytical and test results. Since the model is free flying in the wind tunnel (held by a rod and supported by an air spring), the excitation system had to be built into the model. The vane excitation system, shown in Figure 3 was installed in the external stores.

Another vane was attached to the forward fuselage, to be able to excite the model with the AFS (Automatic Flutter Suppression) switched on.

Several ways of damping and frequency evaluation were tested, considering later application to full-scale flight flutter testing. Producing vector plots (Fig.5) with harmonic excitation or using excitation switch-off decays is too time consuming, because the system takes too long to get to a steady state response due to the low frequencies and dampings involved. Evaluation of frequency sweep responses by statistical methods was more economic. Using transportable special purpose computers the damping trends can be monitored quasi on line by evaluation of the auto-correlation function of the response. A more detailed description of the method is given in (4).

Figure 6 shows a model response to a frequency sweep.

A very powerful method was used during the test. For this method the phase of the AFS vane forces is shifted 180° so that essentially an unstable system is created. This AFE (Automatic Flutter Excitation) has two outstanding advantages:

1. It is automatically tuning the frequency into the store flutter mode providing a suitable sensor signal.
2. Switching off the AFE, one can easily evaluate damping from the logarithmic decrement of the response. In comparison to the frequency sweep response, which cannot be analysed without the help of computers, the signals produced by the AFE can be used directly by the engineer.

Figure 7 shows an application of AFE. Because the model is free flying in the tunnel a high angle of attack could be simulated that caused wing stall and a high noise environment. Figure 8 shows that the AFS reduces the response of the store considerably. The wing response is not attenuated as much. This is due to the fact that the wing mainly responds in its bending mode. Very little damping force can be introduced into this mode at the wing pylon station.

6. AFS APPLICATION WIND-TUNNEL TEST RESULTS

In Figure 9 the measured damping versus velocity is plotted for different phase angles. This picture shows that about 50% increase on flutter speed can be gained by the AFS-system. It is also shown that the 0° phase is nearly optimal.

This could be expected, because there is little phase shift at a frequency of 8 Hz between unsteady aerodynamic force and angle of attack on the vane. Figure 10 shows the measured damping versus velocity for ½ the standard vane area for different phase angles. The aerodynamic damping produced by the AFS (0° phase) is about halved. Figure 11 depicts the damping behaviour for a gain of the AFS of two times nominal and nominal with vane B (see Figure 2). All these measurements were performed with a wing leading-edge sweep angle of $\Lambda_{WG} = 25^\circ$.

7. ANALYSIS RESULTS AND COMPARISON WITH TEST

All analyses were performed with zero structural damping for a wing leading-edge sweep angle $\Lambda = 45^\circ$.

In Figure 12 a comparison of measured and calculated damping values for a configuration with $\Lambda_{WG} = 45^\circ$ is given. The calculated damping values are taken from $v - g$ plots, Figure 13 and Figure 15. Two percent of structural damping was added to mode 2 damping, because the drag force is creating additional damping when the model is supported on its rod in the tunnel. Considering the complicated flutter mechanism, correlation of test and analysis is very good. The analysis underestimates the tunnel flutter speed only by about ten percent (AFS off) and gives the same damping trend (AFS off and on).

Figure 13 and Figure 14 show the calculated damping and frequency versus velocity for $Ma = 0.2$ and $Ma = 0.9$. These two figures demonstrate that there is no pronounced Mach number effect existent, so that for the external store configuration used, the wind-tunnel tests would be representative for the full-scale aircraft. In both figures the relatively mild flutter of mode 2 and the strong flutter of mode 3 can be seen. The $v - g$ plots for AFS on for $Ma = 0.2$ and $Ma = 0.9$ are shown in Figure 15 and Figure 16. Both flutter modes are damped now. The bending mode 1 is very little affected by the AFS. Flutter speed versus gain K of the AFS is depicted in Figure 17. Here it can be seen that for a specific gain setting (about 75% of nominal) there is no more flutter for mode 2. Flutter speed of mode 3 is increased by increasing the gain. For both modes 2% structural damping was considered.

Figure 18 and Figure 19 shows root loci for a variation of K and $\Delta\varphi$ respectively. From Figure 18 one can see that mode 2 and mode 3 are strongly affected by AFS, whereas mode 1 is almost unaffected. Varying the phase φ in Figure 19 shows that mode 1 damping can also be changed with varying phase of AFS. Figure 20 shows an application of AFE. For evaluation of dampings of mode 2 and mode 3, different sensors would be necessary.

Figure 21 shows, in comparison with Figure 15, that there would be no difference in effectiveness of AFS if the vane and sensor are located at the store rear or forward end. This result stems from using linear aerodynamic effects. There are indications from test results, that there could be a pronounced effect, depending upon whether the vane was located in the undisturbed flow stream at the store forward end or at the relatively disturbed flow at the store rear end.

Figure 22 shows the $v - g$ plot for the classical wing bending/store pitch flutter problem by deleting the wing pivot yaw mode.

In Figure 23 the damping and frequency with the AFS on is plotted. Figure 24 shows the effect of AFE. These three figures are only given to show that AFE could be applied directly, without separating different modes by different sensors for fixed geometry airplanes.

8. CONCLUSIONS

It was shown, that a relatively simple control system could be developed and tested on a wind-tunnel model to suppress flutter.

The main reason that the AFS is so effective with relatively small vanes that do not change the flight mechanical characteristics is that mild flutter, very susceptible to small damping changes, occurs when large masses are involved in the flutter phenomenon.

This system was also very valuable in exciting model modes. Very interesting aspects of extension of existing flutter testing techniques were illuminated.

REFERENCES

1. Triplett, W.E. *A Feasibility Study of Active Wing/Store Flutter Control*. J. Aircraft, June 1972.
2. Triplett, W.E., et al. *Active Flutter Control*. 11th AIAA Meeting, Washington, D.C., January 1973.
3. Seidel, W. *Flatteranalyse im frühen Entwurfsstadium mit Hilfe eines Unterschallflattermodells und parallellaufender Rechnungen*. Jahrbuch 1967 der WGLR.
4. Otnes R.K., Enochson, L. *Digital Times Series Analysis*. John Wiley & Sons, London.

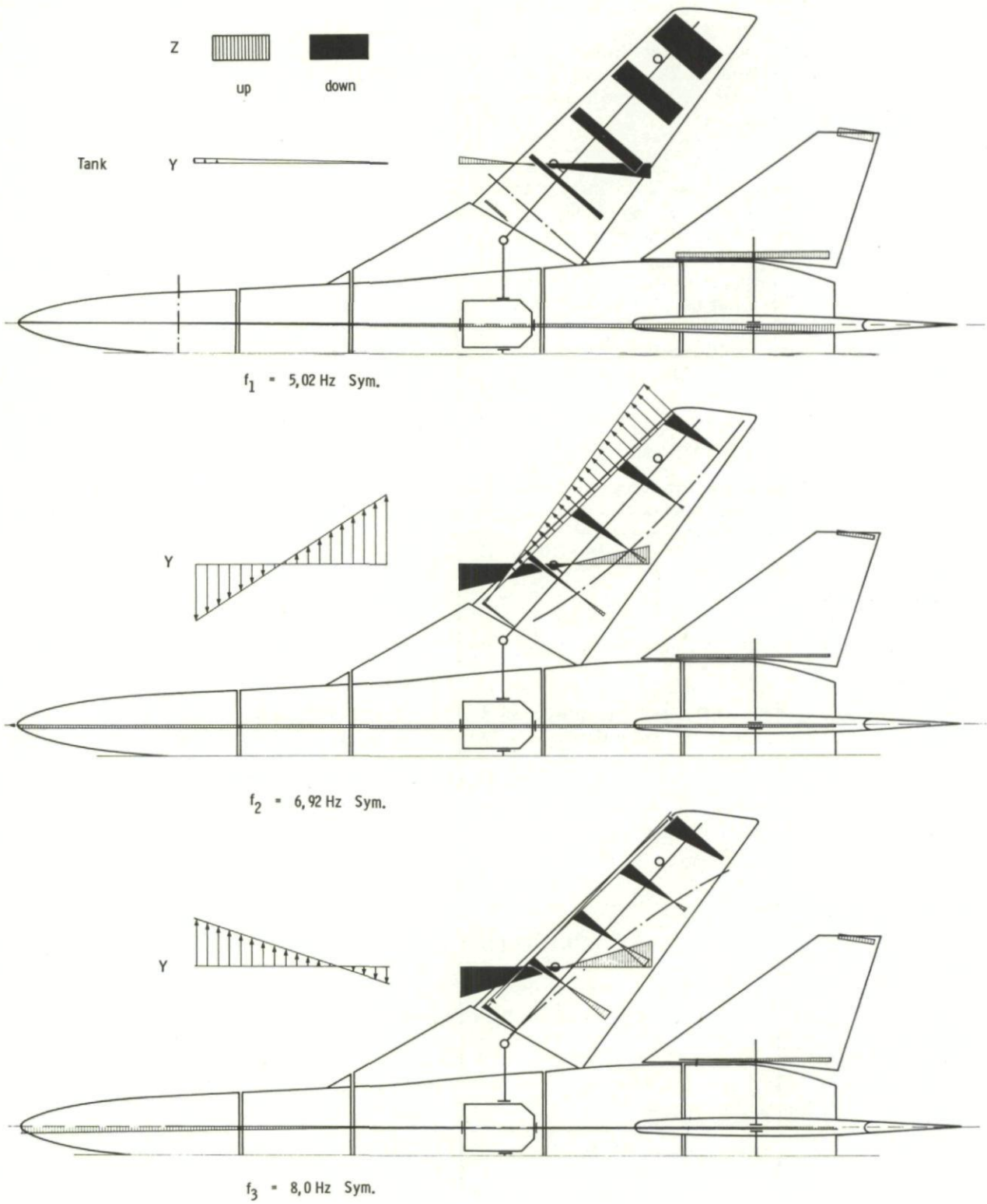


Fig.1 Measured modes with inboard tanks $\Lambda_W = 45^\circ$

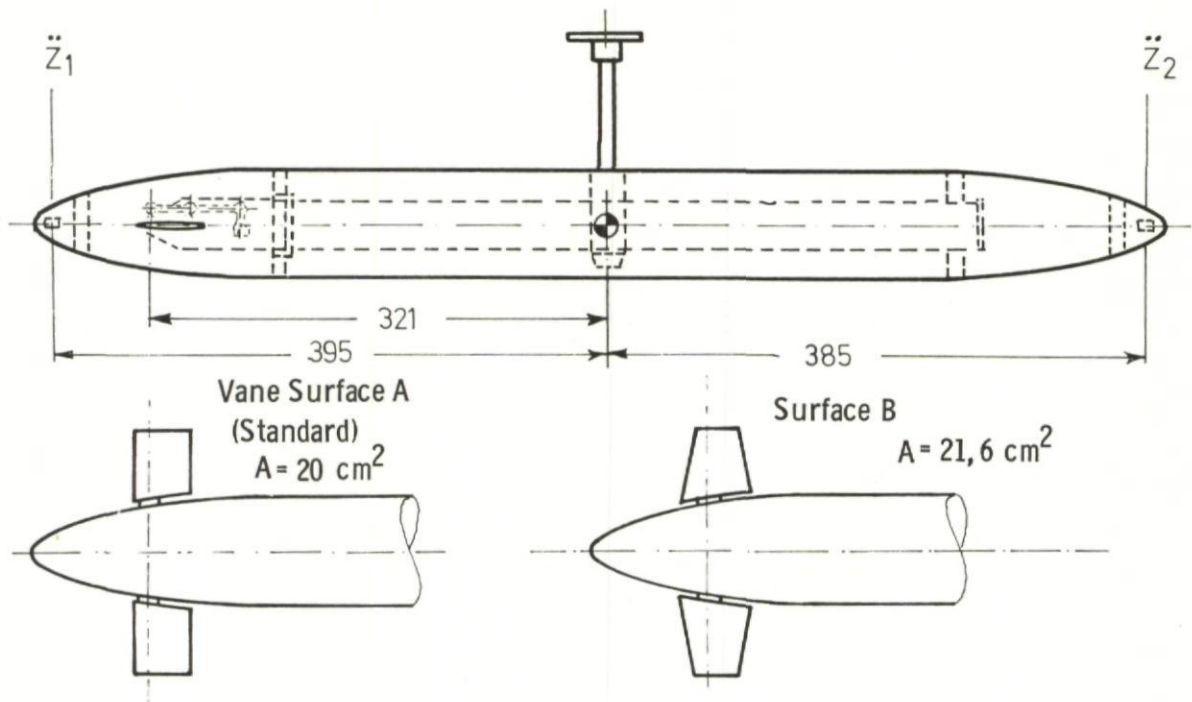


Fig. 2 Vane-tank

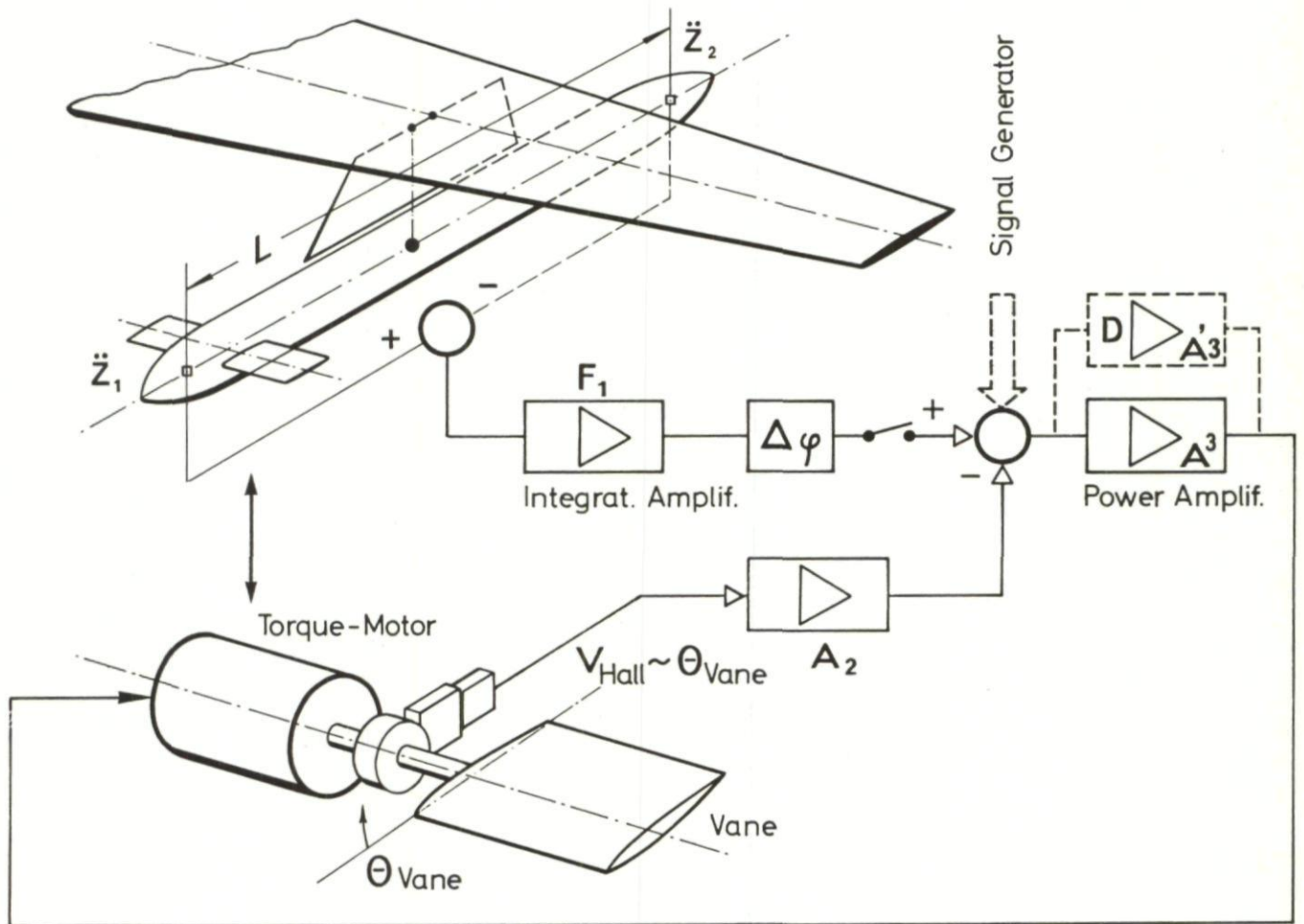


Fig. 3 Block diagram of the vane control system

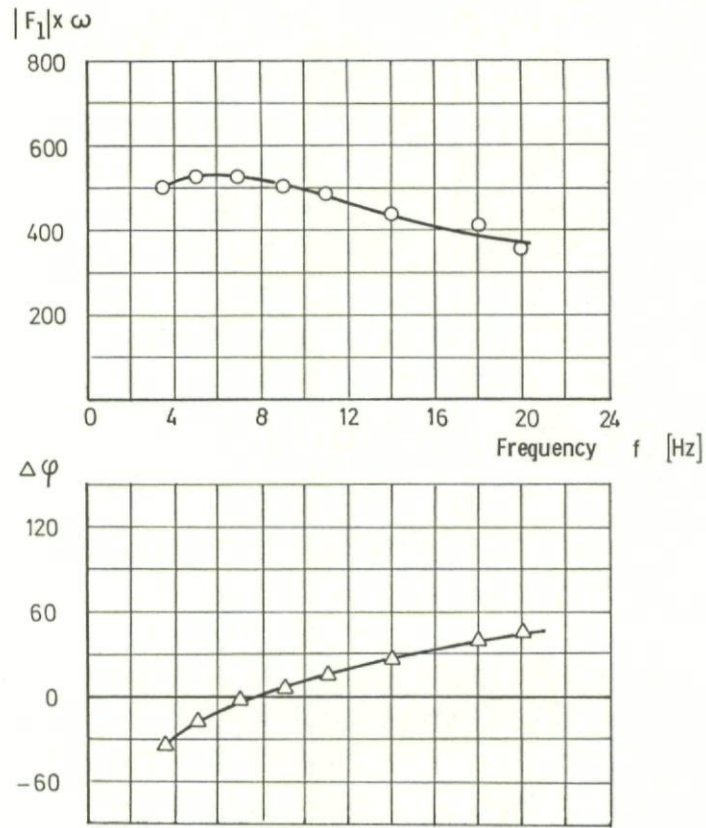


Fig.4 Transferfunction $F_1 \times i\omega$

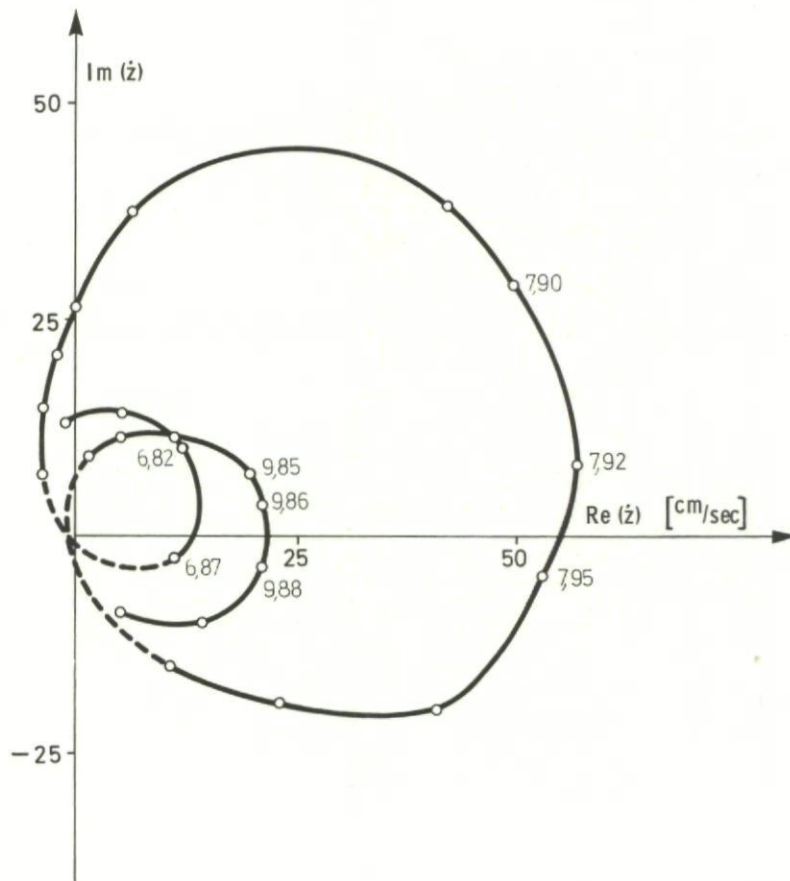


Fig.5 Vector plot at $V/V_{Ref} = 1.11$ $\Lambda_{wing} = 45^\circ$ pickup and vane exciter in rear tank position

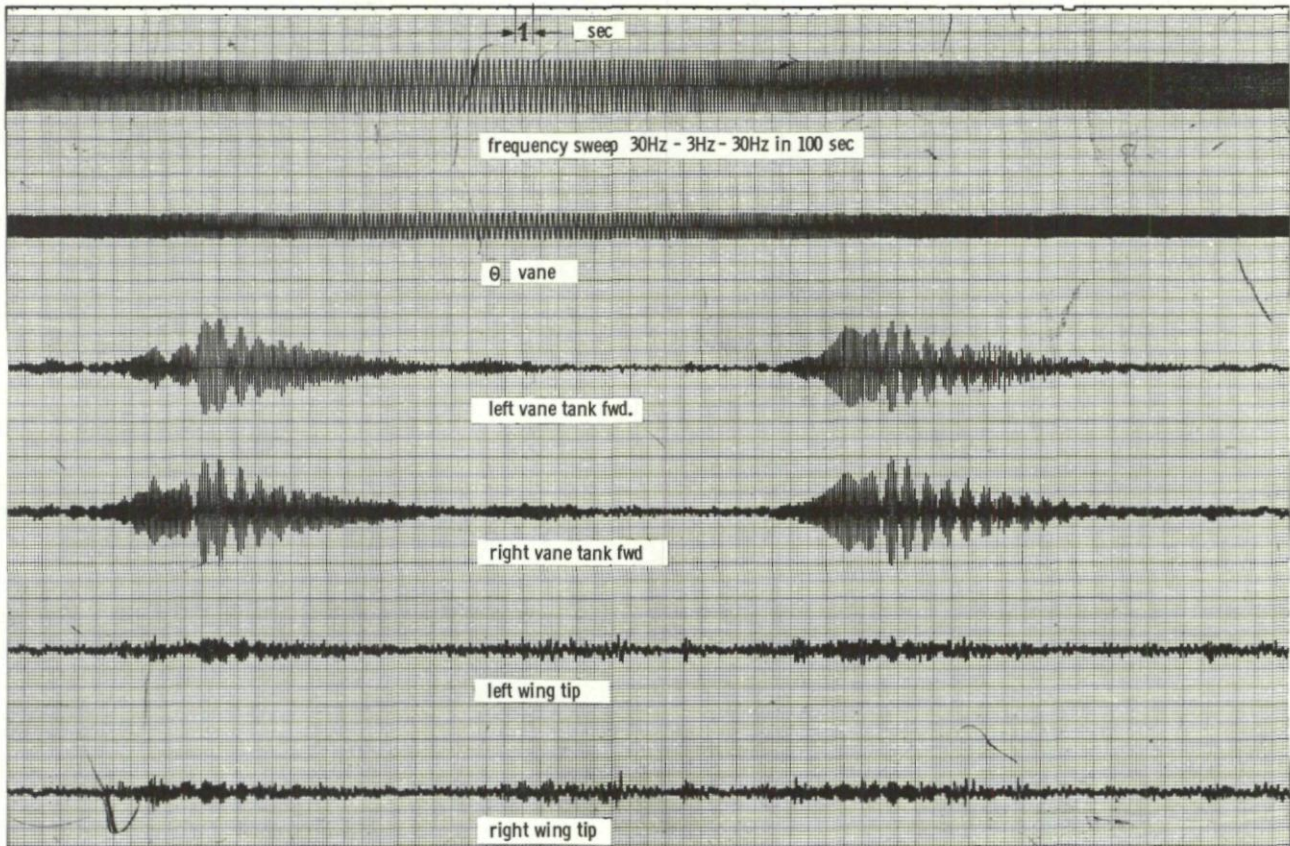


Fig.6 Model responses \dot{Z} to frequency-sweep system excitation with tank vanes $WG = 25^\circ V/V_{Ref} = 0.95$

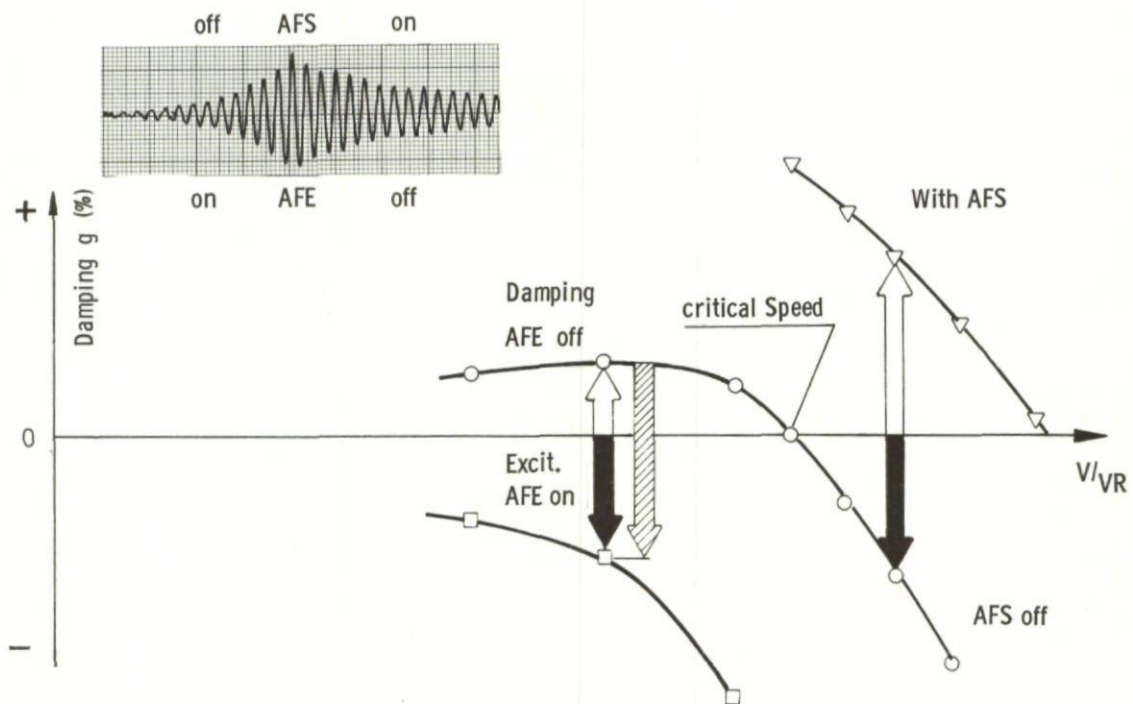


Fig.7 Application of AFE and AFS for damping measurements (MBB patent application P 23493541)

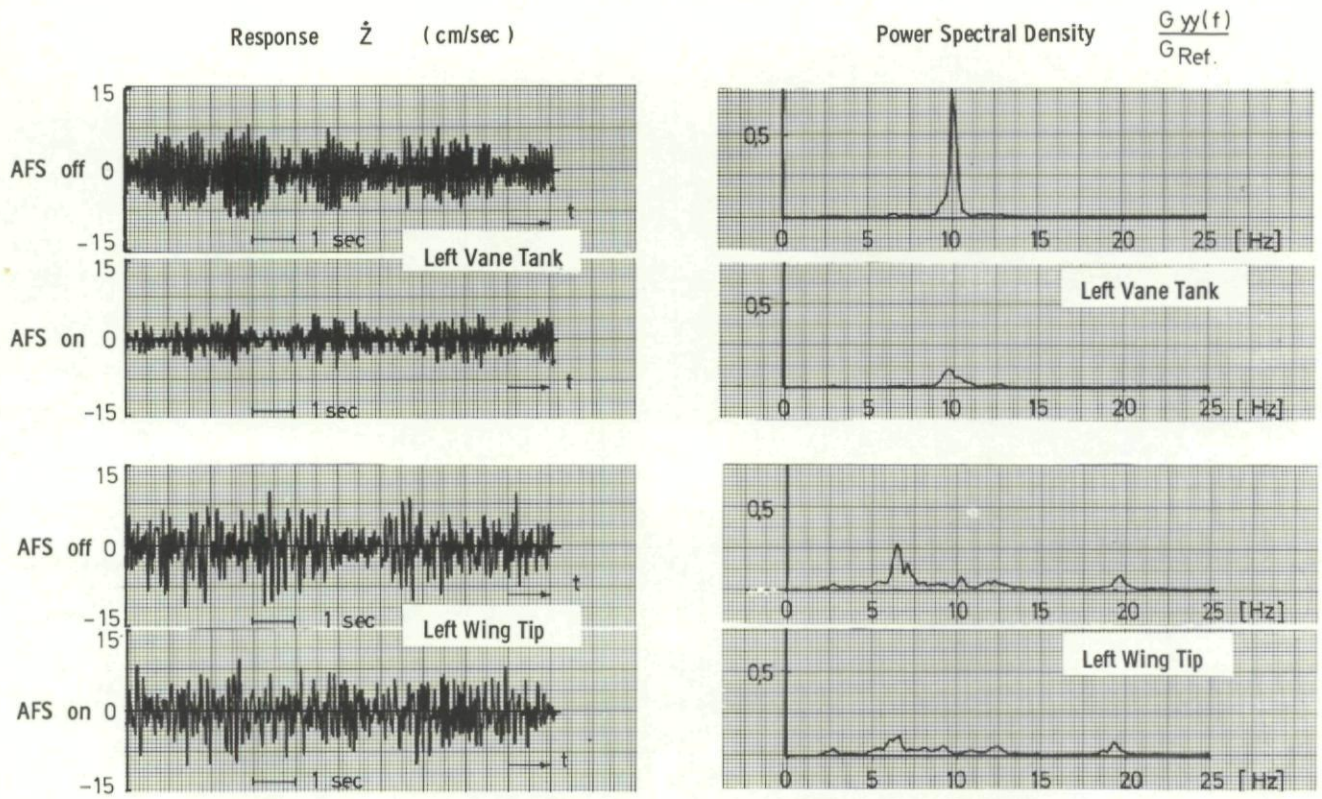


Fig.8 Model response at 12° angle of attack AFS off and on $V/V_{Ref} = 0.77$

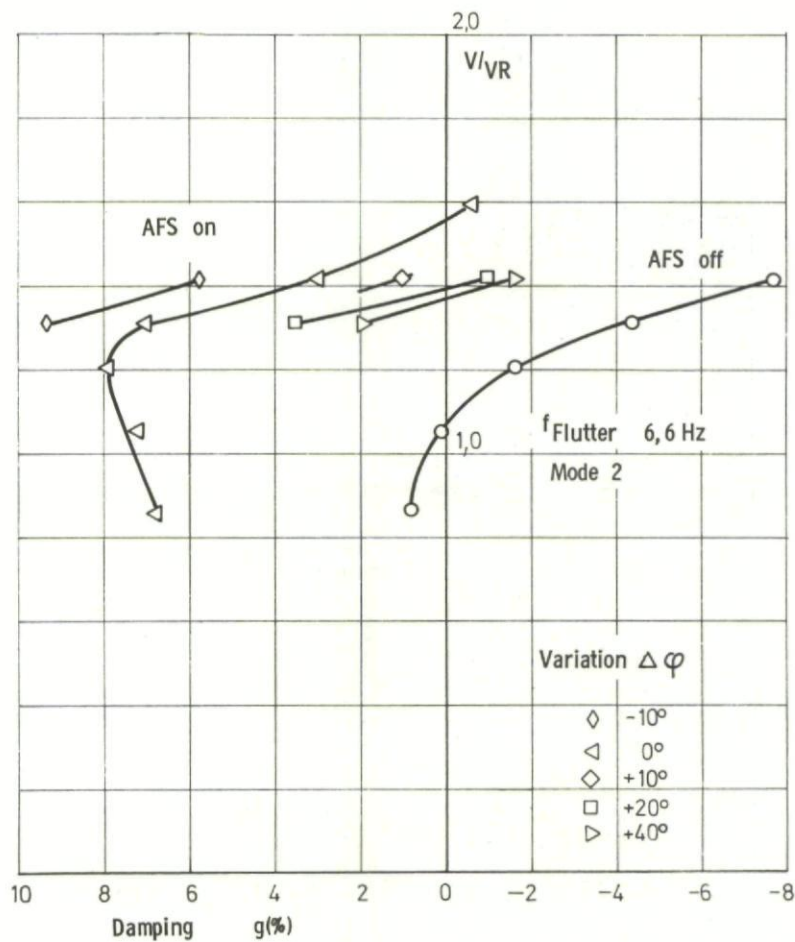


Fig.9 Measured damping versus velocity, $\Lambda_{WG} = 25^\circ$, sensor \dot{z}_1 , vane area = standard

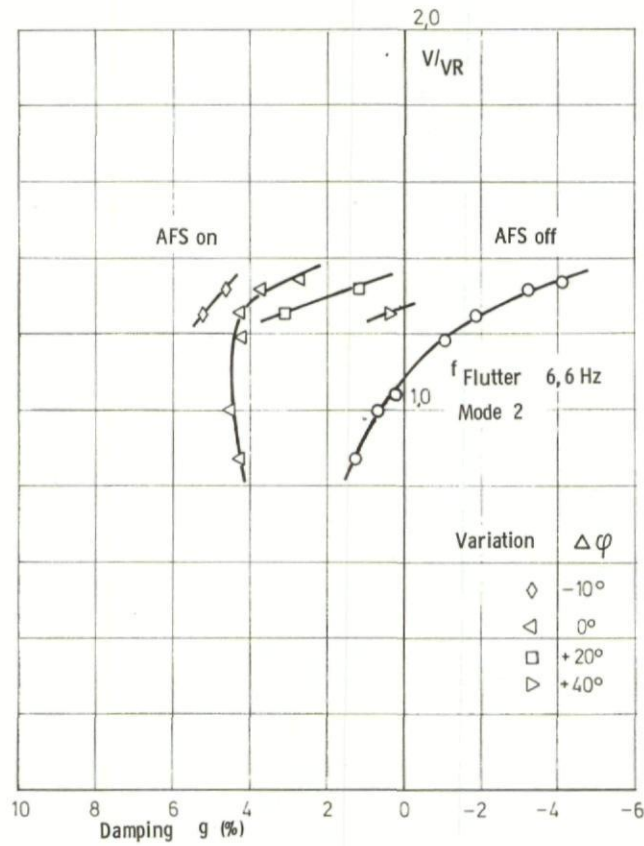


Fig.10 Measured damping versus velocity, $\Lambda_{WG} = 25^\circ$, sensor \ddot{z}_1 , vane area = 0.5 standard

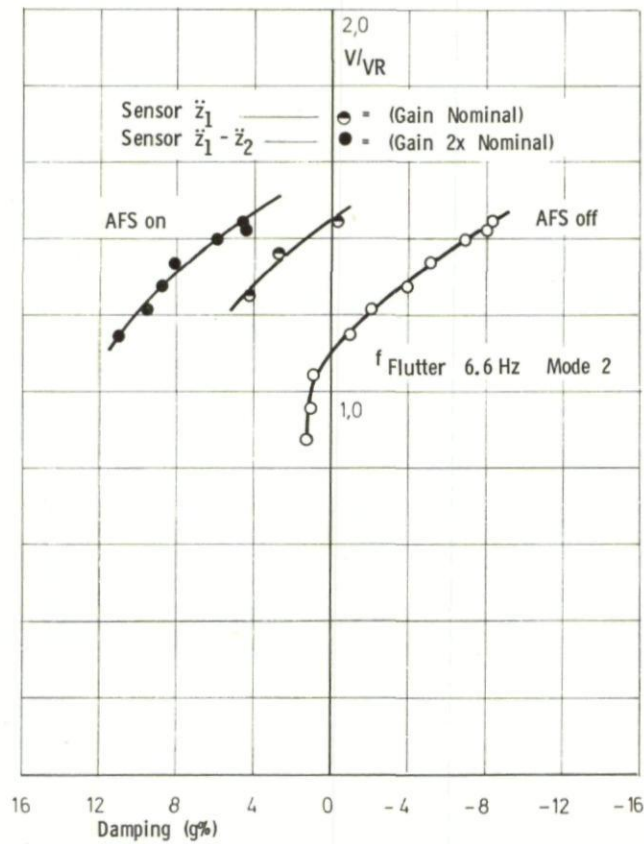


Fig.11 Measured damping versus velocity, $\Lambda_{WG} = 25^\circ$, vane area = 0.54 of standard, (surface B)

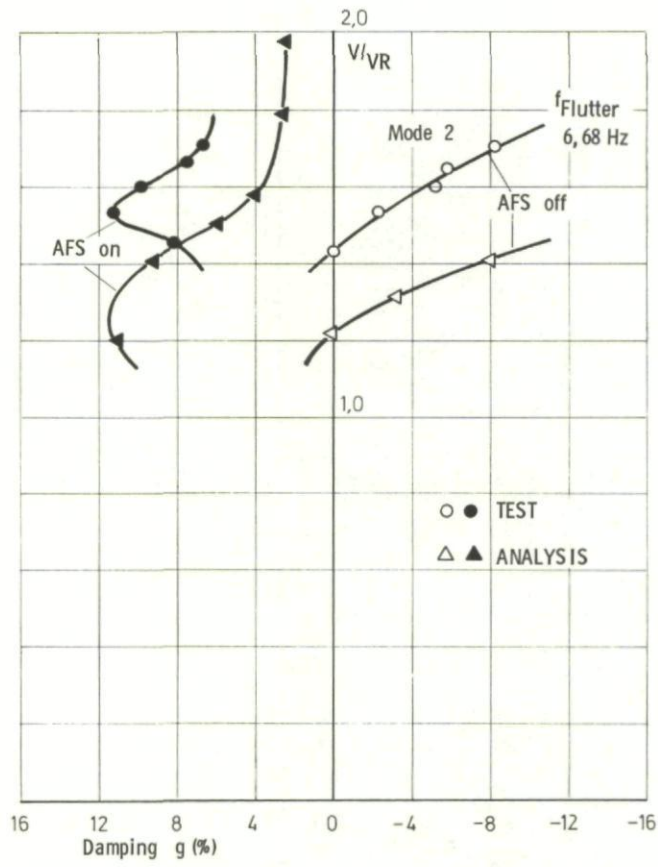


Fig.12 Comparison of measured and calculated damping versus velocity $\Delta_{WG} = 45^\circ$

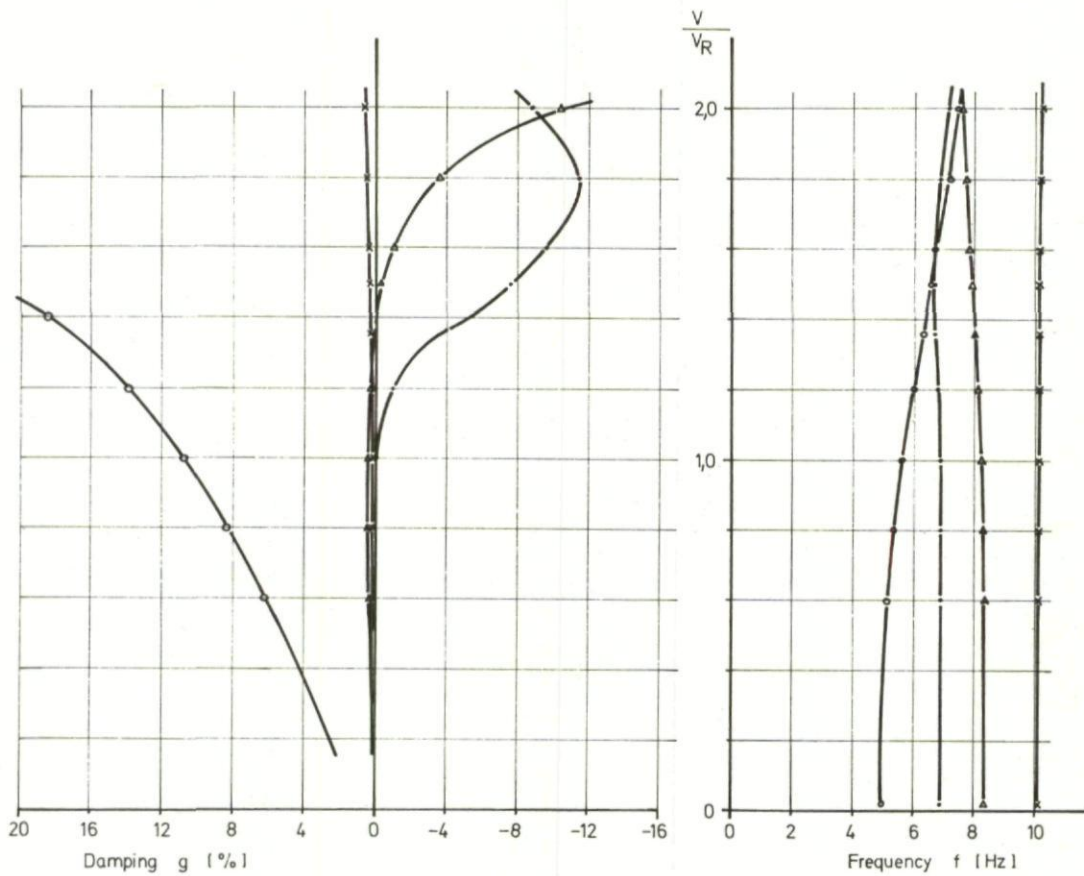


Fig.13 Damping and frequency versus velocity for $Ma = 0.2$ (AFS off), $\Delta_{WG} = 45^\circ$

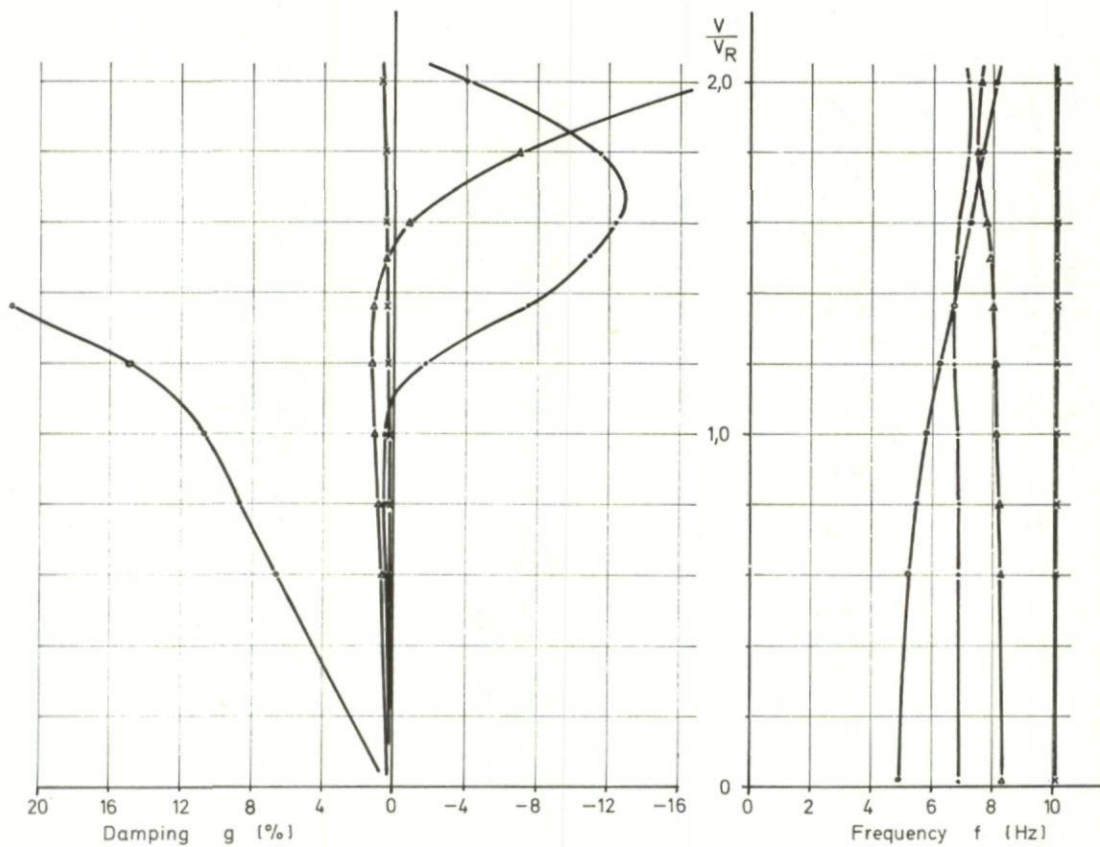


Fig.14 Damping and frequency versus velocity for $Ma = 0.9$ (AFS off), $\Delta_{WG} = 45^\circ$

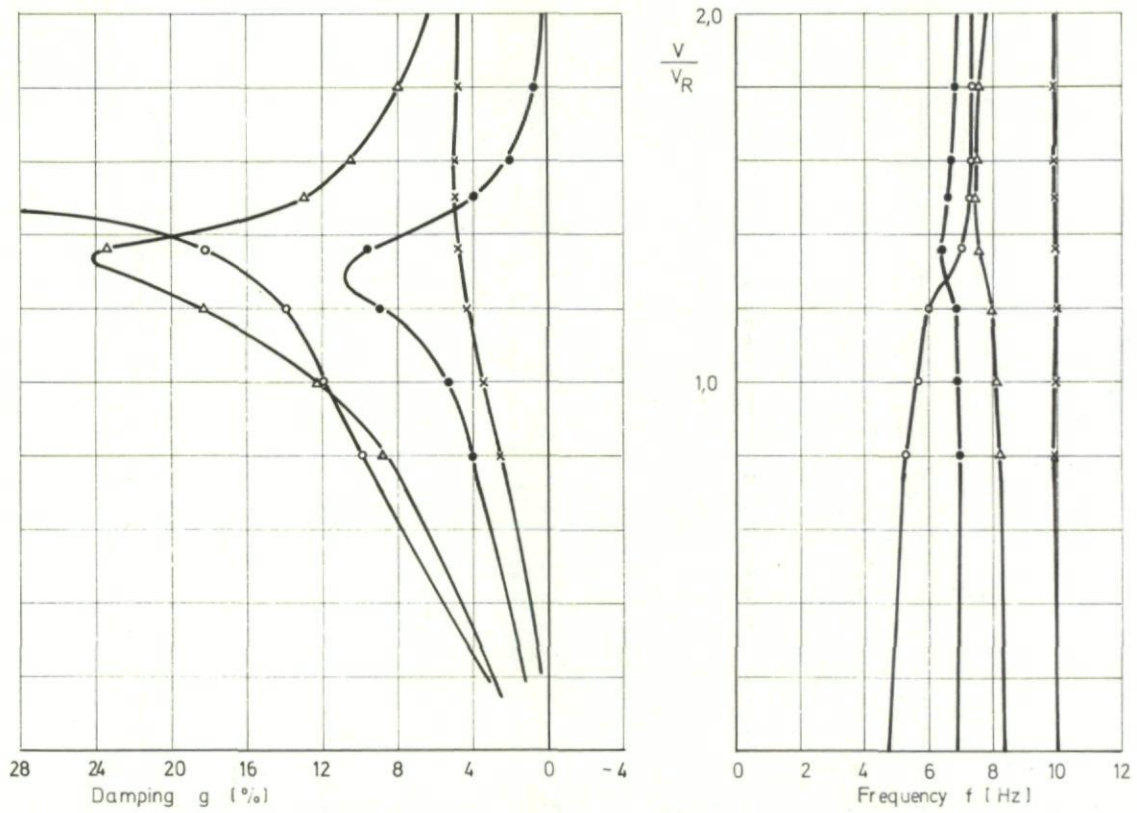


Fig.15 Damping and frequency versus velocity for $Ma = 0.2$ with AFS ($K = 100\%$, $\Delta\varphi = 0^\circ$), $\Lambda_{WG} = 45^\circ$

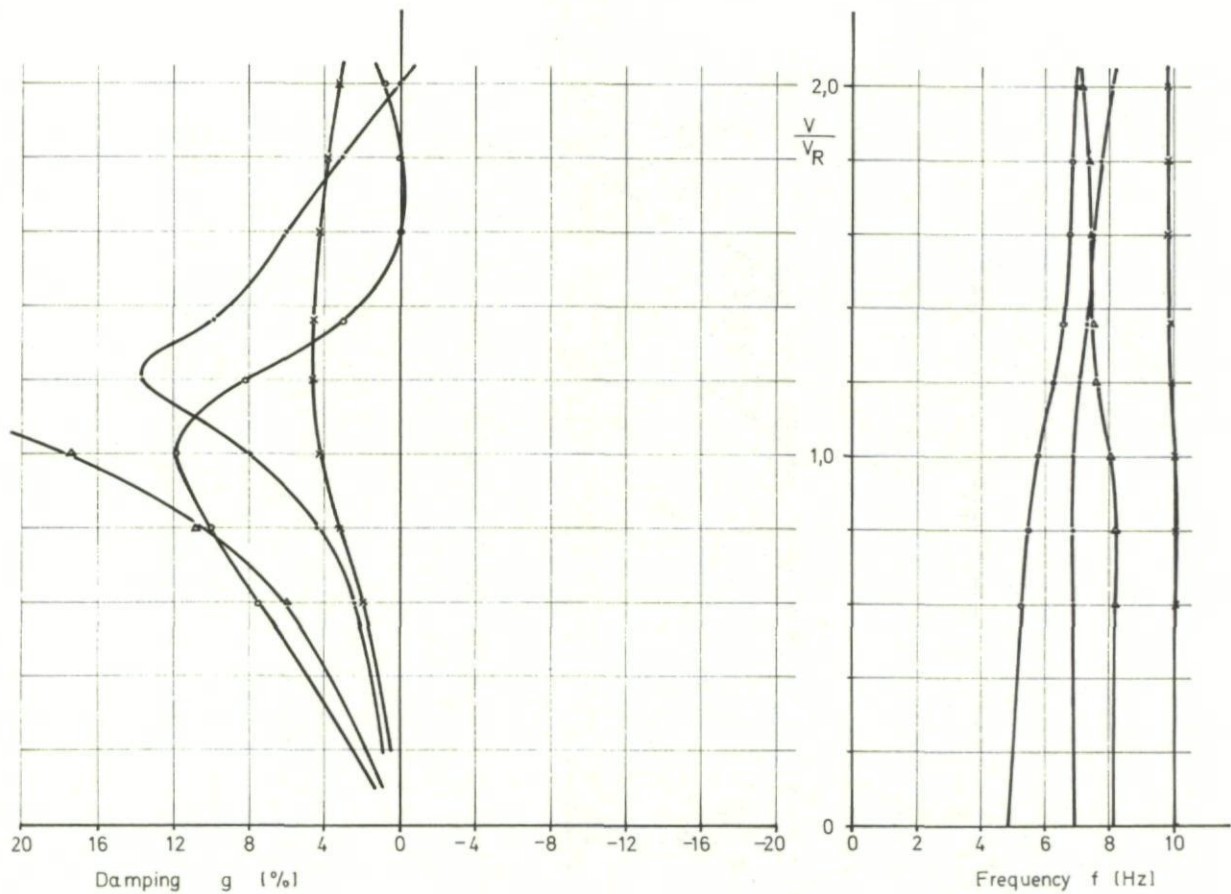


Fig.16 Damping and frequency versus velocity for $Ma = 0.9$ with AFS ($K = 100\%$, $\Delta\varphi = 0^\circ$), $\Lambda_{WG} = 45^\circ$

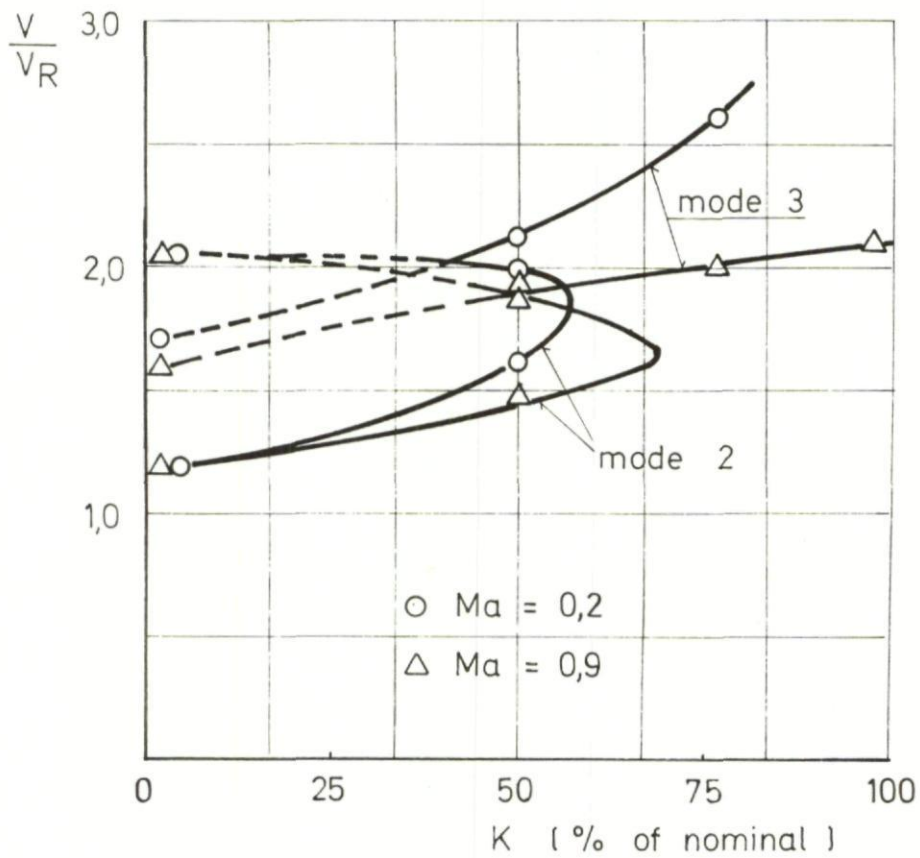


Fig.17 Flutter speed versus K for different Mach numbers, $\Delta\varphi_{WG} = 45^\circ$

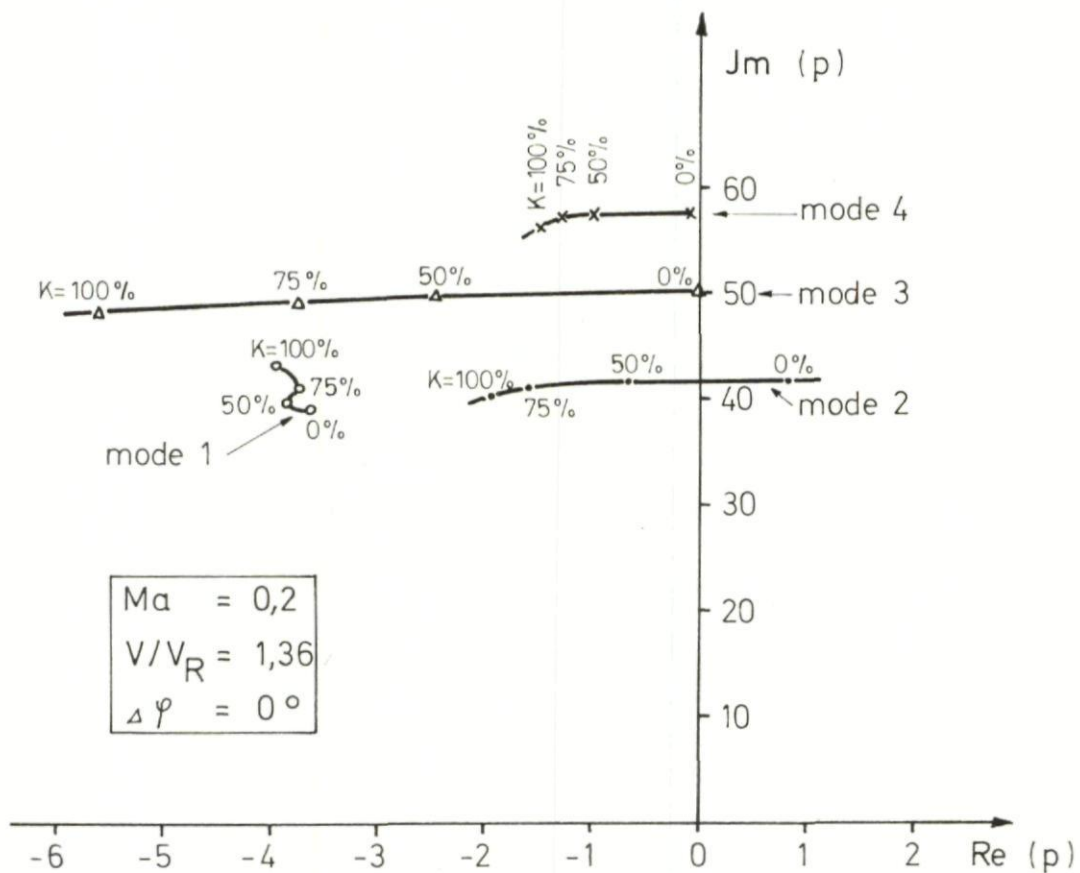


Fig.18 Root locus of the coupled system with variation of K

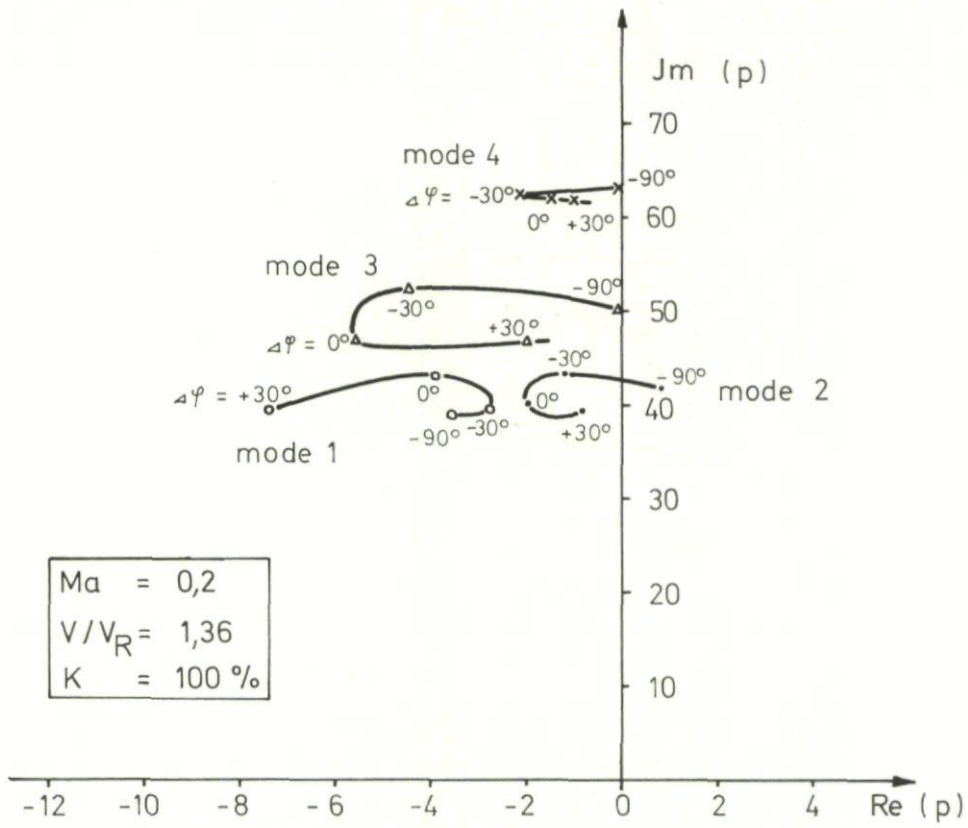


Fig.19 Root locus of the coupled system with variation of $\Delta\varphi$

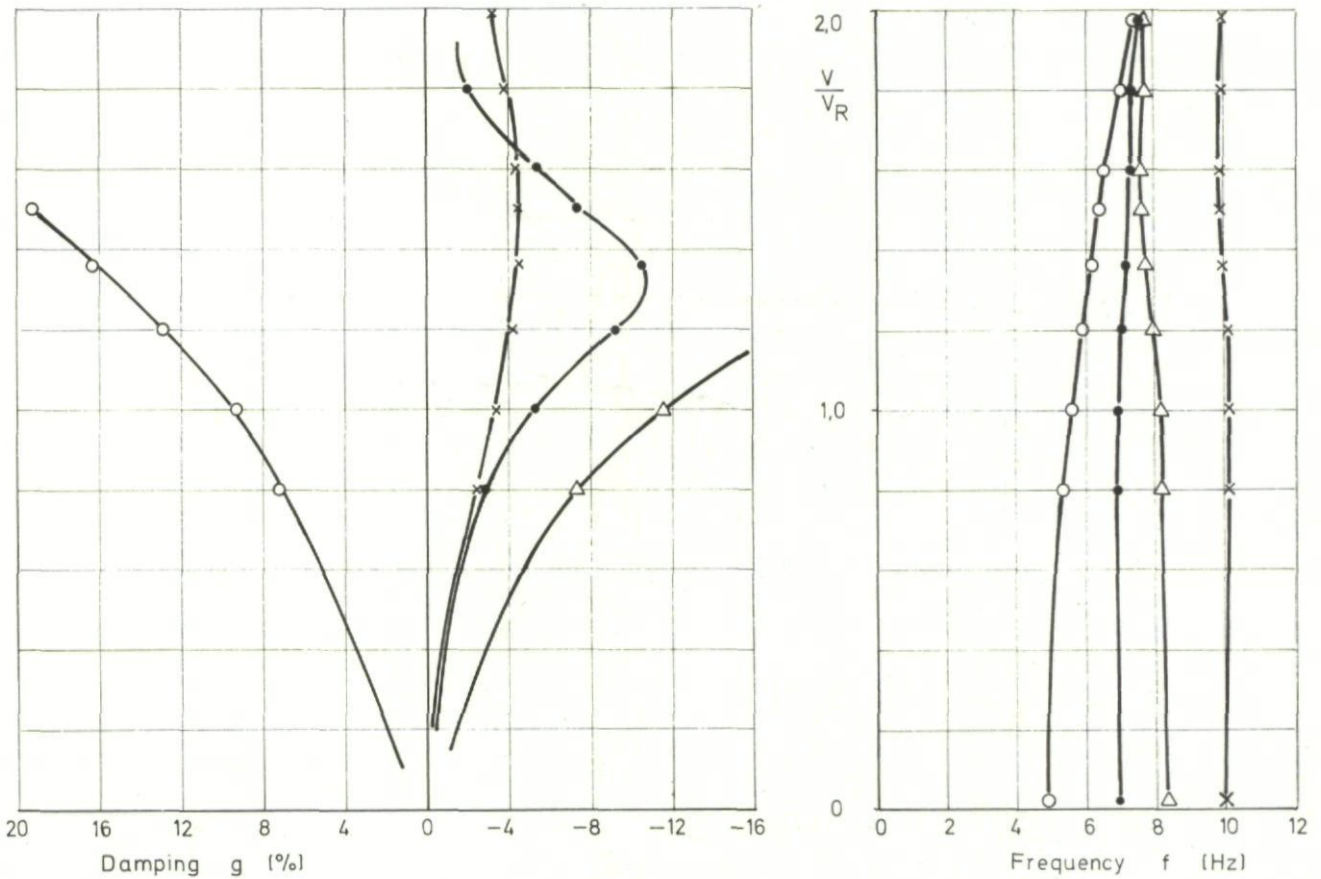


Fig.20 Damping and frequency versus velocity for $Ma = 0.2$ with AFE ($K = 100\%$, $\Delta\varphi = 180^\circ$), $\Lambda_{WG} = 45^\circ$

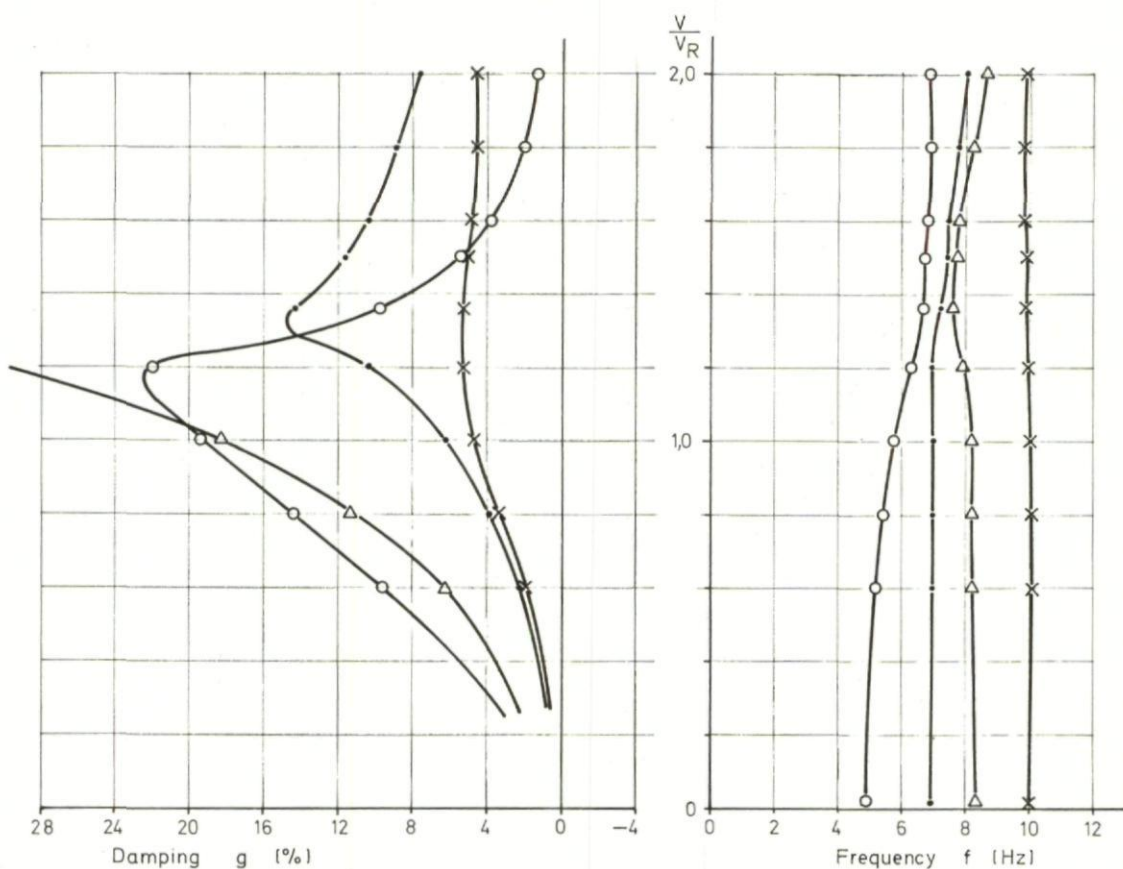


Fig.21 Damping and frequency versus velocity for $Ma = 0.2$ with AFS ($K = 100\%$, $\Delta\varphi = 0^\circ$), $\Lambda_{WG} = 45^\circ$, sensor and vane location: tank rear station

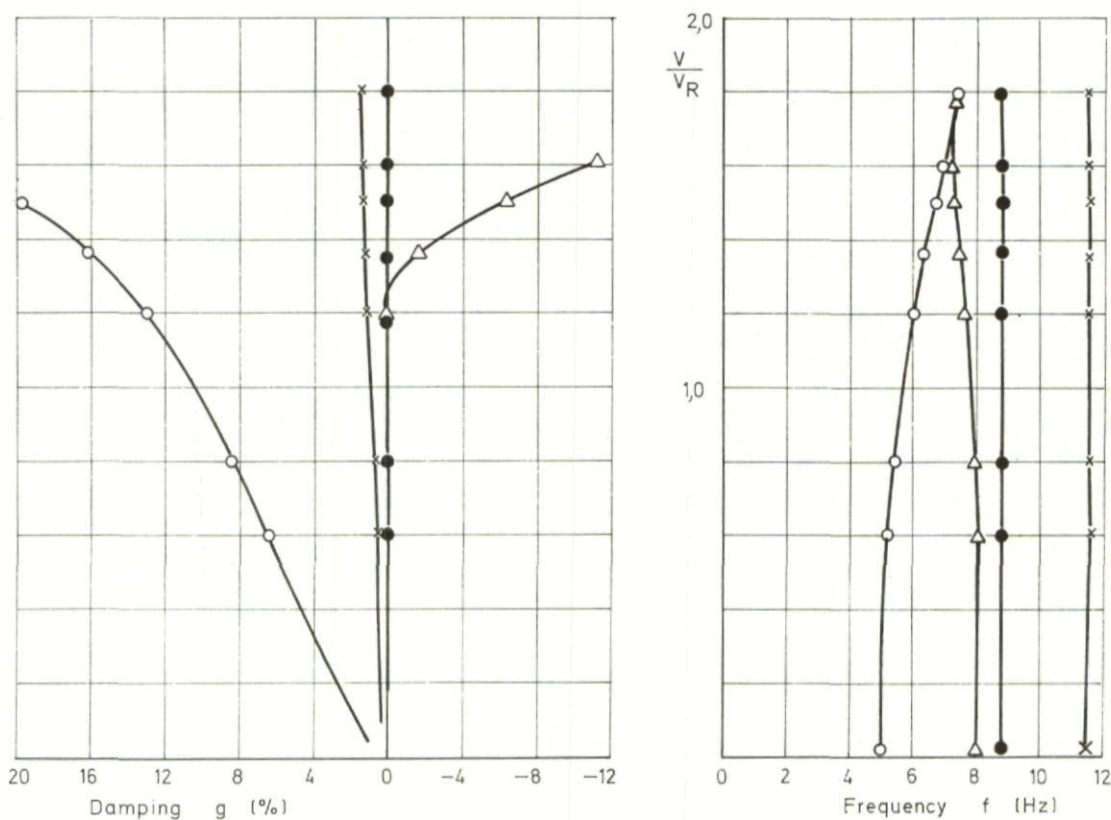


Fig.22 Damping and frequency versus velocity for $Ma = 0.2$ (AFS off), $\Lambda_{WG} = 45^\circ$, wing pivot yaw stiffness rigid

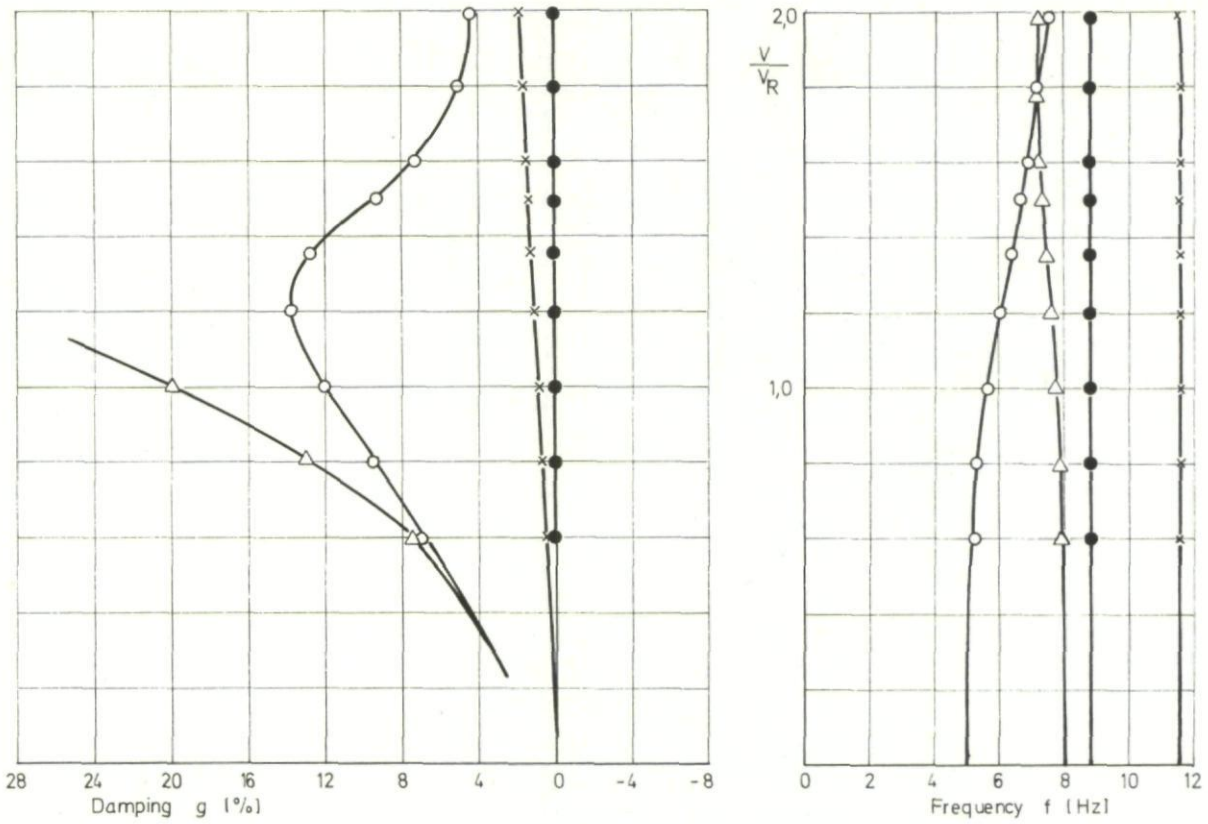


Fig. 23 Damping and frequency versus velocity for $Ma = 0.2$ with AFS ($K = 100\%$, $\Delta\varphi = 0^\circ$), $\Lambda_{WG} = 45^\circ$, wing pivot yaw stiffness rigid

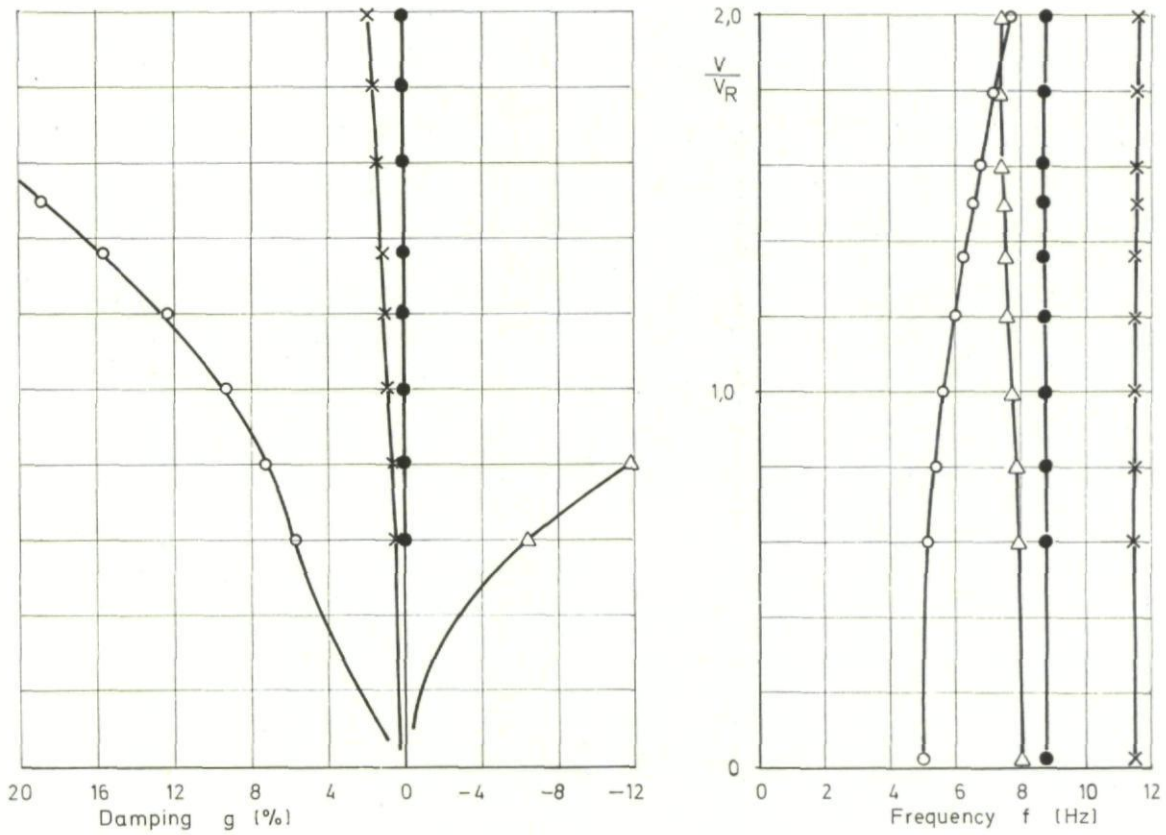
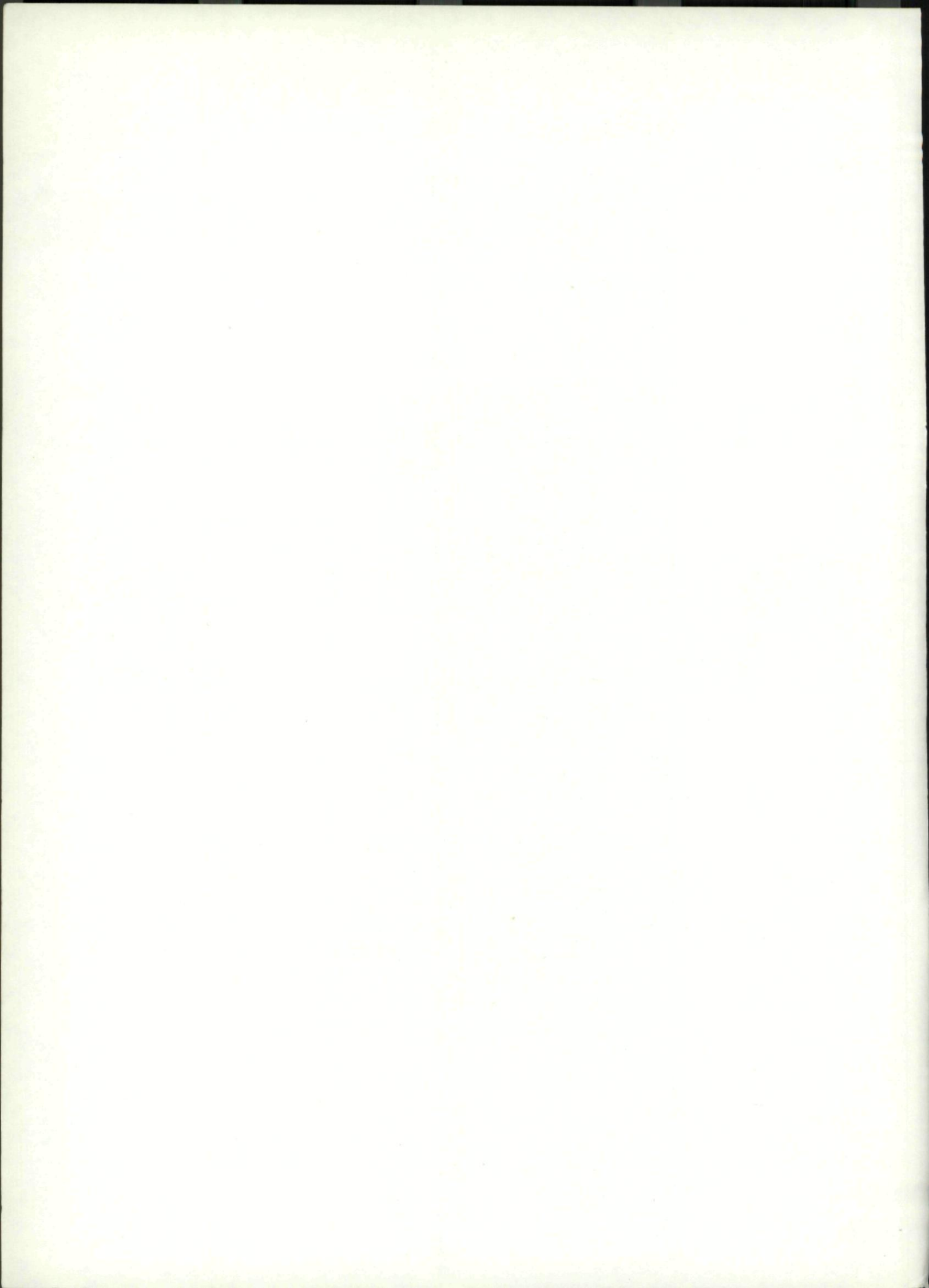


Fig. 24 Damping and frequency versus velocity for $Ma = 0.2$ with AFE ($K = 100\%$, $\Delta\varphi = 180^\circ$), $\Lambda_{WG} = 45^\circ$, wing pivot yaw stiffness rigid





<p>AGARDograph No.175 Advisory Group for Aerospace Research and Development, NATO ACTIVE CONTROL SYSTEMS FOR LOAD ALLEVIATION, FLUTTER SUPPRESSION AND RIDE CONTROL Published March 1974 84 pages</p> <p>Active Control Systems offer potential to: reduce structural loads encountered in maneuvers; improve stability; reduce the size of control surfaces; reduce static design loads; increase flutter speeds and suppress flutter, thereby reducing stiffness or mass required of members; reduce the margin between normal</p> <p>P.T.O.</p>	<p>AGARD-AG-175 629.73.062 – 52 : 533.6.013.422 : 533.6.048.1</p> <p>Aerodynamic loads Flutter Loads (forces) Flight maneuvers Flight control Control equipment</p>	<p>AGARDograph No.175 Advisory Group for Aerospace Research and Development, NATO ACTIVE CONTROL SYSTEMS FOR LOAD ALLEVIATION, FLUTTER SUPPRESSION AND RIDE CONTROL Published March 1974 84 pages</p> <p>Active Control Systems offer potential to: reduce structural loads encountered in maneuvers; improve stability; reduce the size of control surfaces; reduce static design loads; increase flutter speeds and suppress flutter, thereby reducing stiffness or mass required of members; reduce the margin between normal</p> <p>P.T.O.</p>	<p>AGARD-AG-175 629.73.062 – 52 : 533.6.013.422 : 533.6.048.1</p> <p>Aerodynamic loads Flutter Loads (forces) Flight maneuvers Flight control Control equipment</p>
<p>AGARDograph No.175 Advisory Group for Aerospace Research and Development, NATO ACTIVE CONTROL SYSTEMS FOR LOAD ALLEVIATION, FLUTTER SUPPRESSION AND RIDE CONTROL Published March 1974 84 pages</p> <p>Active Control Systems offer potential to: reduce structural loads encountered in maneuvers; improve stability; reduce the size of control surfaces; reduce static design loads; increase flutter speeds and suppress flutter, thereby reducing stiffness or mass required of members; reduce the margin between normal</p> <p>P.T.O.</p>	<p>AGARD-AG-175 629.73.062 – 52 : 533.6.013.422 : 533.6.048.1</p> <p>Aerodynamic loads Flutter Loads (forces) Flight maneuvers Flight control Control equipment</p>	<p>AGARDograph No.175 Advisory Group for Aerospace Research and Development, NATO ACTIVE CONTROL SYSTEMS FOR LOAD ALLEVIATION, FLUTTER SUPPRESSION AND RIDE CONTROL Published March 1974 84 pages</p> <p>Active Control Systems offer potential to: reduce structural loads encountered in maneuvers; improve stability; reduce the size of control surfaces; reduce static design loads; increase flutter speeds and suppress flutter, thereby reducing stiffness or mass required of members; reduce the margin between normal</p> <p>P.T.O.</p>	<p>AGARD-AG-175 629.73.062 – 52 : 533.6.013.422 : 533.6.048.1</p> <p>Aerodynamic loads Flutter Loads (forces) Flight maneuvers Flight control Control equipment</p>

operating speed and design diving speed due to upsets, wind shears, temperature gradients, etc., improve ride control; and reduce stores vibration. Essential to adequate solution of the problem of effective employment of active control devices is the development of systems to detect and counteract disturbing loads by means of properly phased control forces produced by reliable autostabilizing systems. Recent research work and specific applications of active control devices are dealt with in the five papers that comprise this AGARDograph.

This AGARDograph was prepared at the request of the Structures and Materials Panel of AGARD.

operating speed and design diving speed due to upsets, wind shears, temperature gradients, etc., improve ride control; and reduce stores vibration. Essential to adequate solution of the problem of effective employment of active control devices is the development of systems to detect and counteract disturbing loads by means of properly phased control forces produced by reliable autostabilizing systems. Recent research work and specific applications of active control devices are dealt with in the five papers that comprise this AGARDograph.

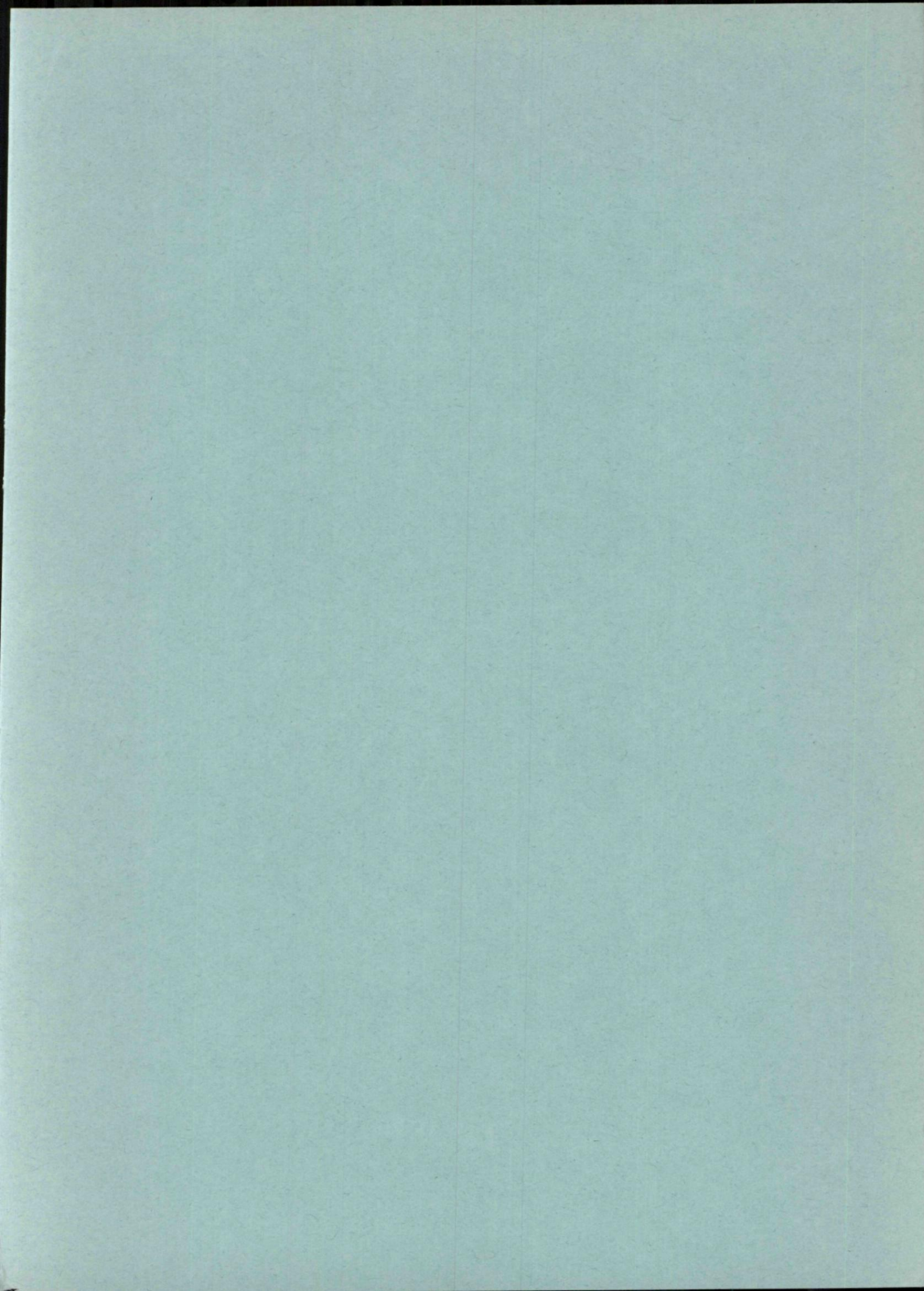
This AGARDograph was prepared at the request of the Structures and Materials Panel of AGARD.

operating speed and design diving speed due to upsets, wind shears, temperature gradients, etc., improve ride control; and reduce stores vibration. Essential to adequate solution of the problem of effective employment of active control devices is the development of systems to detect and counteract disturbing loads by means of properly phased control forces produced by reliable autostabilizing systems. Recent research work and specific applications of active control devices are dealt with in the five papers that comprise this AGARDograph.

This AGARDograph was prepared at the request of the Structures and Materials Panel of AGARD.

operating speed and design diving speed due to upsets, wind shears, temperature gradients, etc., improve ride control; and reduce stores vibration. Essential to adequate solution of the problem of effective employment of active control devices is the development of systems to detect and counteract disturbing loads by means of properly phased control forces produced by reliable autostabilizing systems. Recent research work and specific applications of active control devices are dealt with in the five papers that comprise this AGARDograph.

This AGARDograph was prepared at the request of the Structures and Materials Panel of AGARD.



DISTRIBUTION OF UNCLASSIFIED AGARD PUBLICATIONS

NOTE: Initial distributions of AGARD unclassified publications are made to NATO Member Nations through the following National Distribution Centres. Further copies are sometimes available from these Centres, but if not may be purchased in Microfiche or photocopy form from the Purchase Agencies listed below. THE UNITED STATES NATIONAL DISTRIBUTION CENTRE (NASA) DOES NOT HOLD STOCKS OF AGARD PUBLICATIONS, AND APPLICATIONS FOR FURTHER COPIES SHOULD BE MADE DIRECT TO THE APPROPRIATE PURCHASE AGENCY (NTIS).

NATIONAL DISTRIBUTION CENTRES

BELGIUM

Coordonnateur AGARD – VSL
Etat-Major de la Force Aérienne
Caserne Prince Baudouin
Place Dailly, 1030 Bruxelles

CANADA

Defence Scientific Information Service
Defence Research Board
Department of National Defence
Ottawa, Ontario K1A 0Z3

DENMARK

Danish Defence Research Board
Østerbrogades Kaserne
Copenhagen Ø

FRANCE

O.N.E.R.A. (Direction)
29, Avenue de la Division Leclerc
92, Châtillon sous Bagneux

GERMANY

Zentralstelle für Luftfahrtokumentation
und Information
Maria-Theresia Str. 21
8 München 27

GREECE

Hellenic Armed Forces Command
D Branch, Athens

ICELAND

Director of Aviation
c/o Flugrad
Reykjavik

ITALY

Aeronautica Militare
Ufficio del Delegato Nazionale all'AGARD
3, Piazzale Adenauer
Roma/EUR

LUXEMBOURG

See Belgium

NETHERLANDS

Netherlands Delegation to AGARD
National Aerospace Laboratory, NLR
P.O. Box 126
Delft

NORWAY

Norwegian Defence Research Establishment
Main Library
P.O. Box 25
N-2007 Kjeller

PORTUGAL

Direccao do Servico de Material
da Forca Aerea
Rua de Escola Politecnica 42
Lisboa
Attn: AGARD National Delegate

TURKEY

Turkish General Staff (ARGE)
Ankara

UNITED KINGDOM

Defence Research Information Centre
Station Square House
St. Mary Cray
Orpington, Kent BR5 3RE

UNITED STATES

National Aeronautics and Space Administration (NASA)
Langley Field, Virginia 23365
Attn: Report Distribution and Storage Unit
(See Note above)

PURCHASE AGENCIES

Microfiche or Photocopy

National Technical
Information Service (NTIS)
5285 Port Royal Road
Springfield
Virginia 22151, USA

Microfiche

ESRO/ELDO Space
Documentation Service
European Space
Research Organization
114, Avenue Charles de Gaulle
92200 Neuilly sur Seine, France

Microfiche

Technology Reports
Centre (DTI)
Station Square House
St. Mary Cray
Orpington, Kent BR5 3RE
England

Requests for microfiche or photocopies of AGARD documents should include the AGARD serial number, title, author or editor, and publication date. Requests to NTIS should include the NASA accession report number.

* * *

Full bibliographical references and abstracts of AGARD publications are given in the following bi-monthly abstract journals:

Scientific and Technical Aerospace Reports (STAR),
published by NASA,
Scientific and Technical Information Facility
P.O. Box 33, College Park
Maryland 20740, USA

Government Reports Announcements (GRA),
published by the National Technical
Information Services, Springfield
Virginia 22151, USA

